

Property measurements of thin coatings

by

Obaidur Rehman Khan

This thesis is submitted in fulfilment of the requirements for the degree of doctor of philosophy in the faculty of engineering.

Department of Metallurgy and
Materials Engineering
The University of Aston in Birmingham
February, 1982.

The University of Aston in Birmingham

Property measurement of thin coatings

Obaidur Rehman Khan

Submitted 1982 for the degree of Ph.D.

Summary

Colour and microhardness were the main two properties of thin coatings studied. The thinner the coatings, the more difficult it is to measure the properties of thin coatings (including thickness). The factors that influence the colour of thin coatings were examined. Yellow gold was deposited on white metal substrates by vacuum deposition and electrodeposition. Colour was measured using spectrophotometric techniques. CIE chromaticity co-ordinates were calculated from spectrophotometric data using a computer programme written for the purpose. The minimum thickness of coating required to produce its fixed colour and completely hide the underlying substrate was measured and found to depend on the nature of the substrate and coating, the method of applying the coating and the application operating conditions.

The second part of the thesis covers the measurement of microhardness. A new technique was developed for the production of tungsten microindenters with tips between 0.1 μm and 1.0 μm diameter. The tips were formed by electro-machining tungsten wire in an electropolishing solution controlled electronically to avoid etching. An instrument was developed using the microindenters for determining the microhardness of surfaces within the specimen chamber of a scanning electron microscope. Preliminary results were compared with those of conventional microhardness testing in air.

Keywords: thin coatings, colour, hardness, gold.

Dedication

Some people make the world a better place just by being in it.

My three year old daughter Lubna is one of these people, and that is why I have dedicated this work to her.

Acknowledgements

I acknowledge the assistance and encouragement of my supervisor, Dr. D.J. Arrowsmith. I thank him for his long, patient and helpful supervision during the work, and it is due to this encouragement that I have reached this position of compiling the work and writing it up. I am grateful to Dr. J.K. Dennis, Dr. J. Aston, Dr. W.B. Hutchinson and Professor I.L. Dillamore for their support.

I have received experimental assistance both from the Department of Metallurgy and Materials Engineering of the University of Aston in Birmingham and the Department of Chemistry at Birmingham Polytechnic. I am very grateful to Dr. G. Brown at the Polytechnic for her assistance and suggestions on colour measurements of the coatings and substrate materials.

I am indebted to Mr. T. Watson and Mr. R. Howell for their suggestions for the modification of the micromanipulator's lever to be used as a microindentation tester, and other components used in this work.

Many thanks to Dr. V. Piddock, Mr. B. Mahmoudian, Mr. P.J. Cunningham, Mr. N. Mykura, Mr. J.J. Fuggle, Mr. D. Russell, Mr. S.P. Fuggle, Mr. B. Cox and Mr. K. Smith for their assistance and moral support in the Department.

I am grateful to Mr. P. Cox for his time and assistance with the photographic work. I am also thankful to Mrs. K. Hollingworth

who typed this thesis.

Financial support was provided partially by the M.E.T. (Muslim Educational Trust, London) during this work. Also, I would like to thank my father, Mohammad Ramzan Khan, my wife Anisa, for their long patience, sacrifices and moral support during the research. Finally, how can I forget my three year old daughter Lubna! who kept my spirits high during the entire period of this work.

CONTENTS

	<u>Page No.</u>
<u>Chapter 1</u>	
Introduction.	2
<u>Chapter 2</u>	
Coating techniques.	6
2.1 Introduction.	6
2.2 Electrodeposition.	7
2.3 Vapour deposition.	7
2.4 Sputtering.	7
2.5 Evaporation.	11
Part I The influence of substrate composition on the optical properties of thin coatings.	
<u>Chapter 3</u>	
Theory and determination of the optical properties.	14
3.1 Introduction.	14
3.2 The nature of light.	14
3.2.1 The nature of colour.	15
3.3 The spectrophotometric specification of colour.	17
3.4 Basic principles of the measurement of colour.	18
3.4.1 The function of reflectivity and absorbance.	18
3.4.2 The measurement of colours.	19
3.4.3 Matching methods.	21
3.4.4 Colorimetry.	22
3.4.4.1 Additive colorimeters.	22

3.4.4.2	Visual colorimeters.	24
3.4.4.3	Photoelectric colorimeters.	24
3.4.4.4	Photoelectric spectrophotometers.	24
3.4.5	Graphical representation of colour specification.	25
3.4.5.1	The standard illuminants.	25
3.4.5.2	The colour triangle.	25
3.4.5.3	The spectral locus.	27
3.4.5.4	The dominant wavelength.	29
3.4.5.5	The chromaticity chart/diagram.	29
3.4.5.6	The spectrophotometer readings.	29
3.5	The influence of atomic structure on the colour of metals.	33
3.6	The formation and growth of gold coatings.	33
3.7	The principle of scanning electron microscopy (S.E.M.).	34

Chapter 4

	Results and techniques.	40
4.1	Introduction.	40
4.2	Specimen preparation.	41
4.3	Aluminium coatings.	41
4.3.1	Experimental procedure.	41
4.3.2	The evaporation.	44
4.3.3	The microscopic examination of the coatings (projection microscope).	46
4.3.4	Aluminium evaporated coatings for different timings.	46

4.4	Thin gold coatings.	51
4.4.1	The sputtering electrode.	51
4.4.2	Deposition of gold coatings.	51
4.4.3	Thicknesses of the gold coatings.	53
4.4.3.1	The radial section semi-circular disc.	60
4.4.3.2	Gold coated specimens using the semi-circular discs.	60
4.5	The influence of substrate materials on gold coatings.	62
4.5.1	The coating arrangement.	62
4.5.2	Standard specimen for colour measurement.	68
4.5.3	The measurement of colour.	73
4.5.4	Procedure of measurement.	76
4.5.5	Calculation of the chromaticity co-ordinates.	78
4.5.6	Fortran computer programme OKØØ2	80
4.5.7	The optical properties of gold coatings.	83
4.5.8	Thickness of the gold coatings.	85
4.5.9	Influence of the substrate material on the gold coatings.	92
4.5.9.1	The influence of substrate nickel on the coatings.	92
4.5.9.2	The influence of substrate stainless steel on the coatings.	97
4.5.9.3	The influence of substrate aluminium on the coatings.	97

Chapter 5

	Discussion and conclusions.	107
5.1	Discussion.	107
5.1.1	Thin coatings, techniques and methods.	107
5.1.2	Thickness measurement.	108
5.1.3	Colour measurement.	108
5.2	Conclusions.	112
5.3	Suggestions for the further work.	112

References to the first part.

Part II Thin coating, hardness measurement and micro-indentation techniques.

	<u>Page No.</u>
<u>Chapter 6</u>	
Introduction.	125
<u>Chapter 7</u>	
Methods of hardness testing and microindentation.	127
7.1 Introduction.	127
7.2 Methods of hardness testing.	128
7.2.1 Cone indentation test.	128
7.2.2 The Rockwell test - 120° diamond cone.	129
7.2.3 The pyramid indentation test.	130
7.2.4 The ball indentation test.	131
7.2.5 Microindentation testing.	132
<u>Chapter 8</u>	
Theory of microindentations and microhardness testing.	135
8.1 Basics of the microindentation hardness testing.	135
8.2 Related features of microhardness testing.	138
8.3 Precautions and the experimental conditions for the microindentations.	140
<u>Chapter 9</u>	
Results and techniques.	146
9.1 Introduction.	146
9.2 The stereoscan SEM micro-manipulator as a microindentation tester.	146

		<u>Page No.</u>
9.2.1	Function of the SEM micro-manipulator.	146
9.2.2	Modifications.	148
9.2.3	The microindenter's holder.	148
9.2.4	Function of the microindentation tester.	150
9.3	Indenters for microindentation.	151
9.3.1	The micromanipulator's probe tungsten needles.	151
9.3.2	Choice of suitable micro-indenters.	151
9.3.3	Electropolished tungsten micro-indenters.	155
9.3.4	The preparation of tungsten tips using an automatic switch.	155
9.3.4.1	Function of the automatic switch.	156
9.3.4.2	Circuit characteristics.	156
9.3.5	Preparation of the polishing solution.	159
9.3.6	The tungsten specimens for micro-indenters.	159
9.3.7	The tungsten microindenters.	160
9.4	The microhardness testing, using a Vicker's microhardness tester.	181
9.4.1	Microhardness testing systems.	181
9.5	Microindentation testings on 60/40 brass and aluminium specimens.	184
9.5.1	Reproducibility of the micro-indenters.	188
9.5.2	Calibration of the indentation size and load.	188

9.5.3 Some selected microindentations. 200

Chapter 10

Discussion and conclusions. 206

References to the second part. 210

Appendix. 216

List of the figures and the diagrams

			<u>Page No.</u>
<u>Chapter 2</u>			
(1)	Figure 2.1	A sputtering unit.	9
(2)	Figure 2.2	An evaporation unit.	12
<u>Chapter 3</u>			
(3)	Figure 3.1	Composition of wave length in white light.	16
(4)	Figure 3.2	Illustration of the terms wave length and amplitude.	15
(5)	Figure 3.3	Dispersion of the white light.	16
(6)	Figure 3.4	Illustration of the terms, hue, lightness and saturation.	20
(7)	Figure 3.5	Additive colorimeter.	23
(8)	Figure 3.6	Visual colorimeter.	23
(9)	Figure 3.7	Spectrophotometer.	26
(10)	Figure 3.8	The colour triangle and spectral locus.	28
(11)	Figure 3.9	Definition of dominant wave length and saturation.	30
(12)	Figure 3.10	The colour triangle and spectral locus superimposed on a right angled triangle.	31
(13)	Figure 3.11	The basic principle of scanning electron microscope (SEM).	35
(14)	Figure 3.12	Cambridge stereoscan 150 electron microscope.	38
<u>Chapter 4</u>			
(15)	Figure 4.1	Plastic mould for lapping the discs.	42
(16)	Figure 4.2	The specimen pieces mounted with conducting bakelite in cross section.	43

			<u>Page No.</u>
(17)	Figure 4.3	Experimental set up for aluminium coatings.	45
(18)	Figure 4.4	Rate of aluminium deposition.	50
(19)	Figure 4.5	Sputtering electrode coated with gold deposits of a few thousand Angstrom units.	52
(20)	Figure 4.6 (A)	Six gold coated nickel discs.	54
(21)	Figure 4.6 (B)	Six gold coated glass cover slips with identification labels.	54
(22)	Figure 4.7	Experimental set up of gold coatings.	55
(23)	Figure 4.8	Resistance measuring probes mounted with the non-conducting material.	57
(24)	Figure 4.9	Thickness measurement.	59
(25)	Figure 4.10	Semi circular disc with radial sections.	61
(26)	Figure 4.11	SEM photomicrographs of gold coatings after 3 minutes sputtering on nickel.	64
(27)	Figure 4.12	Gold sputtered coatings on nickel.	66
(28)	Figure 4.13	Punched discs of the substrate materials.	69
(29)	Figure 4.14	Unicam S.P. 800 spectrophotometer.	
(30)	Figure 4.15	The instrumental absorbance/transmittance chart.	
(31)	Figure 4.16	Aluminium jig for holding the discs.	70
(32)	Figure 4.17	Nickel abraded surfaces.	71
(33)	Figure 4.18	The mask used in the spectrophotometric measurement.	74
(34)	Figure 4.19	The optical system of the unicam S.P. 800 spectrophotometer.	75
(35)	Figure 4.20	Unicam diffuse reflectance attachment (No. SP 890).	

			<u>Page No.</u>
(36)	Figure 4.21	The optical system of the diffuse reflectance attachment.	77
(37)	Figure 4.22	The preparation of standard and the sample/standard holder.	79
(38)	Figure 4.23	The chromaticity chart in colour.	
(39)	Figure 4.24	The chromaticity diagram.	
(40)	Figure 4.25	The CIE chromaticity chart for equi-energy conditions.	81
(41)	Figure 4.26	The CIE chromaticity chart for tungsten lamp sp. conditions.	82
(42)	Figure 4.27	Reflectivity curves of an aluminium substrate coated with gold for different times.	84
(43)	Figure 4.28	Positions of the coated glass cover slips.	86
(44)	Figure 4.29	Colour of gold coatings on glass cover slips.	87
(45)	Figure 4.30	Reflectivity curves of glass cover slip coated with gold for different times.	88
(46)	Figure 4.31	Reflectivity curves of glass cover slip coated with gold for different times.	89
(47)	Figure 4.32	Gold coatings.	90
(48)	Figure 4.33	" "	91
(49)	Figure 4.34	Reproducibility of the gold coatings for the same time period.	93
(50)	Figure 4.35	Colour of gold coatings on polished nickel.	94
(51)	Figure 4.36	Colour of gold coatings on polished stainless steel.	98
(52)	Figure 4.37	Colour of gold coatings on polished aluminium.	99
(53)	Figure 4.38	Reflectivity curves of nickel substrate coated with gold for different times.	100

			<u>Page No.</u>
(54)	Figure 4.39	Reflectivity curves of nickel substrate coated with gold for different times.	101
(55)	Figure 4.40	Reflectivity curves of stainless steel substrate coated with gold for different times.	102
(56)	Figure 4.41	Reflectivity curves of stainless steel substrate coated with gold for different times.	103
(57)	Figure 4.42	Reflectivity curves of aluminium substrate coated with gold for different times.	105
(58)	Figure 4.43	Reflectivity curves of aluminium substrate coated with gold for different times.	106
<u>Chapter 5</u>			
(59)	Figure 5.1	Histogram of the island size in a typical coating.	109
(60)	Figure 5.2	Histogram of the inter-island spacing.	109
<u>Chapter 8</u>			
(61)	Figure 8.1	Microindentation phenomenon.	139
(62)	Figure 8.2	Variation of microindentation hardening value with indenter load.	142
(63)	Figure 8.3	Microindentation hardness profile of a grain boundary in a sulphur-segregated iron.	144
<u>Chapter 9</u>			
(64)	Figure 9.1	Function of the micromanipulator.	147
(65)	Figure 9.2	Modified micromanipulators lever as microhardness tester.	149
(66)	Figure 9.3	The holders for the microindenters.	
(67)	Figure 9.4	Microprobes and the load used for microindentations.	

(68)	Figure 9.5	Microindenter's holder.	
(69)	Figure 9.6	Micromanipulator's probe needles.	152
(70)	Figure 9.7	The microindentations with the micromanipulators probe needles.	153
(71)	Figure 9.8	The microindentations with the micromanipulators probe needles.	154
(72)	Figure 9.9	Basic principle of the electro-polishing circuit.	157
(73)	Figure 9.10	Circuit diagram of the automatic switch.	158
(74)	Figure 9.11	Shapes of the tungsten micro-indenters.	161
(75)	Figure 9.12	Shapes of the tungsten micro-indenters polished of the wires	162
(76)	Figure 9.13	of different thickness.	163
(77)	Figure 9.14	Tungsten microindenters.	166
(78)	Figure 9.15	" "	168
(79)	Figure 9.16	" "	170
(80)	Figure 9.17	" "	171
(81)	Figure 9.18	" "	172
(82)	Figure 9.19	" "	173
(83)	Figure 9.20	" "	174
(84)	Figure 9.21	Electropolishing equipment.	177
(85)	Figure 9.22	Tungsten microindenters.	178
(86)	Figure 9.23	" "	180
(87)	Figure 9.24	Used microindenters.	182
(88)	Figure 9.25	" "	183
(89)	Figure 9.26	DM41 microhardness tester.	186
(90)	Figure 9.27	Microindentations made with the Vicker's microhardness tester.	187

			<u>Page No.</u>
(91)	Figure 9.28	Microindentations made on brass.	189
(92)	Figure 9.29	" " " "	190
(93)	Figure 9.30	Microindentations made on aluminium.	191
(94)	Figure 9.31	Microindentations made with different load on brass.	194
(95)	Figure 9.32	Microindentations made with different load on aluminium.	196
(96)	Figure 9.33	Microindentations made with different load on aluminium.	197
(97)	Figure 9.34	Some selected microindentations on aluminium.	202
(98)	Figure 9.35	Some selected microindentations on brass.	204
<u>Chapter 10</u>			
(99)	Figure 9.36	A damaged microindenter.	207

List of Tables

			<u>Page No.</u>
<u>Chapter 4</u>			
(1)	Table 4.1	Thickness of the coatings.	47
(2)	Table 4.2	" " " "	49
(3)	Table 4.3	Thickness of the coatings using different methods.	58
(4)	Table 4.4	Thickness of the coatings using microphotographs.	67
(5)	Table 4.5	Gold coatings series E.	95
(6)	Table 4.6	Gold coatings series F.	96
<u>Chapter 5</u>			
(7)	Table 5.1	A comparison of the results.	111
<u>Chapter 7</u>			
(8)	Table 7.1	Microhardness limits.	134
<u>Chapter 9</u>			
(9)	Table 9.1	The shape of the micro-indenter tips.	164
(10)	Table 9.2	Diameter and the shape of the tips of the microindenters.	175
(11)	Table 9.3	Diameter and the shape of the tips of the microindenters.	176
(12)	Table 9.4	Microindentation sizes.	185
(13)	Table 9.5	" " "	192
(14)	Table 9.6	Microindentation size at different loads on brass and aluminium.	198

List of the Appendices

		<u>Page No.</u>
App. 1	Standard illuminants.	216
App. 2	The computer programme OKØØ2	217
App. 3	The computer programme file OKØØ2	219
App. 4	Cambridge stereoscan 150.	220
App. 5	Nanotech automatic high vacuum coater.	221
App. 6	Procedure metallographic mounting.	222
App. 7	Thickness calculation of the coatings using a gravimetric method.	223
App. 8	Installation procedure for Unicam SP800D spectrophotometer with a Unicam SP890 diffuse reflectance attachment.	224
App. 9	The computer input data files for four specimens.	225
App. 10	The computer output for programme OKØØ2 for a coating.	227
App. 11	The computer output for programme OKØØ2 for a substrate.	229
App. 12	The features of the automatic switch for 231 the electropolishing of the tungsten wire.	
App. 13	Pretreated specimen for microindentation 233	
App. 14	D M41 microhardness tester.	234

Part One

Thickness measurement and the influence of substrate composition on the optical properties of thin coatings.

Chapter One

Introduction

Film fabrication has been developed and studied widely because of its many applications in industry and technology (51, 59, 60, 61, 62). It is a very broad subject and embraces films whose thickness varies from about a nanometer to a few microns.

Metal films have been the subject of many investigations (20, 21, 22, 23, 36, 37). The first films were developed more than one hundred years ago and were mainly precious metal coatings. Later many different coatings were applied for corrosion protection in industry. Nowadays their many uses and applications (59, 60, 61, 62, 63, 64) cover the whole range of surface properties. Films of a few atomic layers thick are called thin films and in most cases the film properties and their reproducibility can vary within rather wide limits. Many basic studies (65, 66) were conducted on the thin films where one dimension was extremely small compared with the other two. Although these studies were aimed at determining the characteristics of the film in the one dimension, the studies of the thin films stimulated great interest for the industry in general and in the electronic industry in particular.

With the rising cost of oil, work on alternative sources of energy has increased. Surfaces with solar absorption characteristics are being sought and research has escalated in the production of the desired properties in thick and thin films employed in solar cells (61).

There are many methods for making thin films (18) but vapour deposition, vacuum evaporation and sputtering, and electrodeposition are those commonly employed in research and industry. Vapour deposition is attractive because of its simplicity. The first vapour deposition was performed in 1893 when de Lodyguine (1893) attempted to coat the carbon filaments of incandescent lamps with tungsten by heating in a mixture of H₂ and WCl₆ (21). Evaporation and sputtering are usually preferred for dry and clean metallic coatings (67, 68). Nahwold (36) and Kundt (37) were the pioneers of the technique while R. Pohl et. al. (38) carried out the first successful evaporation in vacuum. Grove (22) and Plucker (23) studied the basic phenomena of sputtering. Sputtering is a very simple technique in principle, but the practice is comparatively complex. Electrodeposition also is simple but it is not a dry method. The first electrodeposition was done in 1838. It is now a major commercial method for producing decorative and protective coatings (60).

The first problem encountered when studying the properties of the thin films is the selection and characterisation of the initial surface of the substrate before deposition. The crystal structure, lattice orientation and the density of the dislocations at the material surface all affect the formation of film. Surface preparation is essential. This can involve the cleaning of the substrate in vacuum and also various environmental conditions during the cleaning procedure.

Recent developments (51, 67, 68, 69, 70, 71) show various tech-

niques of substrate cleaning and coating. These techniques result in an increase in the reproducibility of the properties obtained on thin coating systems. However, there are still variations in reproducibility even under controlled conditions.

The study of the physical properties of the film, such as the optical, electrical, mechanical and magnetic properties are related to the function of the coating and its use in industry or scientific development. With the progress of sophisticated methods of production and examination, the understanding of many of the unusual characteristics of the thin film behaviour is steadily improving. The reasons for many of the discrepancies in the early experiments on coatings are now known. Advances in many of the necessary accompanying technologies have enabled work on coatings to be carried out under conditions allowing a high degree of control (58). It is also interesting to note that the properties of the thin films differ from the properties of the bulk in many cases (57).

The purpose of the present work was to study the influence of the substrate and film thickness on the optical properties of the coated component. It was also the aim to find the minimum thickness of gold coatings to replace the colour (whiteness) of the substrate completely with the characteristic spectral colour of gold.

The second part of the work was to adapt a micromanipulator (64*)

* References at the back of the second part.

for the scanning electron microscope (SEM) as a microhardness tester. This involved design of a microindenter and holder which was controlled by the manipulator lever with 1-5 gram loads. An automatically switched electropolishing system for making the microindenter tungsten tips (*6) was developed. The reproducibility of tip sizes was assessed and the microindentations made with the tips were compared with microindentations made with the DM41 microhardness tester (*65). The reproducibility of the microindentations made with the tungsten tips was also assessed.

Further work has been suggested for development of the converted micromanipulator (microhardness tester) for use in the scanning electron microscope.

Chapter 2 is a brief review of coating techniques. Chapters 3 to 10 are divided into two areas of property measurements of thin coatings (1) the influence of substrate materials on the optical properties of thin coatings and (2) microhardness measurement and microindentation techniques for thin coatings. General discussion of the relevant theories in the two areas is also included. Experimental techniques and results are described in Chapter 4 and 9. At the end of each discussion section, conclusions and suggestions for future work are made. Appendices contain details of computer use and software.

Chapter 2

Coating Techniques

2.1 Introduction

There are many coating techniques (1, 51, 60, 63, 64, 67, 68) which are widely used in the aeronautical, electronic, mechanical, nuclear and optical engineering industries. They include the following:

- i. Electrodeposition.
- ii. Vapour deposition.
- iii. Sputtering.
- iv. Thermal evaporation.

The last three techniques are broadly classified as the vacuum deposition techniques (51, 52). Depending on the operating conditions, there are many variations which may be subclassified and which were summarised by J.J. Bessot (51).

Chemical vapour deposition (CVD)

Ionic treatments (+ sputtering)
Plasma deposition (+ sputtering)
Plasma polymerisation (+ sputtering)
Low pressure (CVD)

Cathode sputtering

D.C. diode sputtering -
D.C. magnetron
H.F. diode sputtering -
H.F. and ion magnetron.
Triode sputtering - ionic activation.
Reactive sputtering.

Vacuum evaporation

Reactive evaporation.
Ion plating (sputtering).

2.2 Electrodeposition has been used commercially for producing coatings since as long ago as 1838. The process is much more complicated (72, 73) than it seems at first sight. The migration of the metallic ions in a chemical solution to the cathode in the presence of an electric field between the electrodes is the basic phenomenon. The metallic ions are neutralised at the cathode and incorporated into the metal lattice. Complications arise in the cathode layer at the interface of the cathode surface and the electrolyte. This interfacial region acts as a dielectric layer. It also has capacitance due to the electron transfer across the interface.

There are also many operational factors which influence the deposition and include (a) current density, (b) temperature and agitation of the electrolyte, (c) convection in the immediate vicinity of the cathode, (d) migration and diffusion of the ions, and (e) shape and geometric arrangement of the cathode.

The influence of each one of them may be observed in the structure properties of the deposited film.

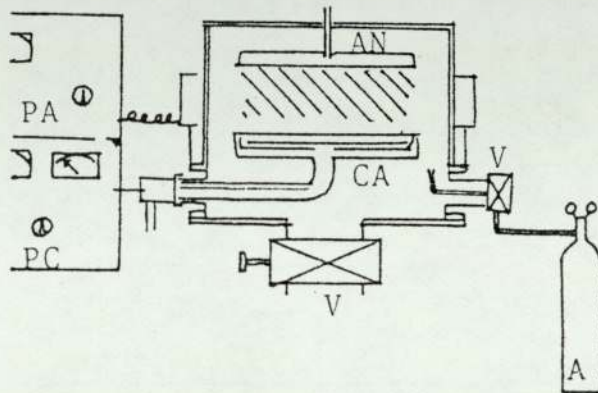
2.3 Vapour deposition. In vapour deposition a volatile compound of the coating material is reduced or decomposed on a heated substrate at a temperature below the melting point of the coating material and the substrate. The deposition parameters include the

temperature of the substrate (21). . The possible formation of an oxide film on the substrate surface, the concentration of the volatile compound in the coating chamber, the total gas pressure and the film rate of the gas in the open tube process, are all factors which influence the properties of the film produced.

2.4 Sputtering. The observation that material can be sputtered from the cathode in the electrical gas discharge was first made by Grove (22) in 1852 followed by Plucker (23) in 1858. The phenomenon is based on ions striking the cathode, having been created by the ionisation of the gas in an electrical discharge. Sputtering has always been an attractive means for film deposition due to the simplicity of the equipment as shown in Figure 2.1. The planar anode substrate is made the earth while the sputtering voltage is applied to the planar cathode. The whole arrangement is evacuated in a vessel or chamber, and deposition commences at a threshold valve after admitting sputtering gas to the chamber. There are many other types of sputtering systems employed choice of which depends on the desired properties of the films (27-32).

Since sputtering can be performed at relatively high pressures of up to several torr or more, there can be impurities in the sputtering atmosphere. Therefore modern sputtering systems employ high vacuum technology in order to obtain low residual gas pressures (32) and sputtering gases of high purity are used. Whener, et. al. (24, 25) have shown that the momentum transfer between impinging ions and the target atoms must be the controlling mechanism. The sputtering threshold atom ejection pattern and the related factors have been

FIGURE 2.1



A Sputtering Unit

- A = Argon gas
- V = vacuum valve
- AN = Anode
- CA = Cathode
- PC = Power supply for cathode
- PA = Power supply for anode

discussed in detail elsewhere (26-32). Since the sputtering rate is proportional to the number of ions impinging on the cathode, i.e. the current density, most films are deposited at pressures in the glow discharge region. Collisions between gas atoms and the sputtered atoms cause back reflection of the sputtered material, forming multi - charged ions and gas occlusion in the film (26). Other parameters which affect the sputtering rates are:

(i) gas temperature; (ii) accelerating voltage which affects the momentum and kinetic energy of the impinging ions; (iii) composition and crystallographic orientation of the cathode; (iv) electrode spacing; (v) cathode surface contamination; (vi) cathode shape and shielding (27).

The temperature of anode and cathode influence the structure of the deposited film and therefore cooling is often utilised in sputtering systems. When volatile compounds are formed through reactions at the cathode, the process is termed 'chemical sputtering' and if the atmosphere contains gases which react with the sputtered films, the process is known as 'reactive sputtering'. In both of these processes the reaction could occur either (a) at the cathode or (b) during transport of the sputtered atoms to the cathode, or (c) during deposition (27).

The process of sputter removal (74) of atoms from surfaces has become a very important adjunct to the technological analysis of surfaces. Argon ions in the energy range 500-3000eV are used, although on occasions, xenon is preferred (75). Compositional depth profiling

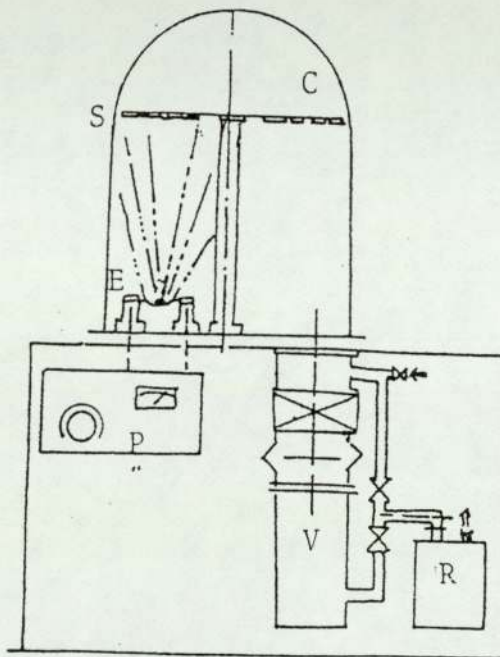
(76) has become a technique for the analysis of surface layers in microelectronics (77, 78), corrosion science (79), evaluating basic parameters such as diffusion constants (80, 81) and the localisation of segregation at grain boundaries (82).

A review of the literature (77, 83) covers the sputtering of a wide range of metals. Whener (86), his co-workers (88, 89) and Oechsner (87) include the data of Weijsenfeld (90), Southern (91) et. al. and Keywell (92) for sputtering 36 metals including gold. Whener (86) has shown the sputtering yield for gold is 2-3 atoms per argon ion.

M.P. Seah (74) has compared the data of Whener (86, 88, 89), and Oechsner (87) with the theoretical predictions of Sigmund (4) and found fit within 20% scatter.

2.5 Evaporation. Film deposition by evaporation of material is a simpler process than sputtering (18). The necessary equipment is shown in Figure 2.2. The first evaporation was carried out by Nahwold (36) in 1887 followed by Kundt (37) in 1888. The earliest evaporation of metal films in vacuo was carried out in 1912 (38). The major difficulties are contamination of the evaporant and incorporation of gas from the residual gas atmosphere. The absorption of gas into the substrate surface depends on the degree of vacuum, the film composition and the nature and temperature of the substrate. For a given gas composition, surface temperature and film composition, the amount of gas occluded in the film will be proportional to the relative

FIGURE 2.2



A thermal evaporation unit

- P = Power supply
- V = vacuum pump
- R = rotary pump
- E = evaporation electrodes
- S = substrate
- C = evacuation chamber

partial pressures (40). The substrate surface, its roughness, composition and crystalline state are of primary importance in the formation of the film; surface mobility also influences the number of collisions among atoms on the surface of the substrate, since the nuclei for the formation of crystallites can result from the collisions.

The rate of deposition and substrate temperature are important in determining the film structure. The binding forces between the atoms of the film and those of the surface determine the mode of growth (continuous, island formation, etc.). Impurities or contamination can alter the growth conditions completely (40).

Evaporation is generally performed at low pressures such that the mean free path of the residual gas molecules is much longer than the distance between the source and the substrate. At such pressures the probability of collisions between the residual gas molecules and the film atoms is small, and the atoms will essentially travel in the straight lines. The evaporation characteristics of the source and the thickness distribution of the film are therefore calculable assuming impurities are avoided.

Chapter 3

Optical properties - theory and measurement

3.1 Introduction

In this chapter theory of colour, the meaning of colour and its measurement are discussed. The theory is outlined of techniques used to measure the thickness and optical properties of coatings in general and of gold coatings in particular. The chapter is arranged in the following sections:

1. The nature of light.
2. The nature of colour.
3. The specification of colour.
4. Basic principles of the measurement of colour.
5. The influence of the atomic structure on the colour of metals.
6. The formation and growth of coatings.
7. The principle of scanning electron microscopy.

3.2 The nature of light

The optical studies of the thin coatings on a metal is a branch of physics. The earliest work on this was reported ninety years ago. Drude (41) examined the influence of a thin superficial film produced on a metal on the measured optical quantities. Clulow (11) states that the colour and light are inseparable and that in order to understand colour we must first understand the nature of light.

Light is a form of electro-magnetic energy. It travels and is transmitted through space. White light consists of light of various wavelengths (λ) from 400 to 700nm (Figure 3.1). The diagram below (Figure 3.2) illustrates the meaning of the terms wavelength and amplitude.

Figure 3.2

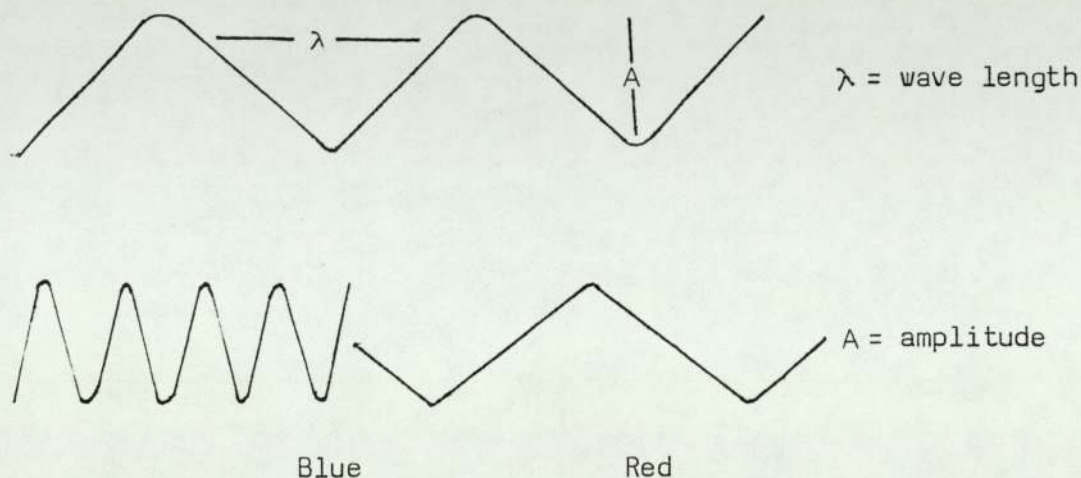
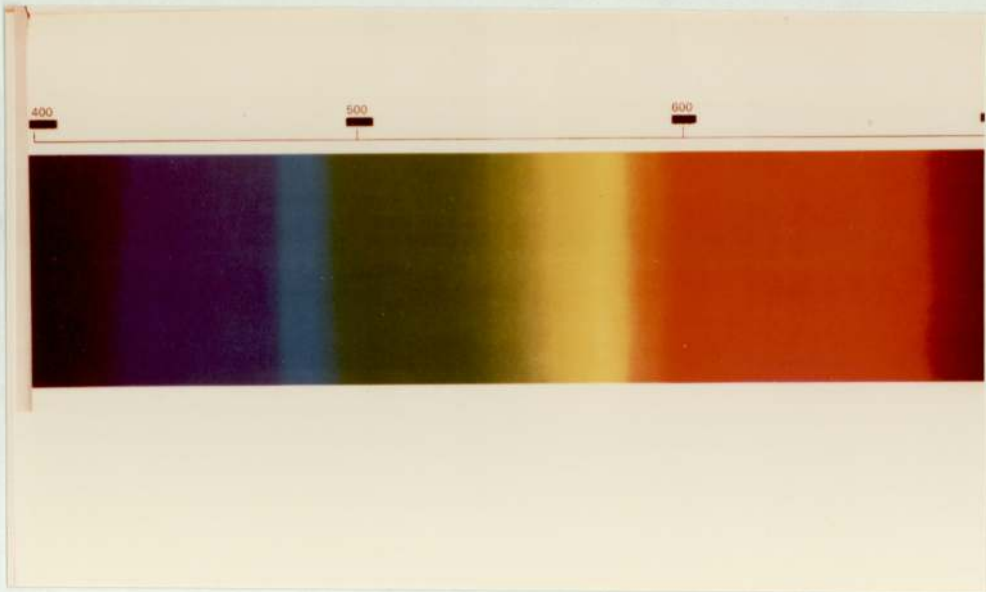


Illustration of the terms wavelength and amplitude

Light stimulates the nerves of the eye to produce the sensation of light. Sunlight contains all the visible radiations and is known as white light. Light rays are not coloured themselves, but when the light of different wavelengths strikes the eye, the sensation of different colours is produced in the brain. An object producing a white 'colour sensation' may be a primary light source or a secondary light source, i.e. a 'white' reflecting surface (10).

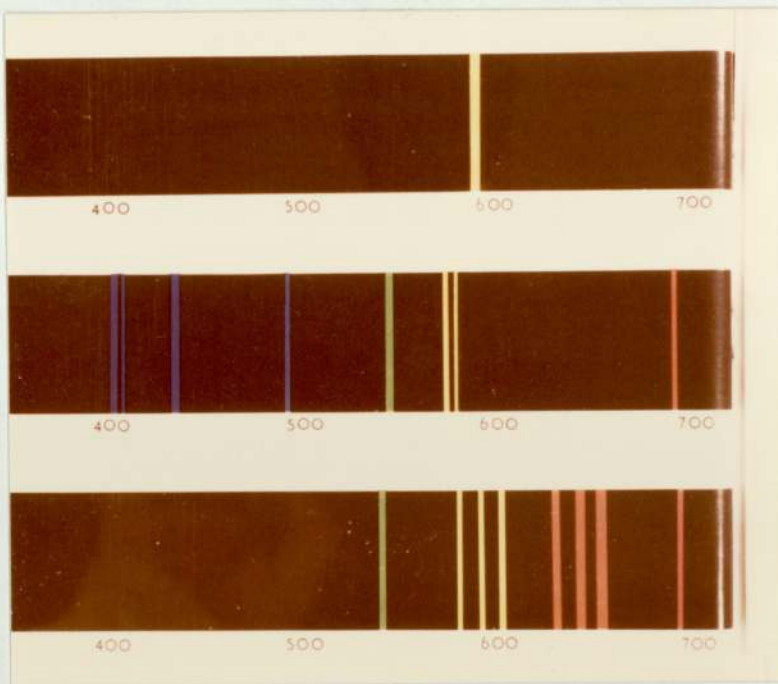
3.21 The nature of colour: The term colour is used by people in different ways. For a chemist it is a generic name for dyes, pigments

Figure 3.3



Dispersion of the white light

Figure 3.1



Composition of wavelength in white light

and similar materials. A physiologist and a psychologist often use this term in a different sense since they are interested primarily in the nature of the visual process, the consciousness of a human observer and colour sensation. The physicist measures and concentrates on the optical properties of the material. The definition of a colour therefore requires a comprehensive physical and objective specification.

3.3 The spectrophotometric specification of colour

A glass prism splits white light into its constituent parts. If the emergent rays are projected on to a screen a visible spectrum of the constituent wavelengths is seen as shown in Figure 3.3. Seven major divisions are recognised as seven colours from violet to red. If, for example, a green object is put under violet illumination, then most of the illuminant light is absorbed and a very small quantity 1% will be reflected back. This amount of light can be accurately measured with an instrument known as spectrophotometer. The reflectance or absorbance of a surface is an inherent property. If the film on the surface is thin (a thickness of a few monolayers of atoms of material), then the optical properties of the film will be dominated by the properties of the substrate surface. The reflection characteristics of the surface or coating do not depend upon the intensity of the incident beam to which it is exposed, but on physical properties of the surface layers which include part if the substrate of the coating is thin.

White magnesium oxide (MgO) reflects back almost all the light in the

visible spectrum. If magnesium oxide is examined in the spectrophotometer and intensity of reflected light is plotted against wavelength, a horizontal line across the whole spectrum at the top of the spectrophotometer chart. On the other hand, a black object absorbs all the light and shows a horizontal line at the bottom of the chart. In this way the colour interpretation or colour mixtures can be standardised. This of course formulates the language of the colour and the stimulation of the colours can be set under any specified conditions.

3.4 Basic principles of the measurement of colour

The colour of the material can be seen on illuminating the material. If the material is transparent we see its colour by the colour of the light transmitted through it. Other properties such as reflection, absorption and refraction are also important in the complete specification of the colour of the material.

3.4.1 The function of reflectivity and absorbance

It is a common fact that a 'perfect' white surface reflects most of the incident light, while a 'perfect' black surface absorbs most of the light incidents upon it. Similarly, transparent colourless materials transmit a high proportion of the incident light. Substances which absorb light from one part of the spectrum and reflect the remainder are said to be coloured. No coloured material exists which reflects light of one wavelength only, but a material of say

red absorbs most of the violet, green and yellow light and reflects mainly red light.

In general, a coloured object reflects a mixture of wavelengths consisting of light of its apparent colour together with the light of the colours adjacent in the spectrum and small quantities of other wavelengths. Reflectivity and absorbance charts are used to characterise the colour of a material.

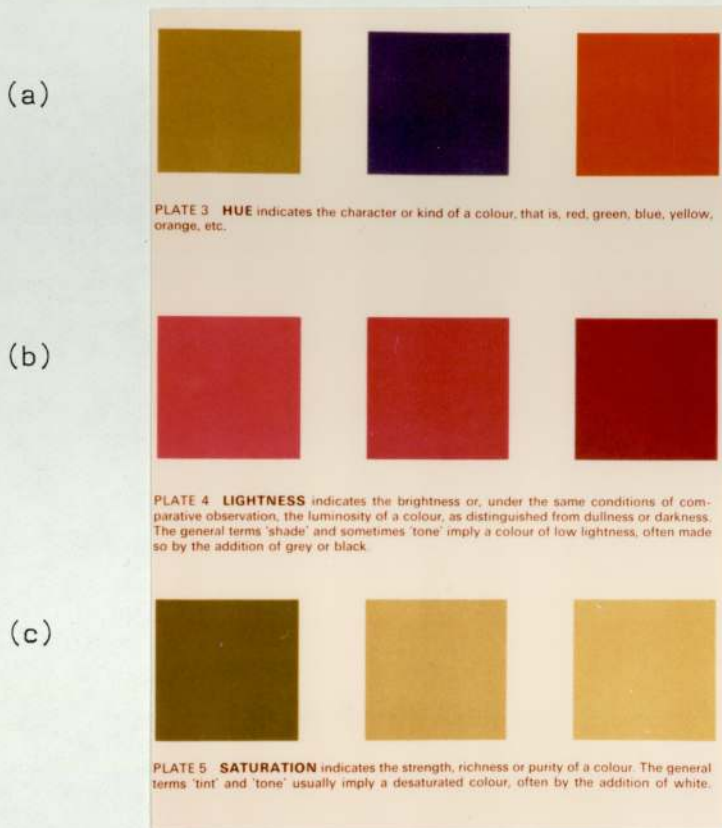
3.4.2 The measurement of colour

Colours and their specification have been standardised by the British Standards Institution (42) and the Commission International de l'Eclairage (CIE) (43). The terms include hue, saturation, lightness and dominant wavelength which are defined as follows:-

Hue This indicates the character or kind of colour, that is, whether it appears green, blue, yellow, orange or red as shown in Figure 3.4(a) (11). It is the property of the material which allows the eye to distinguish different parts of the spectrum.

Lightness This denotes brightness, brilliance or intensity under the same conditions of comparative observation. It is the property of the colour which distinguishes the dullness or darkness as illustrated in Figure 3.4(b) (11).

Figure 3.4



Saturation This indicates the strength, richness or purity of a colour and denotes the extent to which hue is diluted with white colour and appears whiter or greyer as the saturation is reduced as shown in Figure 3.4(c) (11).

Luminosity This is the corresponding term to lightness usually used when referring to light sources but it may also be used for the light reflected back from an object.

The dominant wavelength

White light is composed of seven colours and each colour consists of a band of wavelengths of which there is a dominant wavelength. In the measurement of colour, the dominant wavelength is defined as in Section 3.4.5.4.

There are various methods used to determine the colour of a substance. These can be summarised as follows:

1. Matching methods.
2. Colorimetry.
3. The Commission Internationale de l'Eclairage system (C.I.E. system).

3.4.3 Matching methods

Comparison with standard charts or cards is the simplest method to

specify colour. Many systems based on colour matching have been developed including NU-hue, the colorizer and the Plochere colour systems. Atlases have been produced and a series of charts have been developed including the Ostwald (96) and Munsell systems (97).

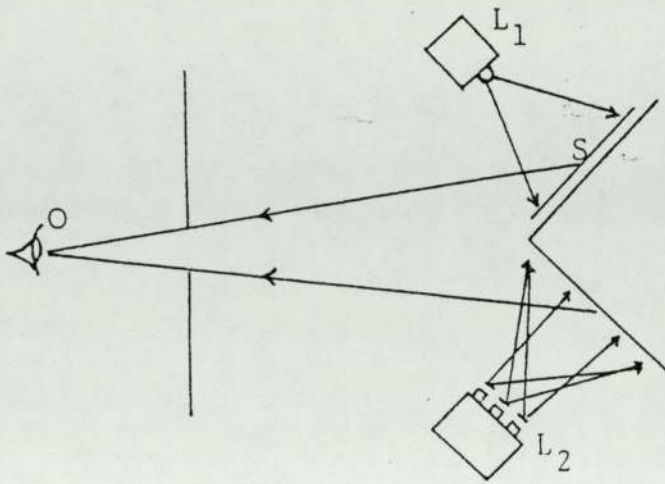
3.4.4 Colorimetry

The principle of colorimetry is based on matching the colour by the correct mixture of three selected radiations, namely, red, green and blue. There are many colorimeters used to match colour. They include additive colorimeters, subtractive colorimeters and photoelectric spectrophotometers.

3.4.4.1 Additive colorimeters

The illustration in Figure 3.5 outlines the basic principle of the additive colorimeter. The instrument allows the three light sources (red, blue and green) to be selected to match the colour under test. The two screens are placed at 90° to each other. The specimen under test is illuminated by a standard white source L_1 while the other screen illuminated by the three primary light beams (L_2). The light beams are adjusted until a match is obtained by the observer's eye (O). The controls of the instrument indicate the relative intensities of the three primary light beams required, and these are termed the tristimulus values. The construction of subtractive colorimeters is similar to that of additive colorimeters but with some differences of application.

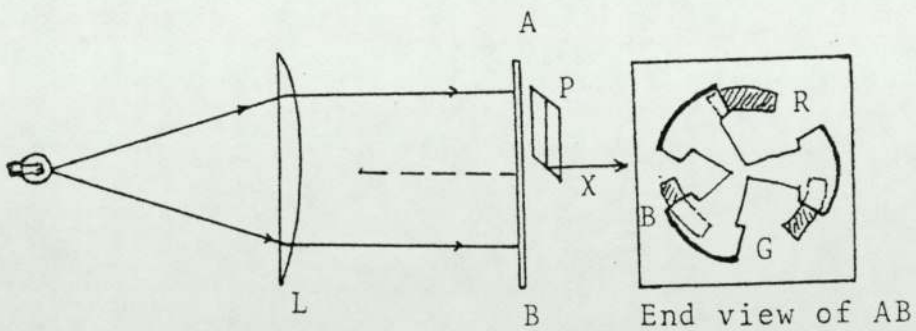
FIGURE 3.5



Additive Colorimeter

- L_1 = Standard white lamp
- L_2 = Standard lamp with three primary filters
- S = Specimen under test

FIGURE 3.6



Visual colorimeter

- R = Red
- G = Green
- B = Blue
- L = Lens
- AB = Adjustable Colour filter
- P = Revolving prism

3.4.4.2 Visual Colorimeters .

The diagram in Figure 3.6 illustrates the basic principle of the visual additive colorimeter. After being collimated by a lens L, light is passed through three adjustable colour filters (AB). The emerging rays are then passed through a revolving prism which combines them to give the appropriate colour. The radial shutters are adjusted by the operator until the test colour is matched. The results tend to vary from observer to observer.

3.4.4.3 Photoelectric colorimeters .

Subjective variation from observer to observer has been overcome by using a photo-electric cell instead of the human eye. The cell is calibrated against a white standard such as magnesium oxide. The modified version of the photoelectric colorimeter in which light is transmitted via several fibre optics to a photo-electric photomultiplier (94) is known as a fibre optic colorimeter.

3.4.4.4 Photoelectric spectrophotometers

The basic principle of photoelectric spectrophotometers is illustrated in Figure 3.7. White light from L_1 is collimated through Lens L_2 and is then split into its constituent parts by the prism P. A moveable screen (M) allows the monochromatic light to impinge onto the specimen (S) after passing through the lens L_2 . The reflected rays from the specimen are allowed to fall onto a photocell (C) which transforms the light energy into an electrical

signal. In this way a graph is obtained of the variation either reflectivity or absorbance with wavelength over the visible spectrum. Measurements were made in this way in the present study.

3.4.5 Graphical representation of colour specification

The absorbance or reflection/transmittance values of a substance at each wavelength can be used to specify the colour of the substance (the spectrophotometric specification). There are many methods to evaluate a stimulus that an eye accepts as equivalent under certain standardised conditions. To represent hue (kind of colour) or visual efficiency, dominant wavelength and purity of a colour, a method was introduced in 1931 known as the C.I.E. system. It involved defining the standard illuminants, the colour triangle, the spectral locus and the CIE chromaticity chart.

3.4.5.1 The standard illuminants

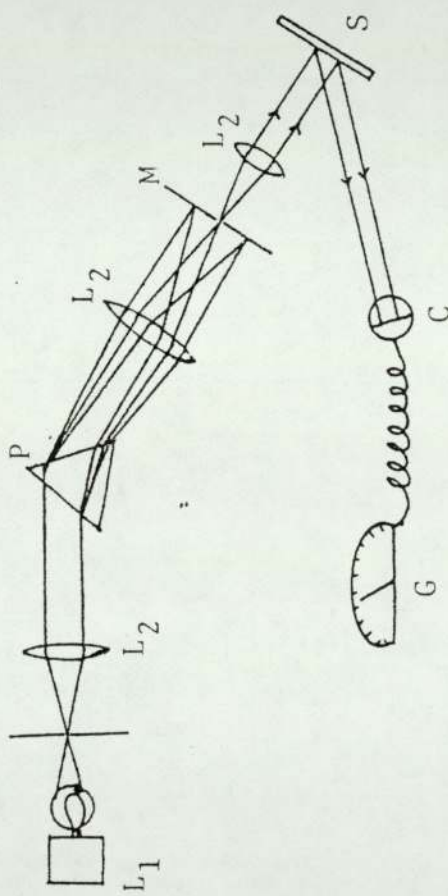
For the perception of colour, the character of the incident light is very important. Three standard illuminants were adopted by the CIE in 1931. They consist of SA (tungsten lamp), SB (sunlight) and SC (overcast sky) and are defined for the wavelength range 400-700nm. For the range 300-830nm which includes ultra-violet and infra-red D6500, D5500 and D7500 illuminants are used. All the standard illuminants are detailed in Appendix 1.

3.4.5.2 The colour triangle

The CIE gives numerical values which indicate the amount of redness,

FIGURE 3.7

Basic principle of the spectrophotometer



Spectrophotometer

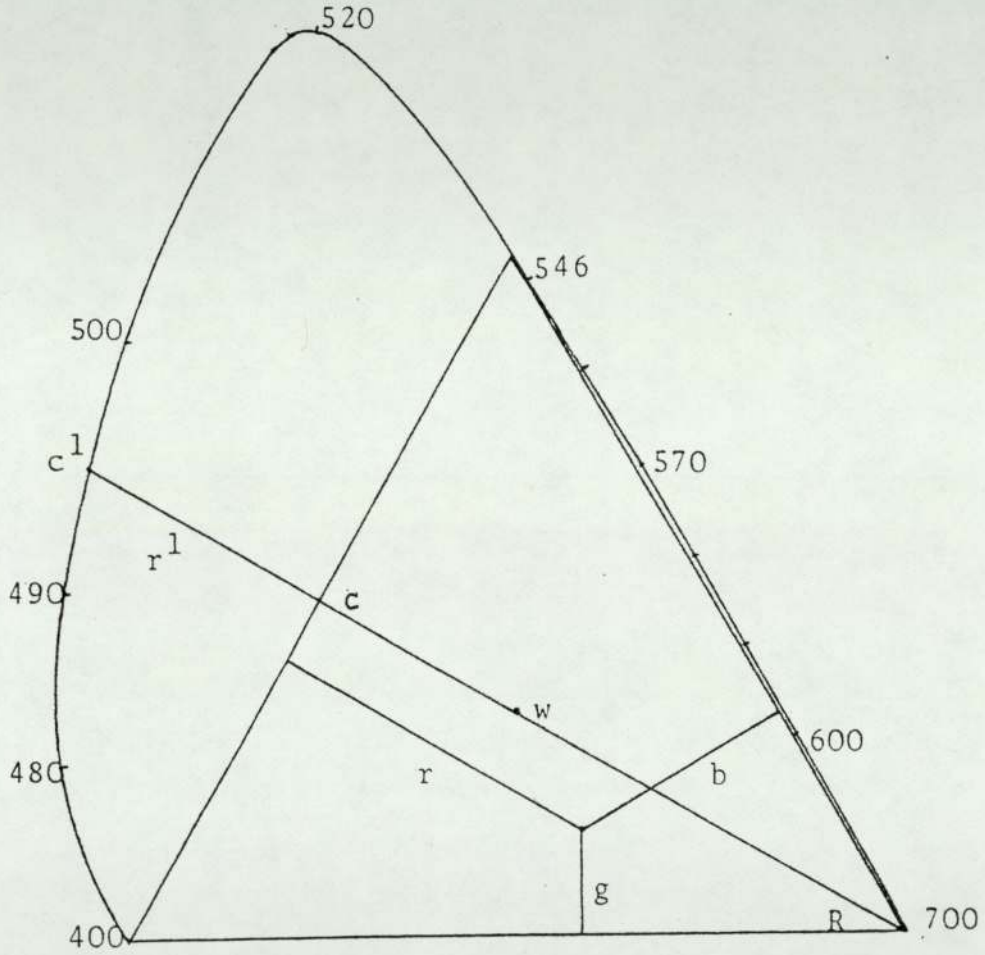
- L₁ = Lamp
- L₂ = Lenses
- P = Prism
- C = Photocell
- S = Specimen
- G = Galvanometer
- M = Moveable screen

greenness and blueness in a colour and these values can be plotted on to a colour triangle in order to indicate the colour. The triangle may be constructed by placing at each apex of an equilateral triangle a spectral primary light (red, green and blue) $\triangle BGR$ Figure 3.8. If the lamps are placed at the apexes such that their intensities are zero to each other, the centre of the triangle shows a white point (W). By dropping a perpendicular from each primary (R) to the opposite side (C^1), the colour directly opposite to the primary will be the complementary colour. Such a triangle BGR is called the colour triangle and is shown in the Figure 3.9.

3.4.5.3 The spectral locus

It has been noticed that there are some colours for which a match cannot be obtained within the actual triangle. These are colours of the spectrum which are more saturated than any of the saturated mixtures of any two of the primaries. These spectral colours can only be matched by first mixing some of the third primary with the spectral colour and therefore the spectral colours must be outside the triangle. For example to match the spectral cyan (495nm), some red is required to add to the blue and green primaries. The amount of red added corresponds to $c-C^1$ in Figure 3.8. The colour equation is now $g+b-r=1$. The spectral locus can be plotted in a similar way for other spectral colours, giving a curve shape called spectral locus as shown in Figure 3.9. The base of the spectral locus is straight, because purple or magentas are not spectral colours.

FIGURE 3.8



The colour triangle and spectral locus

3.4.5.4 The dominant wavelength

Consider a colour M (Figure 3.9) in the spectral locus. If a projection line is drawn through the white point W to the spectral locus, the point P where this line cuts the spectral locus is called dominant wavelength. For a colour N in the magenta segment the dominant wavelength is defined by its complementary wavelength by drawing a line from N through W to the spectral locus (Q).

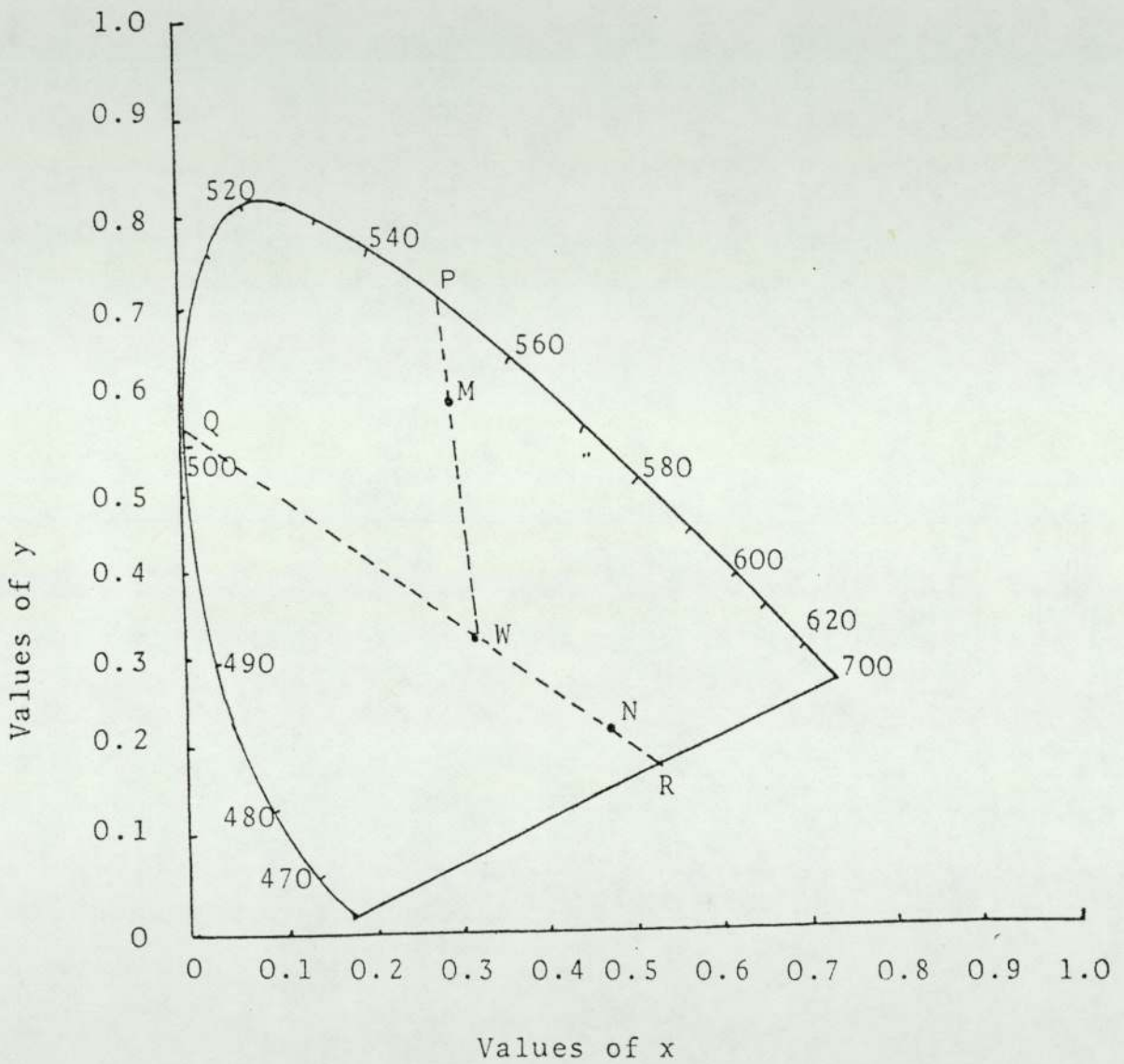
3.4.5.5 The chromaticity chart/diagram

Since the postulated three primaries with a greater degree of saturation do not exist physically, they are termed as stimuli and designated x, y and z. These three values are the arbitrary values such that they surround or superimpose on a right angled triangle with apexes accommodating the spectral locus. The chromaticity co-ordinates may then be plotted on ordinary rectilinear graph paper as shown in Figure 3.10. The values of x and y can be plotted while z is implicit, because the sum of x, y and z is one. Any visible colour can be specified within the spectral locus using xyz stimuli and such a representation on a graph paper is called the CIE chromaticity chart.

3.4.5.6 The spectrophotometer readings

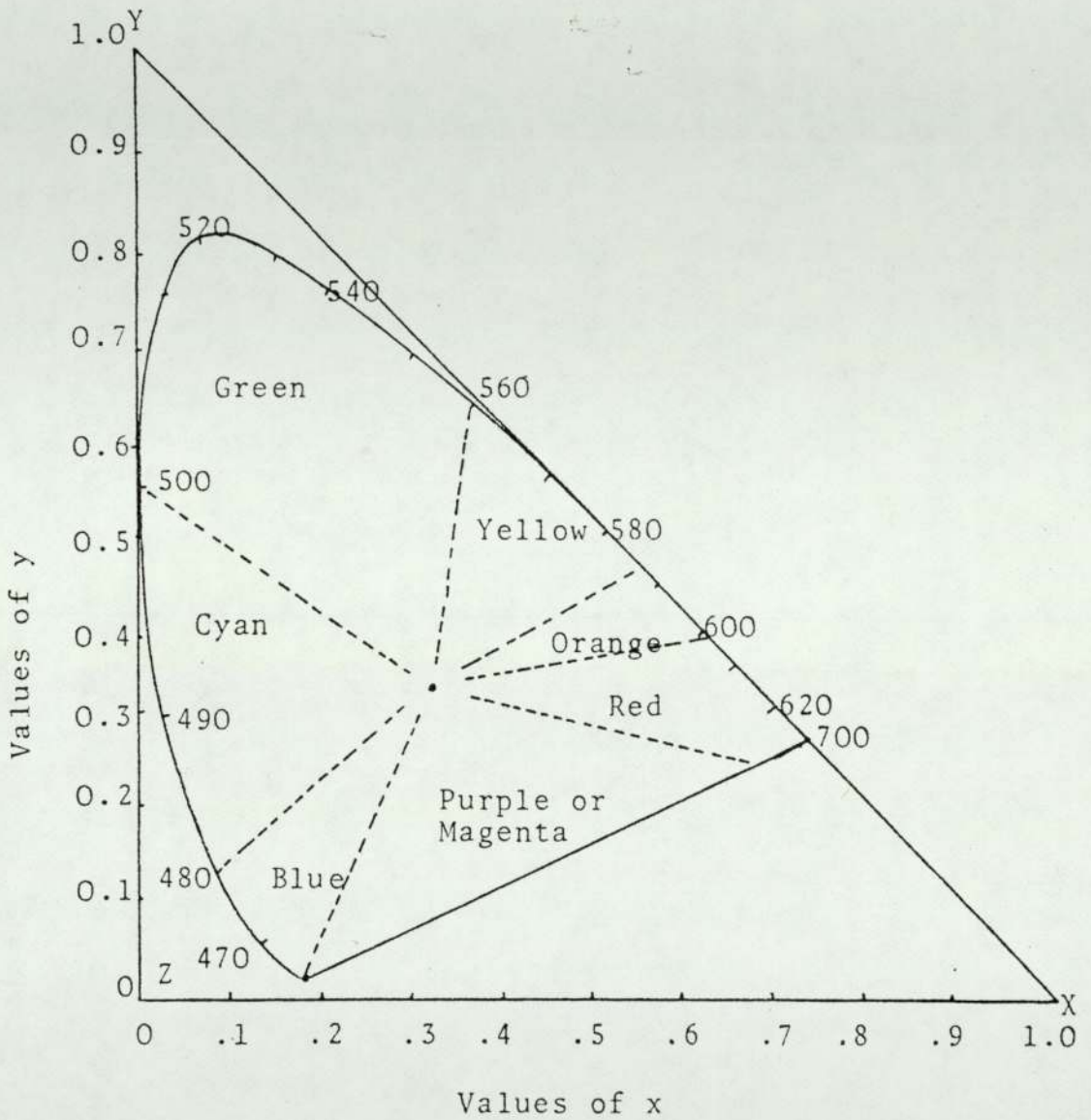
The measurements from a spectrophotometer given reflectance values over a range of wavelengths of incident light. To specify the colour

FIGURE 3.9



Definition of dominant wavelength and saturation

FIGURE 3.10



The colour triangle and spectral locus superimposed on a right angled triangle

it is necessary to convert the values obtained into CIE chromaticity co-ordinates. Tables of distribution co-efficients by standard observers are used by measuring the amounts of X, Y and Z stimuli corresponding to each wavelength of the spectrum under different conditions of illumination. The tristimulus values for the spectral wavelength are designated X, Y and Z. The distribution co-efficient for X is multiplied by the reflectance at each wavelength and the sum of these values obtained. Similar calculations are carried out for the Y and Z values obtained. These totals then express the redness (X), the greenness (Y) and the blueness (Z) of the sample. The redness, greenness and blueness are expressed as proportions of the total red, green and blue to give numbers between 0 and 1 called the chromaticity co-efficients such that

$$x + y + z = 1$$

By convention the y total indicates luminosity. The colour position may now be plotted on the CIE chart and the dominant wavelength and saturation can be calculated.

A Fortran computer programme using the ICL 1900 computer hardware at Aston University was used. The software (programme) is given in Appendix 2. The tristimulus values of distribution co-efficient under equi-energy conditions and under SA for a gap of 5nm were kept in two permanent files. The list of one file is given in Appendix 3.

3.5 The influence of atomic structure on the colour of metals

In the present study thin coatings of gold were sputtered on different substrate materials and the optical properties determined. Saeger and Rodies (7) have related the optical properties of gold and its alloys to the influence of incident light on the free electron distribution in gold. They explained that the gold colour is governed by the dependance of its reflectivity upon the incidence of light. A material of high reflectivity for the low energy end of the visible spectrum (red and yellow light) than for other parts of the spectrum will have a red or yellow colour.

Thus the yellow colour of gold is caused by the pronounced step in the reflectivity curve at an energy of incident light of approximately $3.7 \times 10^{-19} \text{J}$ (2.3ev) (7). Absorption processes in metals are due to the band transitions of electrons from the conduction band to energetically higher bands or the transitions from lower bands to energy states of the conduction band situated above Fermi level. Osborne, Fletcher and Miller(1974) and Fong et.al.in 1975 carried out the complex band calculations for the pure metals, a number of inter-metallic compounds, and a few dilute alloys. In the case of gold the conditions for an intense absorption process are met at the energy $3.7 \times 10^{-19} \text{J}$ from the d band to unoccupied states in the conduction band.

3.6 The formation and growth of gold coatings

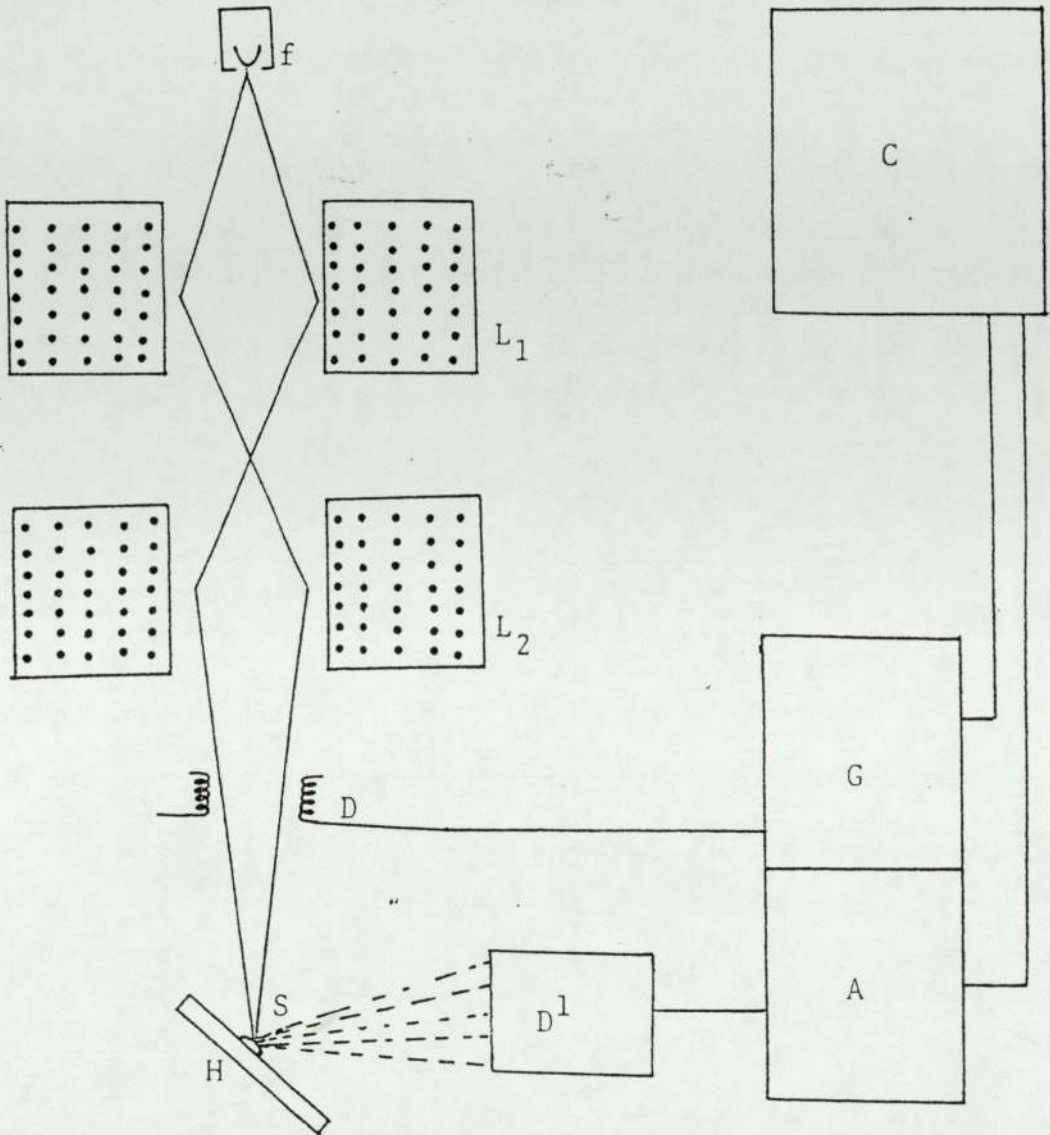
Vook (102) has shown that the mode of growth for gold on copper is the

formation of small islands, which grow to about 4-5 monolayers thick. These islands then widen by thin extensions, which are estimated to be about 1 monolayer thick and tend to thicken as more deposition takes place. At the thickness of \sim 0.6 to 1.1nm the coating is said to be continuous. In the present study the coatings were deposited on the white metals nickel, aluminium and stainless steel and the influence of the substrate on the similar gold coatings was studied. The structure of the materials in the thin coatings depends on so many factors that only rather broad generalisations are possible. In the case of thermal evaporation and sputtering these factors which are related to the coating methods are discussed in Chapter 2.

3.7 The principle of scanning electron microscopy (SEM)

The principle of scanning electron microscopy is illustrated in Figure 3.11. The basis of the principle is analogous to an optical microscope with a fine beam of electrons replacing the light beam. Electrons are very easily absorbed so it is necessary for the electron microscope to operate in a system evacuated to a pressure of less than 10^{-4} torr. Electromagnetic lenses L_1 and L_2 focus the beam of electrons generated from the filament (f). Deflector coil D is used to scan the beam across the surface in a raster. The magnetic lens system is analogous to that in an optical microscope, but the focal length of the lenses is controlled by regulating the current through the coils of the lenses, and magnified images of up to 100,000 times may be obtained on the viewing screen.

FIGURE 3.11



The basic principle of scanning electron microscopy (S.E.M.)

- f = Electron generating source
- L₁, L₂ = Condensing lenses (electromagnets)
- D = Deflecting coil
- S = Specimen
- H = Specimen holder
- D¹ = Signal detector
- A = Amplifier
- G = Scan generator
- C = Cathode ray tube

The wave-like character of electrons was most clearly demonstrated by de Broglie's experiments showing the diffraction of electrons by crystals. The inter-relation can be seen by equating the well known Einstein equation for energy and mass.

$$E = mc^2 \text{ ----- } 3-1$$

where E = energy

m = mass

c = speed of light

According to Planck, energy in the form of radiation can only be emitted in units or quanta of magnitude:

$$E = h\nu \text{ ----- } 3-2$$

where ν = frequency of the radiation and

h = Planck's constant of action.

$$\text{or } h\nu = mc^2$$

$$\text{Also } c = \nu\lambda \text{ ----- } 3-3$$

where λ = wavelength of light

$$\text{Therefore } m = \frac{h\nu}{c^2} = \frac{h}{\lambda c}$$

$$\lambda = \frac{h}{mc}$$

The wavelength of the electrons in the electron microscope is dependent upon the accelerating voltage (V) applied to the electron gun, and is given approximately by $\lambda = \sqrt{\frac{150}{V}} \times 10^{-10} \text{ m} \text{ --- } 3.4.$

Normal operating voltages are of the order 100kv, so that λ may be about 3.5×10^{-12} m.

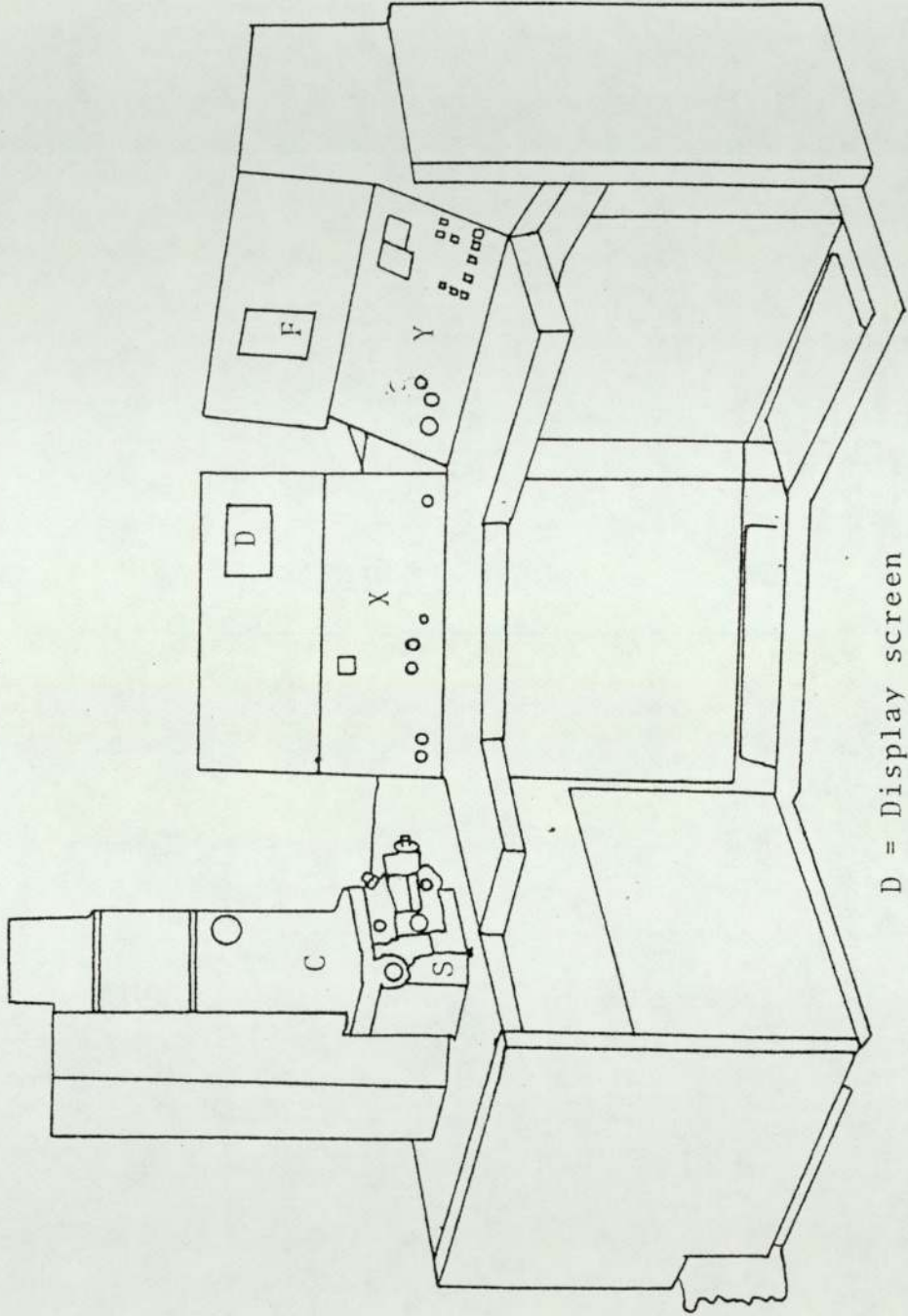
In order to form an image in any optical system, the wavelength has to be small compared to the size of the features which is desired to distinguish or to resolve. Therefore the optical microscopes have limitations while the magnification and the resolution of the electron microscope is very much dependent of accelerating voltage and the functions of the microscope. A scanning electron microscope obtains topographic information directly from a metal specimen. An electron beam of $\sim 2-3 \times 10^{-8}$ m diameter scans a small area of the specimen (s) in the same way that a television screen is scanned and the electrons scattered (secondary electrons) are collected by the detector (D) and the signal from this detector is used to modulate the brightness of a beam scanning the fluorescent screen of a cathode ray tube (C) in synchronism with the electron beam scanning the specimen. A television 'picture' of the small area of the surface is thus produced.

The scanning electron microscope can be used for examining metal fracture surfaces at high magnifications (i.e. up to 50,000 times), and also with high depth of field. It is also used to study wear processes on abraded surfaces, as well as the early stages of oxidation and film formation of the metallic and non-metallic surface.

In the present study, a Cambridge Stereoscan No. 150 (Figure 3.12) has been used to determine the thickness of the coatings and to check the reproducibility of the tungsten microindenters and the micro-

FIGURE 3.12

Cambridge Stereoscan 150 electron microscope



- D = Display screen
- X, Y = Controls
- C = Column containing electron beam gun and electromagnetic lenses
- S = Specimen chamber
- F = Camera fittings

indentations made on aluminium and brass samples. Appendix 4 includes the basic features of the scanning electron microscope used in the present work.

Chapter 4

Results and Techniques

4.1 Introduction

The experimental procedures, techniques and results are described in this chapter. To determine the influence of the substrate materials on thin gold coatings, the following experimental research programme was carried out.

(1) The working conditions and the operation parameters of an existing automatic coating unit (Appendix 5), using both the evaporation and the sputtering options, were tested and checked.

(2) A semi-circular disc with the radial sections (Figure 4.9) was designed and used in attempt to achieve exact and systematic changes in the thickness of the coating.

(3) The thicknesses of the gold coatings were also examined and determined using scanning electron microscopy, resistance measurement and gravimetric methods. Calculated and observed values were compared.

(4) A spectrophotometric method of measuring the colour of gold coatings on various substrate materials was tested and used.

The influence of the substrate on thin gold coatings was observed and discussed. A computer programme (Appendix 2) was designed and used to calculate the colour co-ordinates and to draw the reflectivity curves obtained from gold coatings on different substrate materials.

4.2 Specimen preparation

Most of the work was done on nickel supplied as discs cut from $1\frac{1}{4}$ " diameter bar. Stainless steel and aluminium sheets were polished and pre-treated from which specimen discs were punched. The nickel discs were approximately 1.75mm in thickness and 32mm in diameter. Before coating the nickel discs, different pre-treatments were applied. These included:

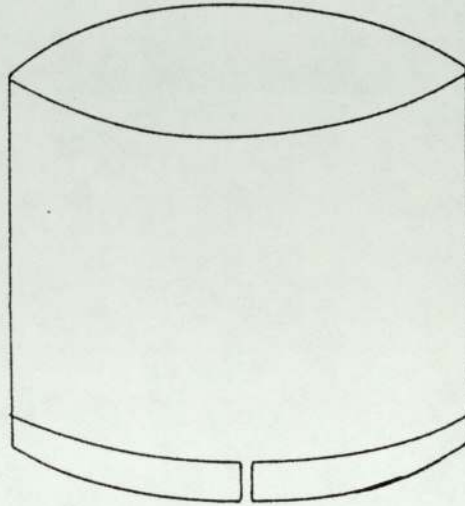
- (i) Abrading of the discs by normal metallographic techniques, i.e. use of silicon carbide papers of increasing fineness, turning through 90° on changing grade, both on paper supported on glass plates and on rotating wheels. During abrading water was used as lubricant and coolant.
- (ii) Discs were machine lapped down to 600 grit.
- (iii) Discs were polished on a diamond wheel down to either 1 to 6 μ diamond, utilising either a plastic mould holder (Figure 4.1) to hold the discs on the rotating wheel or they were hand held on the wheels. During all the pretreatment steps all the specimens were secured to a conductive Bakelite metallographic mount as shown in Figure 4.2. The pretreatment steps are mentioned in Appendix 6. Preliminary experiments also included the pretreatment of the substrates of the brass pallets.

4.3 Results of aluminium coatings

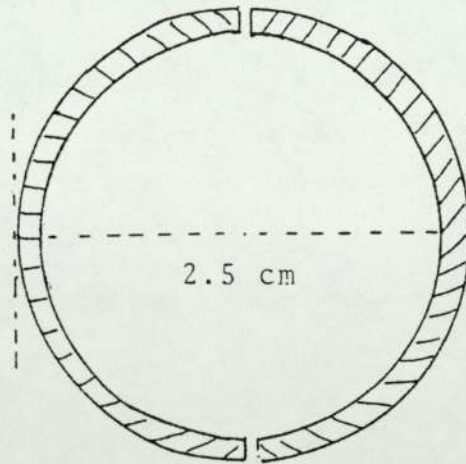
4.3.1 Experimental procedure

To determine the working conditions and the operating parameters of a

FIGURE 4.1

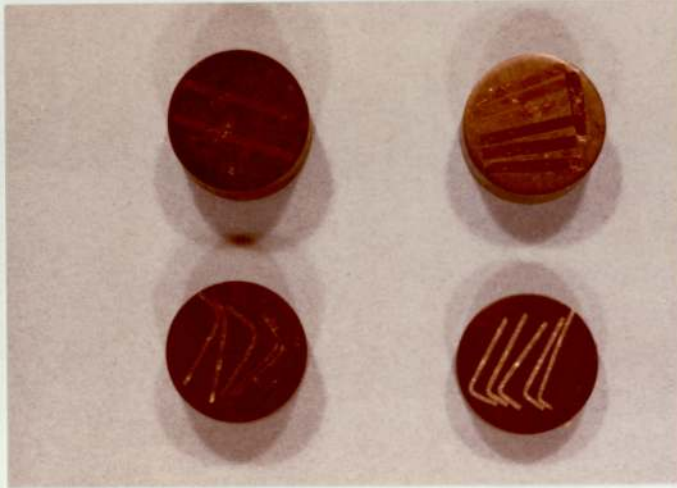


Plastic mould for lapping the discs



Cross-section of the holder mould

Figure 4.2



The coated specimen pieces mounted with
conducting Bakelite in cross sections.

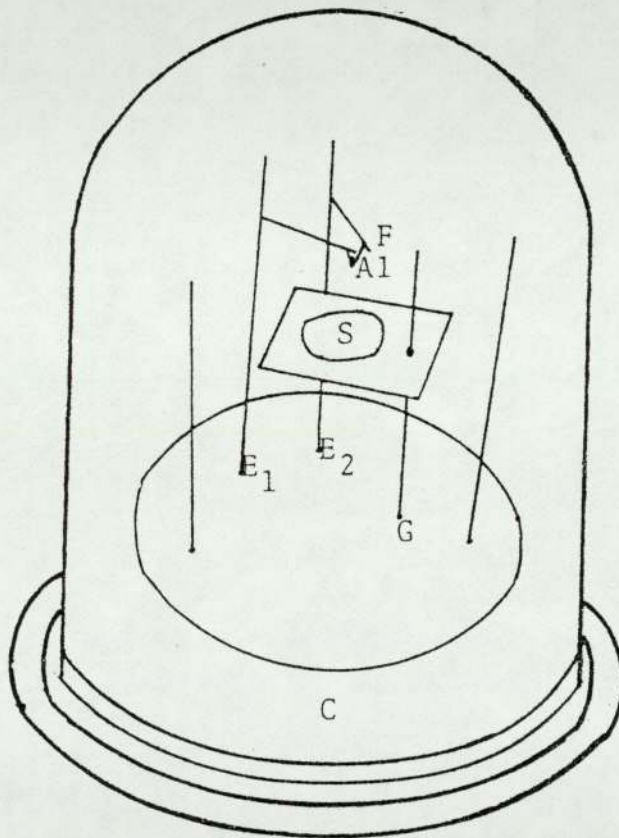
Nanotech vacuum coating unit brass specimens were coated with aluminium by thermal evaporation. The brass specimens were discs of 2.5cm diameter and 1mm thick machined from bar. Each disc was polished mechanically from 150 grade silicon carbide paper to 1 micron diamond grade sprayed cloth. A plastic mould holder was made and used when abrading the specimens. All pretreated specimens were kept in a desiccator before and after being coated. Brass and aluminium were chosen for the contrast in their colour and optical properties.

4.3.2 The evaporation

Equal lengths of aluminium wire, each weighing ~0.0001g were cut and each piece was mounted around the tungsten filament to be evaporated. The substrate was mounted beneath the filament for convenience at a distance of 10cm. Figure 4.3 illustrates the experimental set up. The system was subjected to vacuum of the order of 10^{-5} Torr and the filament was heated electrically. It caused the aluminium wire to melt and on further increasing the filament voltage up to 3kV evaporation started. Five brass specimens coated with aluminium were obtained (Series A) for a coating (evaporation) time of 30 seconds under the same conditions.

To test the operating parameters of the coating unit cross sections of the coatings were examined using the optical projection microscope and coating thickness measured. These specimens were prepared as mentioned in Appendix 6. Four of such metallographic specimens are shown in Figure 4.2.

FIGURE 4.3



Experimental set up for Aluminium coatings

- C = Evacuation chamber
- E_1 and E_2 = Electrode
- F and Al = Filament and Aluminium source material
- G = Ground potential

4.3.3 Optical microscopy of the coatings (projection microscope)

The metallographic specimens were examined using the projection microscope at 560 times magnification ($1\text{cm} = 17.86 \mu$). The thickness of the coatings at three positions are tabulated in Table 4.1.

The thickness at various positions show a wide variation; the values are higher in the middle than at the sides. The weighted mean of all five mean values has a standard deviation of 5%. These results show that the operating parameters of the coating unit for evaporation are quite adequate to achieve reasonable reproducibility.

4.3.4 Aluminium coatings produced by evaporation for different times

A few experiments were carried out to examine the relation between the coating thickness and the evaporation time for aluminium on polished brass and to determine the minimum thickness of aluminium to replace the colour of the brass substrate with that of aluminium.

These experiments involved the development of a mask used within the existing coating unit, which produced layers of coating of equal areas but different thicknesses. The thickness of each layer was proportional to the time it was exposed to evaporation.

Six brass discs of the similar size were polished as described previously and coated with aluminium under the same operating conditions.

Table 4.1

Specimen No.	Thicknesses at three positions μ			Mean μ	Weighted Mean
	Middle	Right	Left		
1	23.22	17.86	14.29	18.46	
2	21.43	19.65	17.86	19.65	19.4 \pm 0.9
3	25.00	17.86	14.29	19.05	\pm 5%
4	26.79	14.29	12.50	19.05	
5	25.00	21.43	16.07	20.83	

but for different evaporation times. Duplicate specimens were coated each time. A glass slide was also used each time and its weight was noted before and after the coating procedure. The coating weight was used to calculate its thickness using density area and mass relation (gravimetric method) in each case. The metallographic specimens of the coatings were prepared as detailed in Appendix 6 and their thicknesses were measured from cross sections examined using the projection microscope. The mean values of the thickness were calculated. Evaporation times ranged from the minimum practicable to those which ensured complete replacement of the colour of the brass substrate by the colour of aluminium. The results are tabulated in Table 4.2.

The mean values of the thicknesses for different evaporation time were plotted respectively and a curve (Figure 4.4) drawn. The curve indicates a decreasing trend in the deposition rate which is expected because of the loss of source material with time.

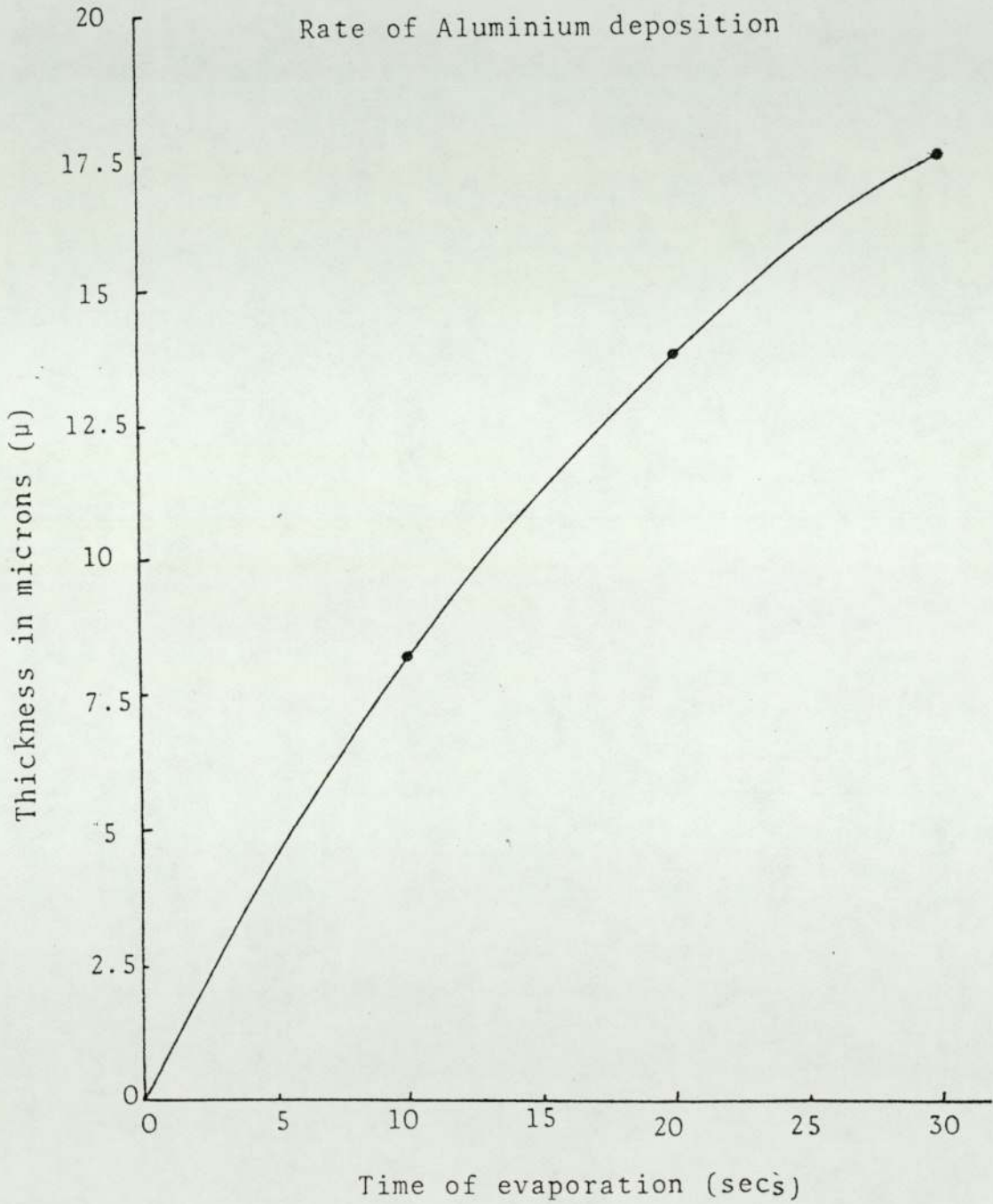
The table 4.2 shows a reproducibility of 91% to 96.4% on the coatings. It was noted previously of the 5% spread on the coating thickness on the same specimen which may be due to the unmeasurable changes in the operating parameters; therefore 4% error was due to the deposition rate making the total error \sim 64% on the reproducibility of the coatings.

Table 4.2(Series A)

S. No.	Specimen No.	Evaporation time (sec.)	Thickness in cm lcm = 17.86 μ m Specimen Specimen 1 2	Mean thickness μ	Thickness (μ m) weighted mean
1	3, 4	10	0.6	0.402 \pm 0.035	7.18 \pm 8.8%
			0.5		
			0.7		
			0.4		
			0.5		
			0.4		
			0.4		
2	5, 6	20	0.7	0.775 \pm 0.028	13.84 \pm 3.7%
			1.0		
			0.8		
			0.7		
			0.8		
			1.0		
			0.7		
3	7, 8	30	0.9	0.984 \pm 0.036	17.57 \pm 3.6%
			1.2		
			1.0		
			0.8		
			1.2		
			1.1		
			1.0		
	0.8				
	1.4				
	1.5				
	1.4				
	1.4				
	1.3				
	0.9				
	1.0				

FIGURE 4.4

Rate of Aluminium deposition



4.4 Thin gold coatings

The Nanotech vacuum coating unit used previously as a thermal evaporation unit may also be used as a sputtering unit for gold. Basically it is used to prepare specimens for examination in the electron microscope. Thin gold conducting coatings make materials, particularly non-conducting materials, ready for the examination. The use of this facility was extended to study the properties of gold coatings and particularly determination of the thickness of a gold coating needed to replace the colour of the substrate.

4.4.1 The sputtering electrode

For the study of thin gold coatings, a brass disc similar to the existing sputtering electrode in the Nanotech vacuum coating unit was made (Figure 4.5) and a gold film of several hundred angstrom units was deposited on to it. This sputtering electrode was used for coating the surfaces of aluminium, nickel, stainless steel and glass slide cover slips, the latter used for comparative purposes.

4.4.2 Deposition of gold coatings (series B)

Nickel was selected as a substrate material because of its whiteness and non-tarnishing properties. 2mm thick nickel discs were cut from a nickel rod of 3.2cm diameter (Figure 4.6). The discs were polished as described in Section 4.3.1. Usually a few monolayers of gold atoms on a non-conducting material are sufficient to conduct heat and electrons. To produce such coatings takes

Figure 4.5



Sputtering electrode coated with gold
deposits of a few thousand Angstrom units.

approximately 2 to 3 minutes in argon at 200 torr, when a current of 15 to 20 mA is passed through the sputtering electrode at a distance of approximately 1.5cm from the substrate. For such coatings the colour of the nickel substrate predominated over the gold colour. The experimental set-up of substrate and cathode is shown in Figure 4.7. Five of the polished nickel discs were coated alongside glass slide cover slips (Figure 4.6), ensuring sputtering conditions. Sputtering times were 3, 6, 7, 8 and 9 minutes timed by stopwatch.

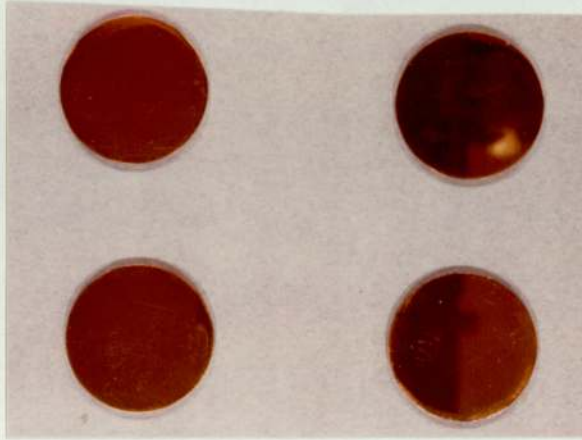
4.4.3 Thicknesses of the gold coatings

Determination of the thickness of the thin coatings is difficult and is more difficult the thinner the coating. G. Brown (94) used a gravimetric method to calculate the thickness of gold coatings about $1\mu\text{m}$ thick (Appendix 7(a)). F. Ogborn et. al. (13) measured thickness by examining the cross section of the specimen in a scanning electron microscope (SEM). SEM magnification is calibrated with a stage micrometer scale and measurement made on conventional photomicrographs. For improved accuracy, measurements are made on photographs of the SEM video waveform signal. Ogborn also discussed the uncertainty involved in their thickness measurements which was estimated to be about $0.06\mu\text{m}$ at a magnification of 10,000.

Coating thickness has also been calculated by determining the resistance of the coating to a passage of a known current. Since

Figure 4.6

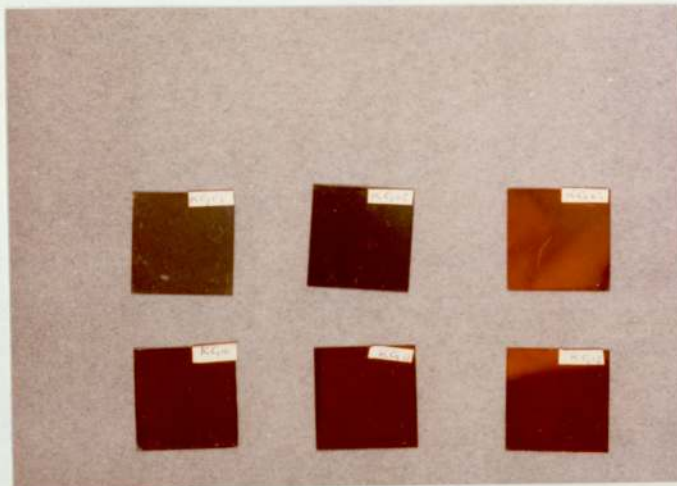
(A)



Four gold coated Nickel discs.

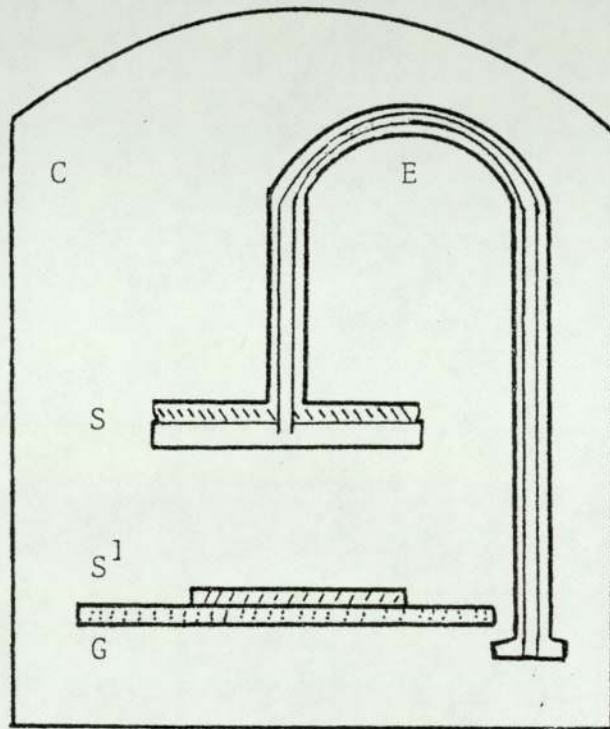
Figure 4.6

(B)



Six gold coated glass cover slips with identification labels.

FIGURE 4.7



Experimental set up of gold coatings

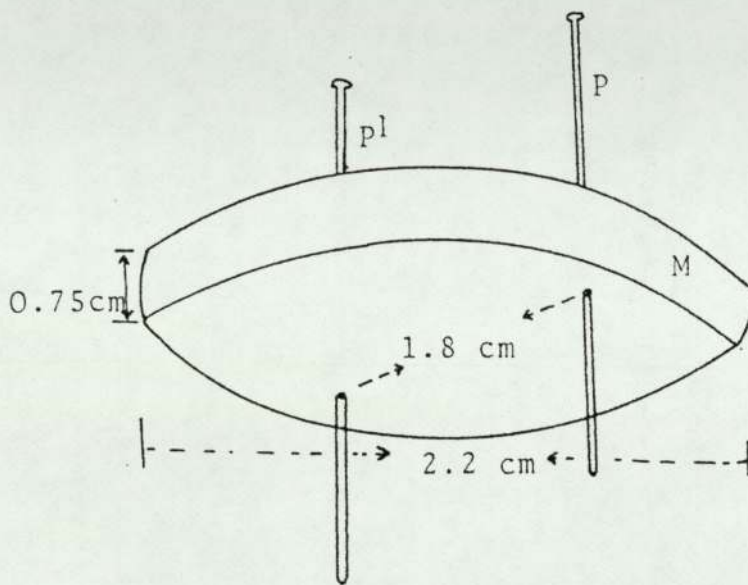
- C = Sputtering chamber
- E = Electrode lead
- S = Sputtering material
- S¹ = Substrate
- G = Ground potential

the resistivity of the material is known, the thickness can be calculated (Appendix 7(b)). P.G. Borziak et. al. (100) measured the thickness by electrical conduction in discontinuous gold films with a mean thickness of 30-60Å⁰.

The thickness of the coatings, prepared by sputtering (as detailed in Section 4.3.2) were determined gravimetrically and electrically as detailed in Appendix 7(a) and (b). The resistance of the coatings was determined using a holder designed for the purpose (Figure 4.8). To check the thicknesses of the coatings so obtained, the coated nickel discs were cut and the metallographic specimens were prepared as detailed in Appendix 6. The metallographic specimens of the five discs were examined in the scanning electron microscope. Photomicrographs were obtained and measurements from these prints, together with the results of thicknesses calculated using resistivity and gravimetric methods, are tabulated in Table 4.3.

The results indicate that the values of the thicknesses of the thin coatings determined by the resistivity and gravimetric methods are closer to each other than the values measured from the photomicrographs of the metallographic specimens of the same coatings. The latter are higher than the calculated values. The values from the photomicrographic prints are plotted against their respective coating time (curve A) and shown in Figure 4.9. The values of the coating thicknesses calculated from the values of their respective weights (B) and resistances (C) are also plotted

FIGURE 4.8



Resistance measuring probes mounted with the non conducting coatings

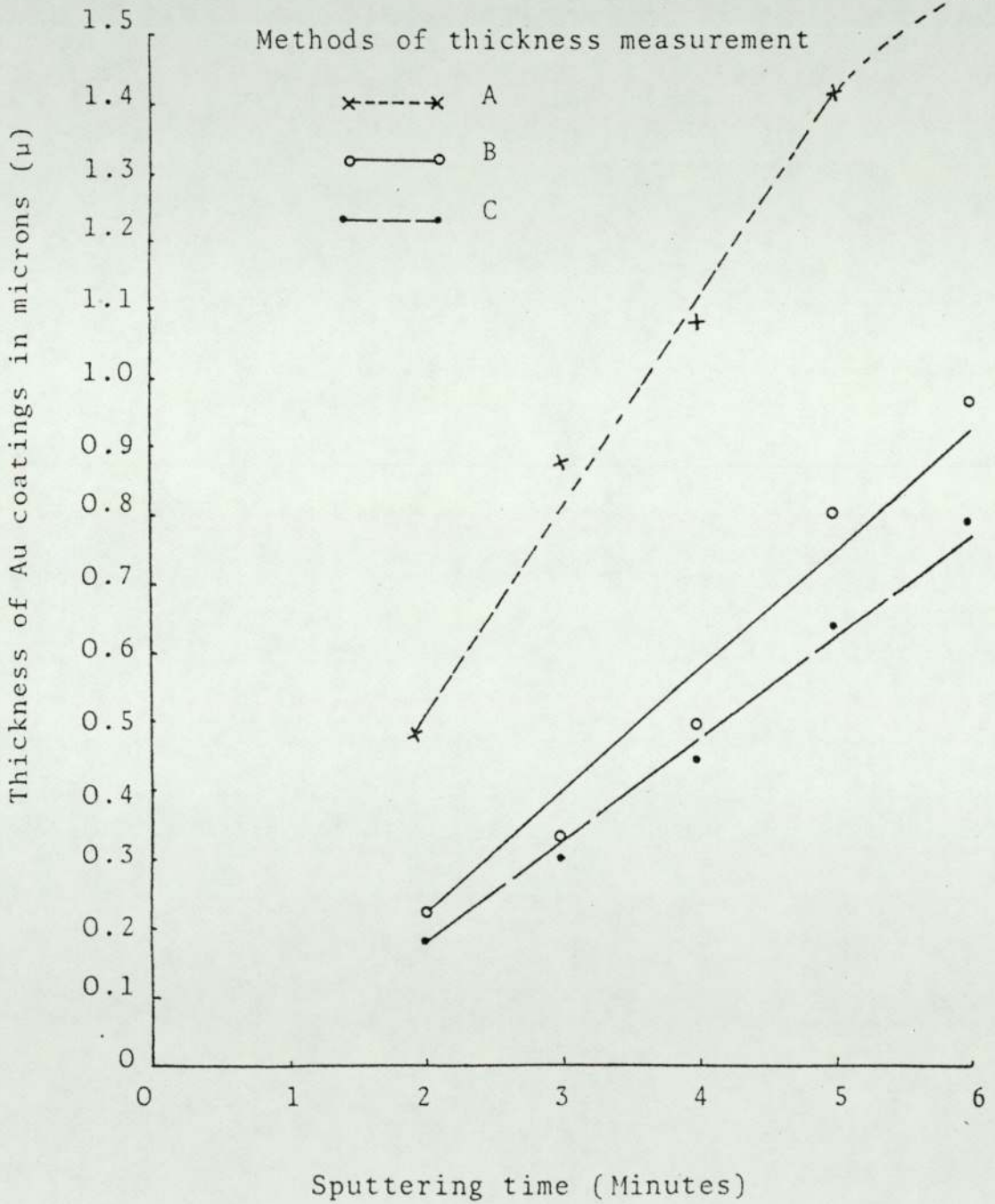
P and P¹ = Resistance measuring probes

M = Non conducting materials

Table 4.3 (Series B)

No.	Specimen No.	Sputtering Time Minutes	Resistance measured $\Omega \times 100$	Mean thickness (resistivity) μm	Mean thickness (photographic) μm	Thickness (gravimetric) μm
1	OKB5	6	1000	0.62	1.54	0.996
2	OKB6	5	1200	0.49	1.34	0.567
3	OKB7	4	2000	0.34	1.08	0.353
4	OKB8	3	3000	0.23	0.82	0.130
5	OKB9	2	4200	0.14	0.56	0.0064

FIGURE 4.9



in Figure 4.9. An almost linear relation between the coating thickness and the coating time is obtained by each method. To obtain better results on the thinnest coatings and to improve reproducibility a moving mask system was designed for use in the existing coating unit and is described in the following section.

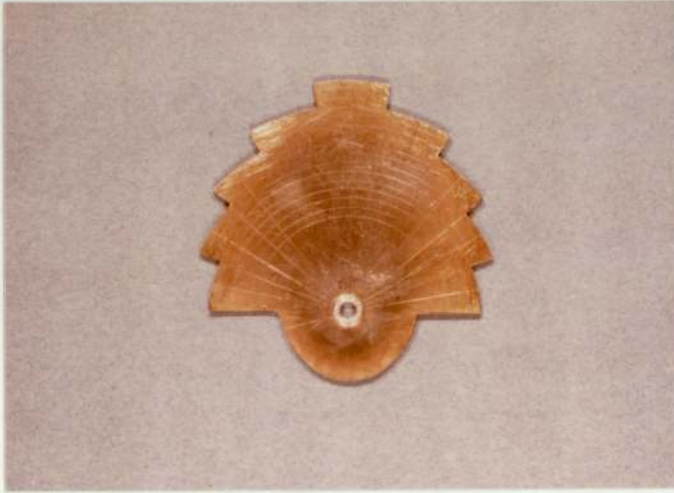
4.4.3.1 The semi-circular disc with radial sections

An aluminium semi-circular disc with radial sections (Figure 4.10) was made to mask the substrate to be coated for various periods of time. The disc was rotated over the specimen under the sputtering electrode during the coating process. The disc rotated in the horizontal plane driven by an electrical motor at a predetermined rate. The radial sections were cut in such a way that they produced coatings of different thicknesses, i.e. related to each other in fixed ratios provided that the motor remained constant. Using the rotating mask it was possible to obtain a series of coatings of increasing thickness all exposed under identical sputtering conditions in a single experimental run.

4.4.3.2 Gold coated specimens obtained using the semi-circular disc (series C)

Those polished nickel discs (series C) were coated with gold using the sputtering electrode and the semi-circular disc for 3, 6 and 9 minutes. The coated specimens were cut and mounted in such a way to show the decreasingly thick layers of gold. Two metallographic

Figure 4.10



Semi circular disc with radial sections.

cross-sections were examined in the SEM. Photomicrographs of the thickest coating and an intermediate coating are shown in Figure 4.11. The thicknesses of the two sections and their mean values are tabulated in Table 4.4.

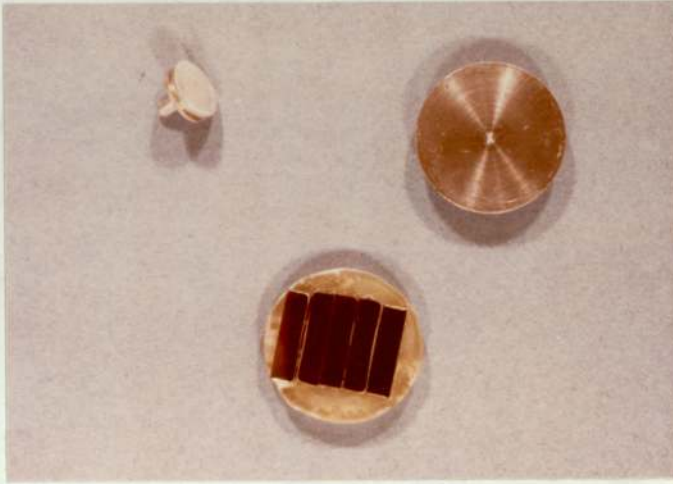
The values of the thicknesses in both regions of the specimens coated for 3, 6 and 9 minutes, are plotted alongwith the results of the coating thicknesses of series B (Figure 4.12). On comparing the three different series of coatings, it is obvious that the thicknesses of the coatings of the series B are higher than the thicknesses of the coatings at the series C, i.e. specimens coated using the semi-circular disc. Although the coating conditions were approximately the same, the deposition rate is non-linear with time. Comparing the thicknesses at the extremities (i.e. Section 1 and Section 2) values of the thicknesses are not in the ratio of 2:1 expected from a linear relationship.

Although the mask gave results different from those expected it was nevertheless useful in experiments to determine the minimum thickness of gold required to replace the colour of the substrate with that of gold. The mask resulted in a series of samples with increasing thickness of coating.

4.5 The influence of substrate composition on the colour and properties of gold coatings

4.5.1 The coating arrangement

To study the influence of substrate composition on the optical

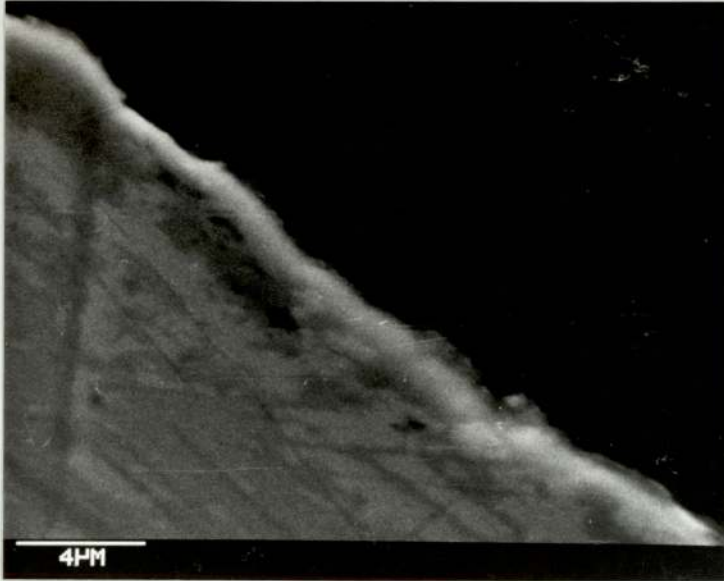


SEM specimen stage mountings and the mounted coating pieces

Figure 4.11

Section 1

(A)



SEM photomicrographs of gold coatings after 3 minutes sputtering on Nickel.

Section 1

(B)

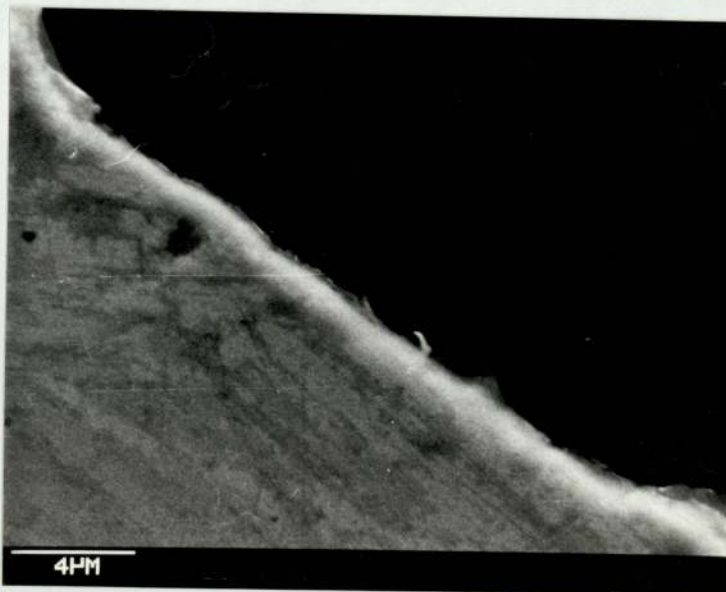
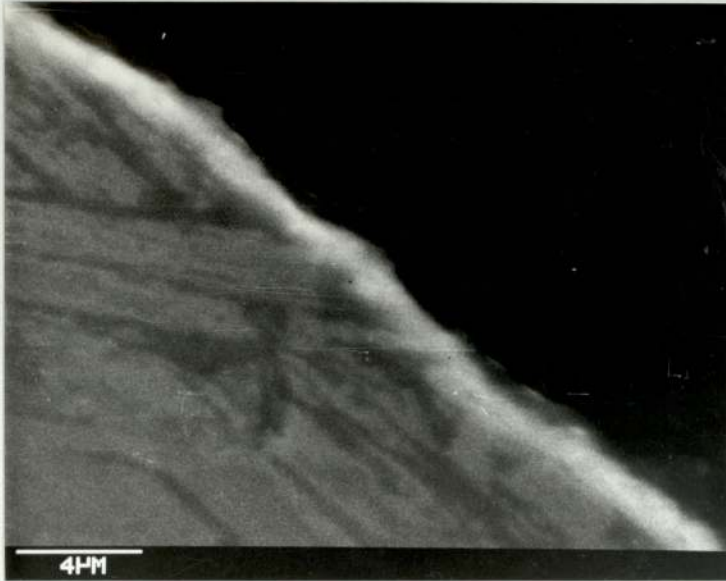


Figure 4.11

Section 2

(A)



SEM photomicrographs of gold coatings after 3 minutes sputtering on nickel.

(B)

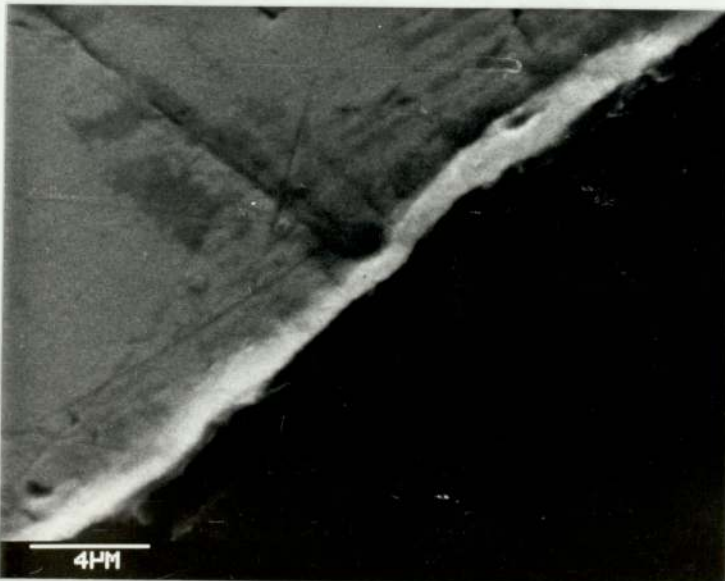


FIGURE 4.12

Gold sputtered coatings on Nickel

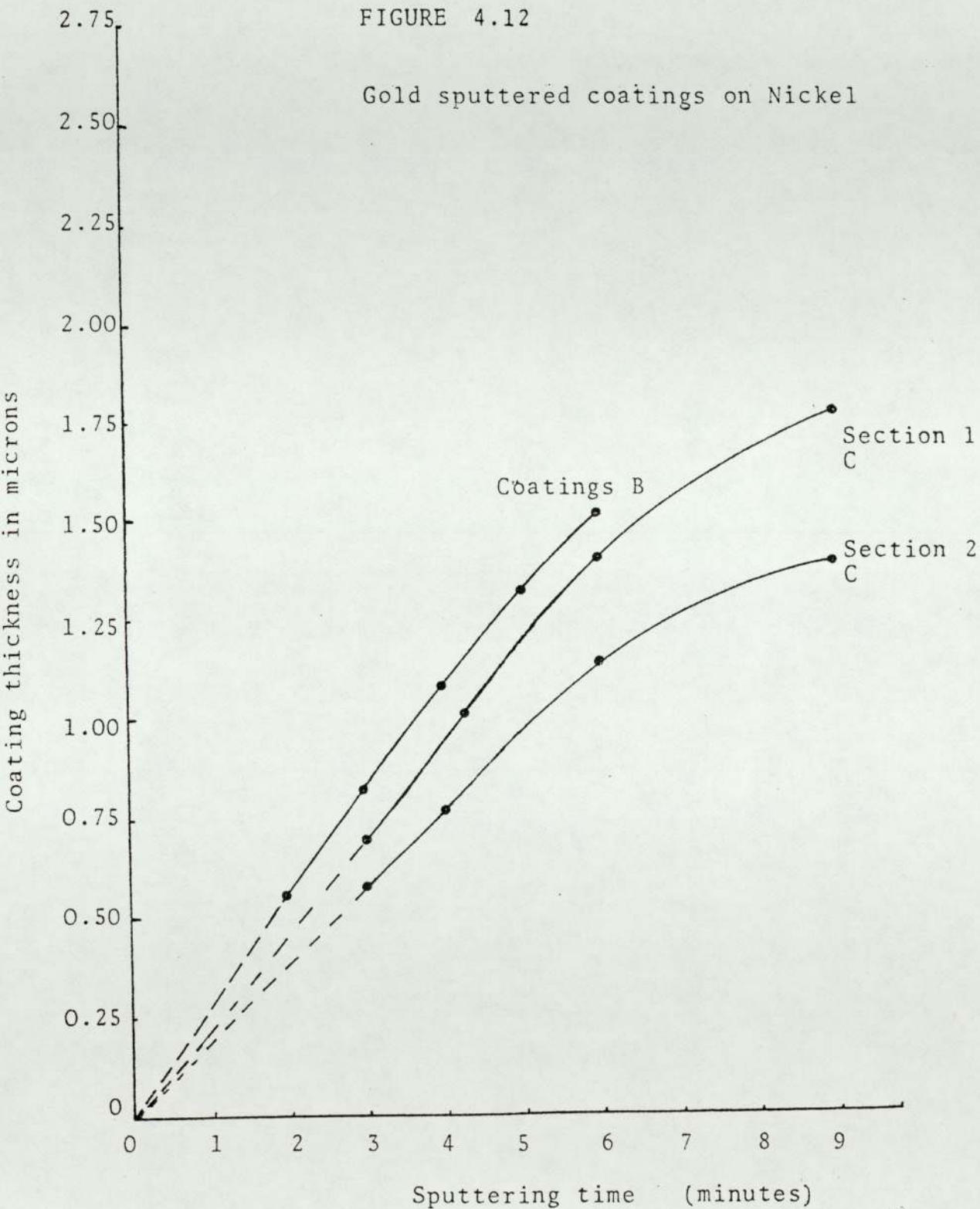


Table 4.4 (Series C)

No.	Specimen	Sputtering time	Section	Thickness (micro- photographs) cm	Mean	Thickness in μm
1	OKC1	3 minutes	1	3, 2.5, 3, 3, 4, 4, 5, 4	2.43 \pm 0.46	0.61 \pm 0.12
			2	2, 2, 2, 1.5, 1.5, 3, 2.5, 1.5	1.94 \pm 0.5	0.48 \pm 0.12
2	OKC2	6 minutes	1	4.25, 4.5, 4.5, 4.5, 4.25, 5, 5, 5	4.24 \pm 0.7	1.40 \pm 0.36
			2	4, 3.5, 3.5, 3, 3, 3.5, 3.5, 4	3.45 \pm 0.6	1.15 \pm 0.28
3	OKC3	9 minutes	1	6.5, 6, 6, 6, 5.5, 5, 5.5, 6	5.28 \pm 0.9	1.78 \pm 0.47
			2	5, 5, 4.5, 4, 4.5, 4.5, 4, 5.	4.15 \pm 0.34	1.40 \pm 0.34



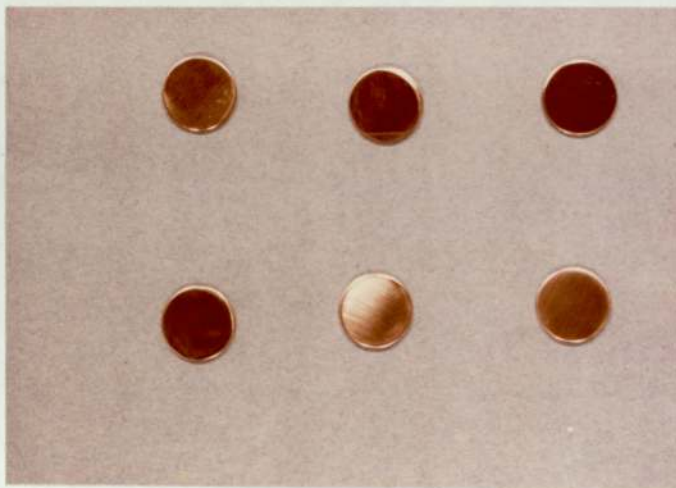
properties of gold coatings, it was planned to use polished stainless steel, aluminium and nickel. Polished sheet was used in attempt to have similar standard surface conditions. The specimens were punched discs of 1.5cm diameter (Figure 4.13). Glass cover slips were also coated at the same time as the metal substrates were coated. The glass cover slips were obtained to enable calculation of the coating thickness using the gravimetric method. Coating times of 2, 3, 4, 5 and 6 minutes were used. Repetition of the experiment was made to assess reproducibility. Altogether, twenty-four specimens were coated (series E) and the colour of each was determined using a Unicam SP800 spectrophotometer (Figure 4.14). The output of the instrument was as absorbance/transmittance chart (Figure 4.15).

The above experimental procedure was repeated (Experimental Series F) in order to check reproducibility. When coatings on the same substrate material under the same operating conditions. The influence of surface roughness of the substrate was studied by abrading the surface with silicon carbide paper. An aluminium holder (Figure 4.16) was made for holding the specimens while being abraded. A few of the photomicrographs are shown in Figure 4.17 A, B, C, D after abrading with different grades of silicon carbide paper.

4.5.2 Standard specimen for colour measurement

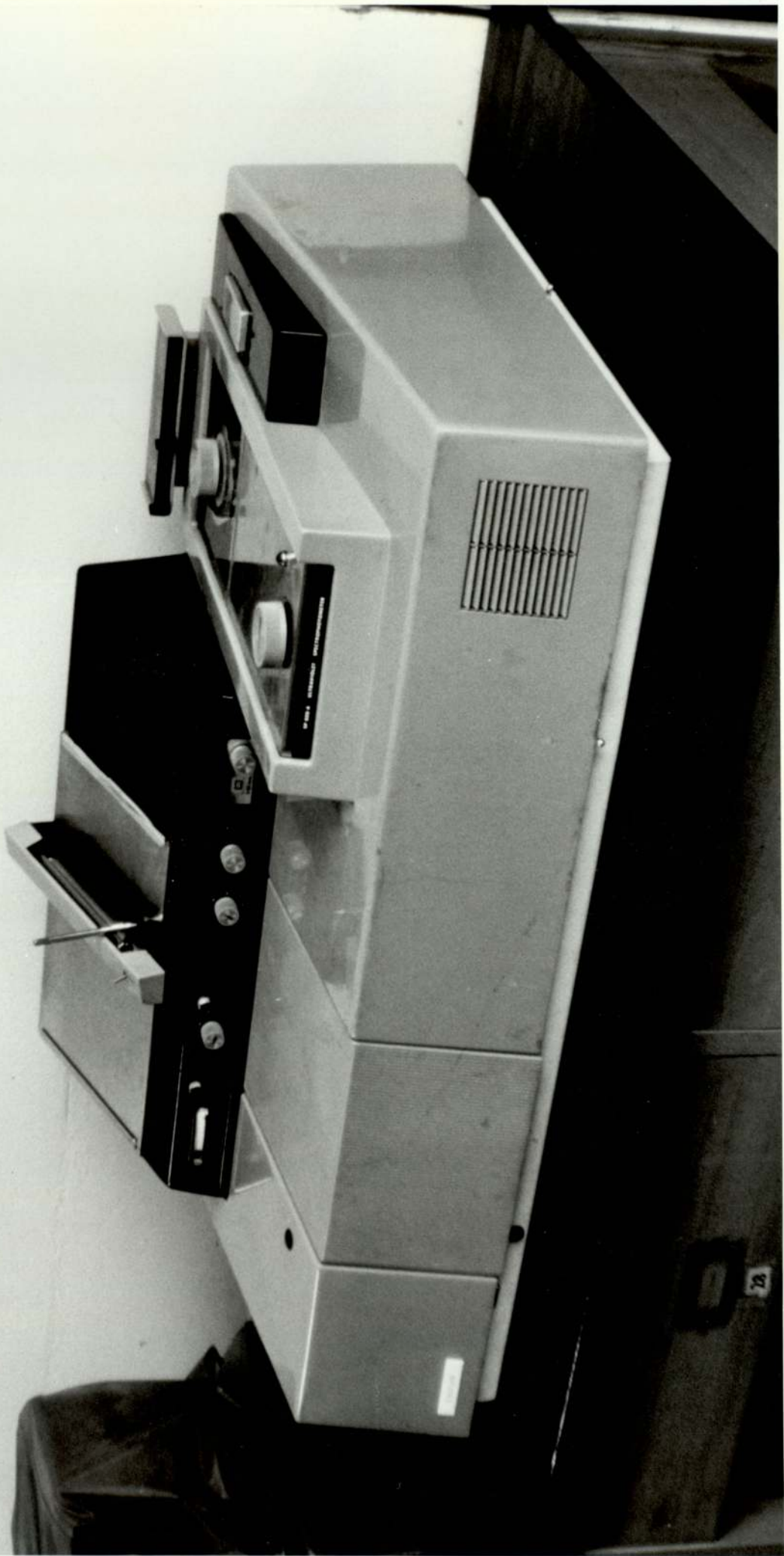
Before measuring the colour of gold coatings on various substrates, it was necessary to establish a 'white' standard. G. Brown (94)

Figure 4.13



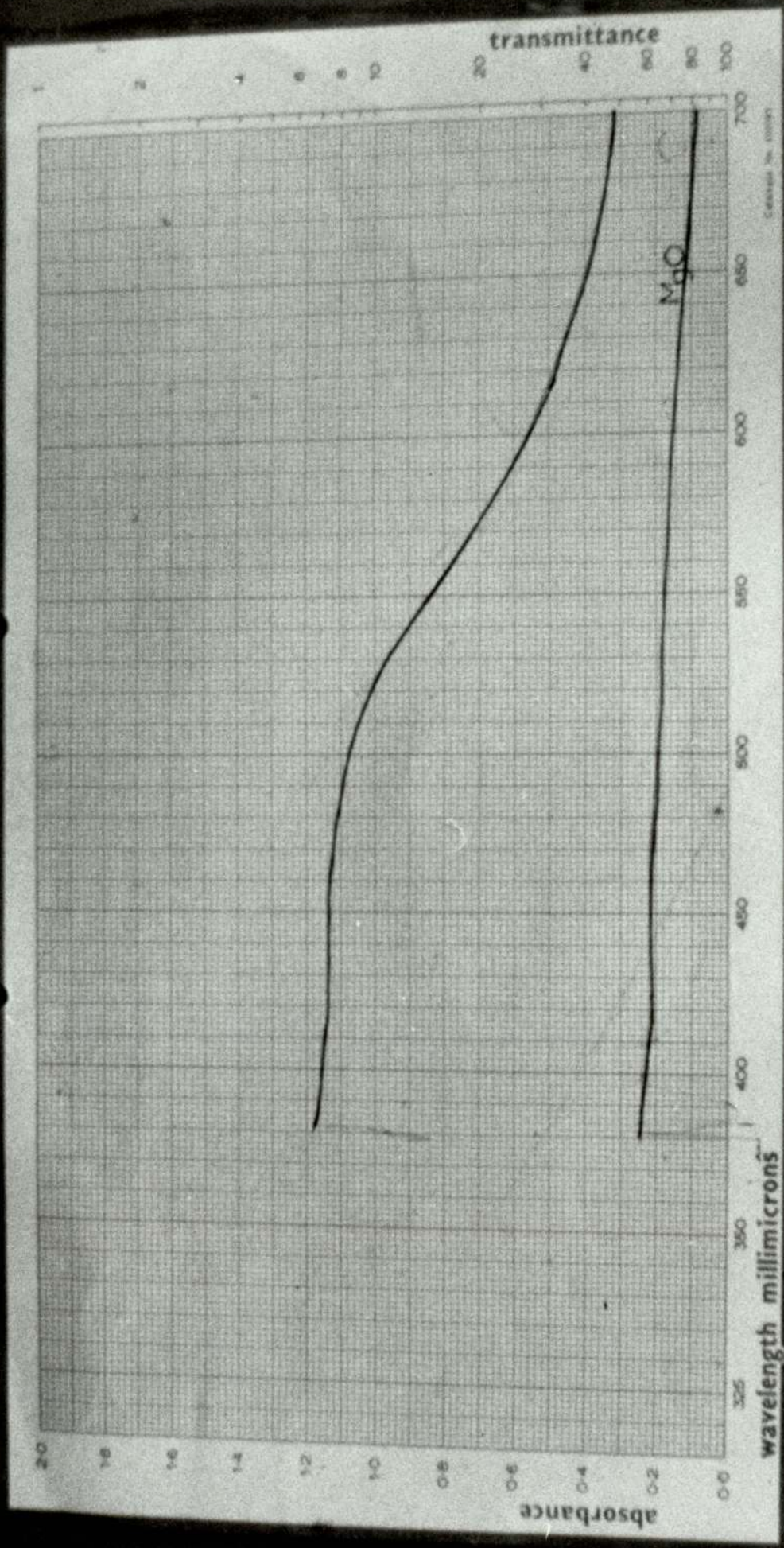
Punched discs of the substrate materials.

FIGURE 4.14
Unicam SP.8000 Spectrophotometer



UNICAM SP. 800

ULTRAVIOLET SPECTROPHOTOMETER



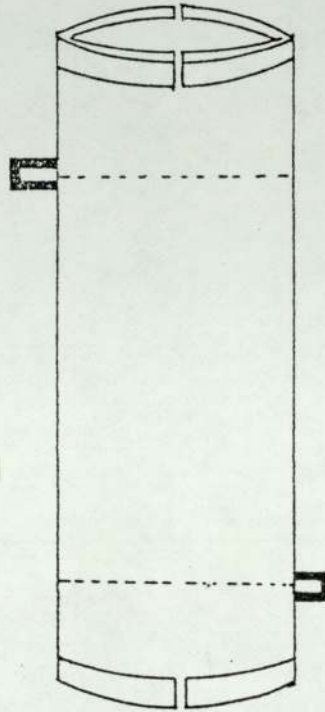
56 FIGURE 4.15
Absorbance/transmittance Chart

SCALE USED: ABS TRAN
DATE: 13-1-80
OPERATOR: J. B. ...

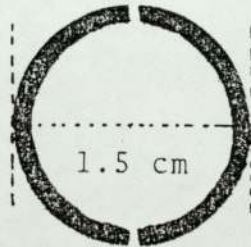
CONCENTRATION:
REFERENCE:
PATH LENGTH:

READ WITH INDEX
ON THE RECORD

FIGURE 4.16



Aluminium jig for holding the discs



Cross-section of the holder jig

Figure 4.17

(A)



15 x nickel surface abraded with 120 grit

(B)



15 x nickel surface abraded with 240 grit.

Figure 4.17

(C)



15 x nickel surface abraded with 400 grit.

(D)



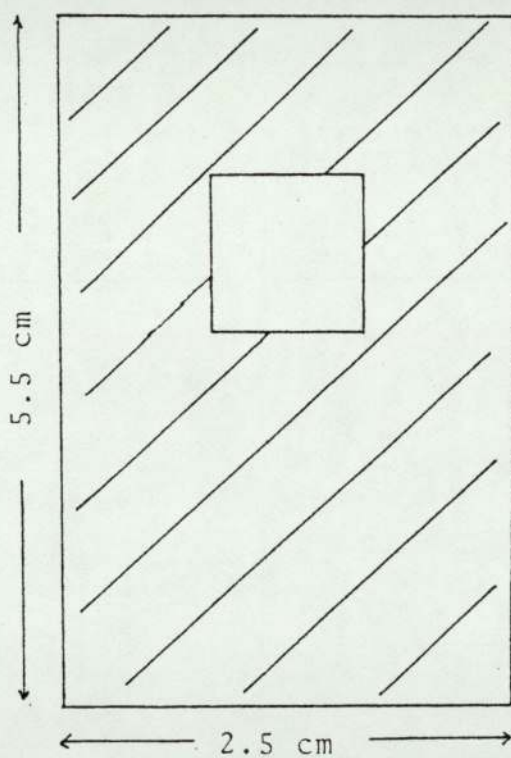
15 x nickel surface abraded with 600 grit.

has done a study on various materials in order to determine the most suitable for convenience and reproducibility. Absorbance wavelength graphs for Analar grade magnesium oxide (MgO), condensed MgO vapour, Barium sulphate ($BaSO_4$), magnesium carbonate ($MgCO_3$) and white paper were obtained. The spectrophotometer was zeroed at 700nm and the graphs were drawn over the range 700-380nm. The general shape of the graphs was very similar except that for white paper, which showed slightly greater absorbance at the violet end of the spectrum. There was negligible difference between the graph for pressed magnesium oxide and condensed MgO . Therefore a freshly pressed magnesium oxide (MgO) standard was used before each experiment and the spectrophotometer zeroed. A standard mask was designed and used in the diffuse reflectance attachment of the spectrophotometer to illuminate with equal intensity equal areas the standard and the specimen to be measured. Figure 4.18 illustrates the mask and its size.

4.5.3 The measurement of colour

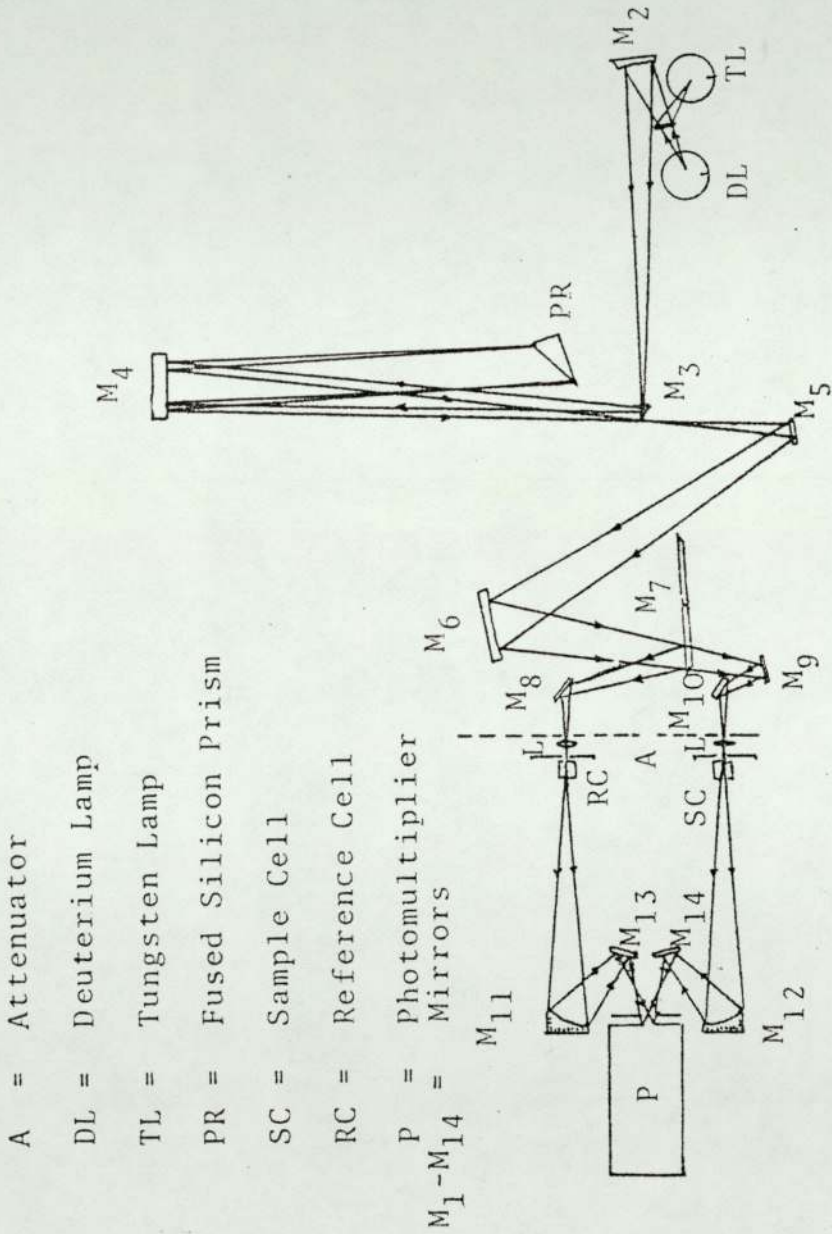
The optical properties of the coatings were measured with a Unicam spectrophotometer type SP800 fitted with a diffuse reflectance attachment type SB 890 photographed in Figure 4.14. The optical system of the spectrophotometer is shown in Figure 4.19. Light from a standard tungsten lamp source splits into its constituent wavelengths. For chemical analysis of coloured liquids each increment in wavelength is directed through the liquid and its absorbance measured and recorded over the spectrum of wavelengths.

FIGURE 4.18



The mask to expose an equal amount of light energy from a square hole on the specimens and standards

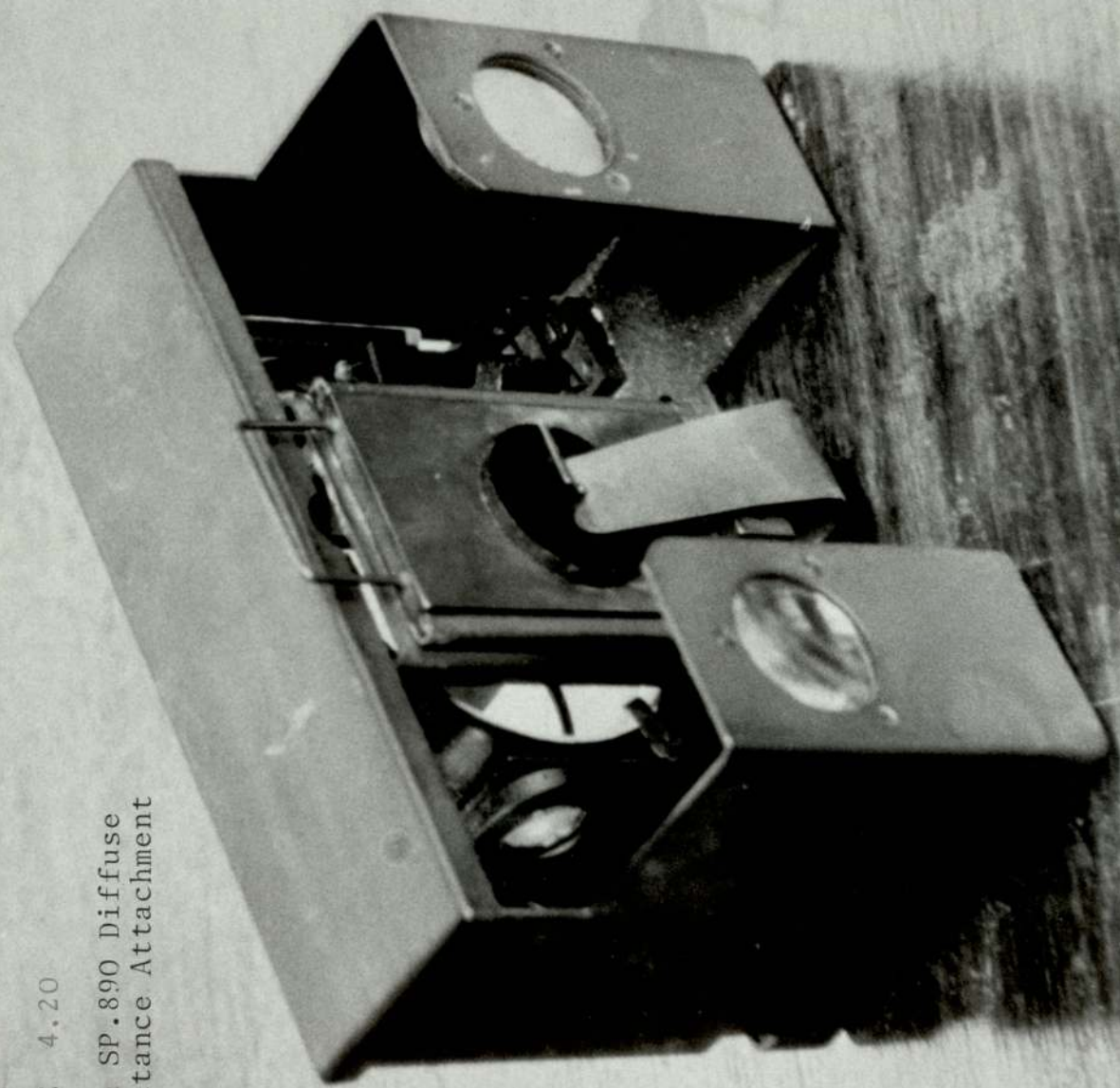
FIGURE 4.19



The Optical System of the Unicam SP.800

FIGURE 4.20

Unicam SP.890 Diffuse
Reflectance Attachment



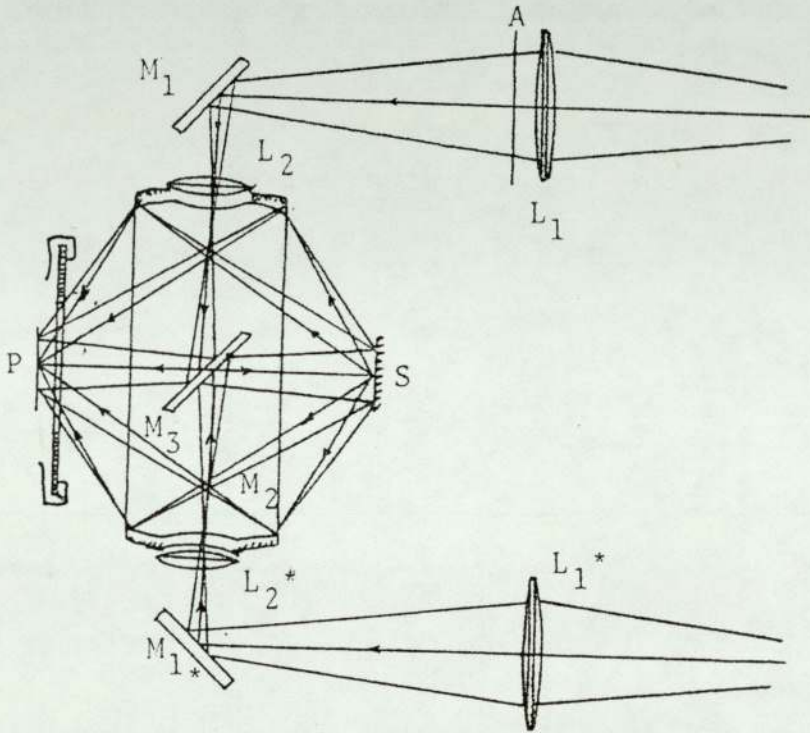
For solid materials the apparatus was modified, and a Unicam diffuse reflectance attachment SP890 is substituted as shown in the photograph (Figure 4.20). Figure 4.21 shows the optical system of the diffuse reflectance attachment. Light from the sample and the reference beams of the spectrophotometer are focussed by the lenses L_1 , L_1^* to form images of the monochromator slit at the apertures in the side of the ellipsoidal mirror M_2 . Light from the sample beam falls upon one side of mirror M_3 and then illuminates the sample over a small range of angles near normal incidence. An image of the prism is formed on the sample by lens L_2 , thus ensuring even illumination of the sample. Light from the reference beam is reflected by the rear of mirror M_3 on to the face of the photomultiplier (94).

The light which is diffusely reflected by the sample is collected by the ellipsoidal mirror over a range of angles of reflection between approximately 35° and 55° , and is focussed on to the face of the photomultiplier. The ellipsoidal mirror collects about 30% of the total diffusely reflected light and to compensate for this, an attenuator A is fitted in the reference beam. The main instrument plots absorbance over the range of wavelengths of the visible spectrum as shown in the photographic print in Figure 4.15.

4.5.4 Measurement procedure

(i) The diffuse reflectance attachment (Figure 4.20) was substituted for M_{13} to M_{14} section of the spectrophotometer as explained in Appendix 8 and the designed mask mounted with it.

FIGURE 4.21



Optical system of the Diffuse Reflectance Attachment

- L_1, L_1^* = Lenses
- L_2, L_2^* = Lenses
- M_1, M_1^* = Reflecting Mirror
- M_2 = Ellipsoidal Mirror
- M_3 = Double sided reflecting mirror
- S = Sample
- P = Photomultiplier
- A = Attenuator

(ii) A standard specimen of magnesium oxide was prepared in a hollow disc using the jig shown in Figure 4.22. A glass slide was used to apply the pressure so that a smooth surface was obtained.

(iii) The magnesium standard was placed in the jig with the mask which was positioned in the diffuse reflectance attachment.

(iv) The zero of the instrument was then adjusted and the absorbance of the standard measured over the spectrum of wavelengths, resulting in a graph as shown in Figure 4.15.

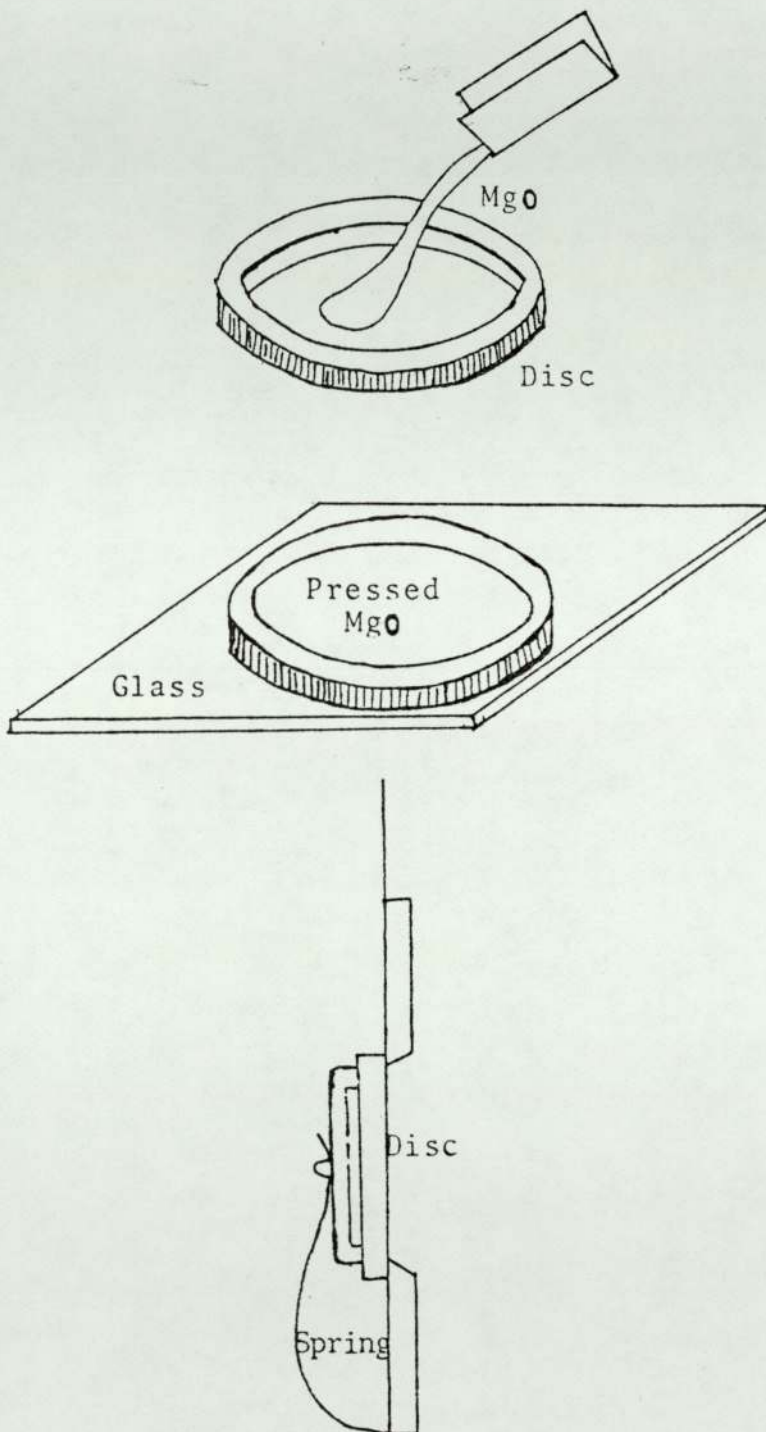
(v) The disc under test was then substituted for the standard and the absorbance measured.

(vi) The difference in absorbance (A) the standard and the disc was then derived from the graph at 5nm intervals. From this information the reflectivity (R) was derived using the relation $R = 10^{2-A}$.

4.5.5 Calculation of the chromaticity co-ordinates

Each reflection value was multiplied by the chromaticity coefficients (C.I.E. value) (Appendix 3) for both equi-energy and for the illuminant SA to get the C.I.E. tristimulus values (X, Y and Z). They indicate the amount of the three theoretical primary stimuli that would be required for a colour match. The chromaticity co-ordinates x, y and z for a colour are calculated from its C.I.E. tristimulus values by dividing each of these values with their total

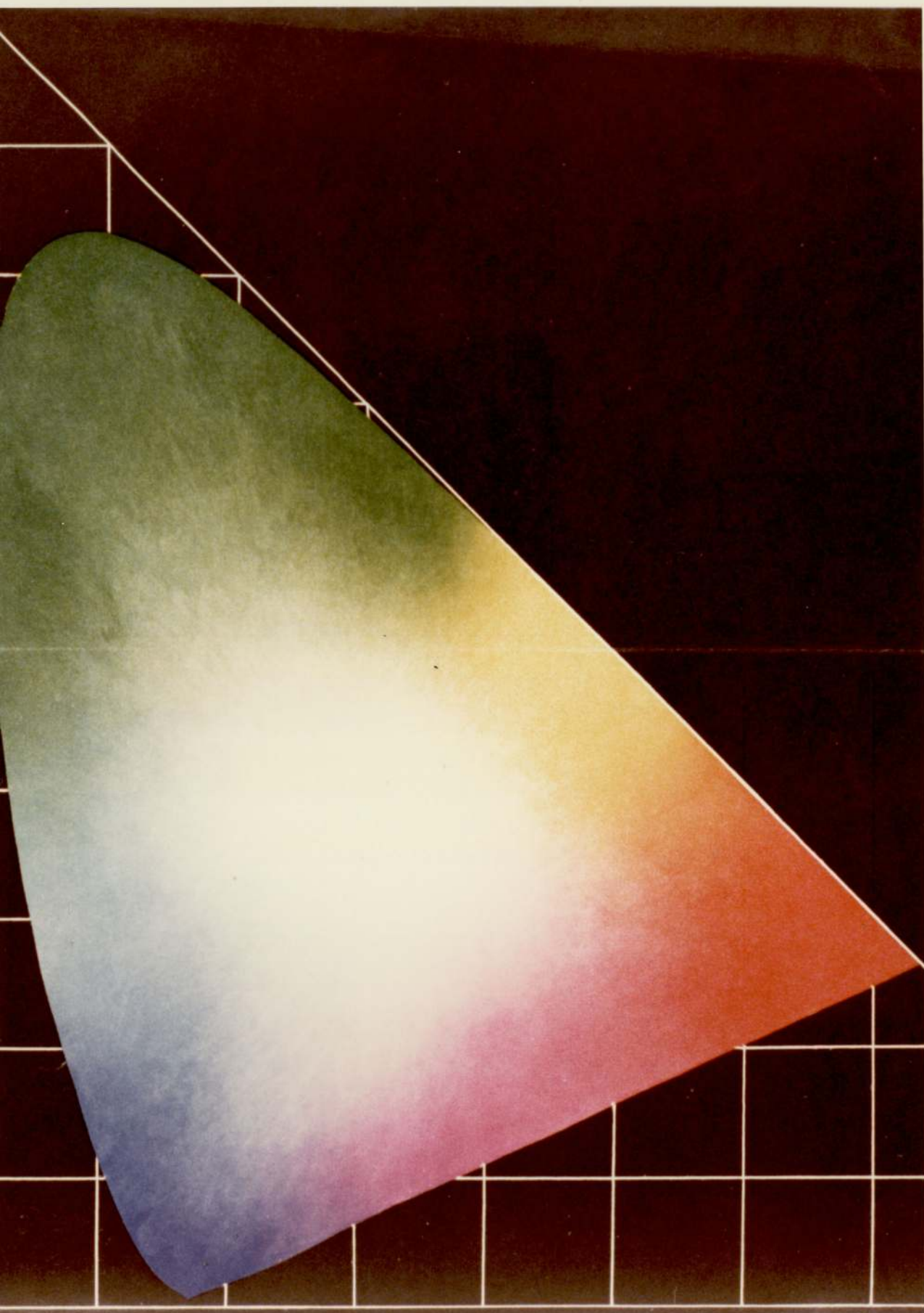
FIGURE 4.22



The preparation of standard and the sample and standard holder

FIGURE 4.23

Chromaticity diagram in Colour



sum, i.e. $x = \frac{X}{X+Y+Z}$, $y = \frac{Y}{X+Y+Z}$, and $z = \frac{Z}{X+Y+Z}$.

The resulting co-ordinates add up to unity as required for the chromaticity chart (Figure 4.23), i.e. $x+y+z = 1$. The co-ordinates are the proportions of x , y and z that constitute a particular colour. The values of x and y define the hue and saturation of the specimen by fixing its position on the chromaticity chart. The box in the chromaticity diagram (Figure 4.24) represents the limits of the yellow colour, part of which is used in defining the colour co-ordinates of the gold coatings and the influence of the substrate material on them in the present study.

4.5.6 Fortran computer programme OK002

A computer programme was designed to do the calculations and to print and plot the required output. Appendix 2 shows the programme, which required an input data file for the absorbance values for the standard and each specimen at 5nm wavelength steps from 380nm. Examples of such files are shown in Appendix 9. The programme also requires an input data file for the standard illuminants. The sets of values for the two standard illuminants used in the present study i.e. for equi-energy (EE) Figure 4.25 and for tungsten lamp SA Figure 4.26 were required. One of them is listed in Appendix 3.

All of the data files were stored through the MOP terminals to the magnetic tape memories of an ICL 1904 computer. The absorbance values of approximately fifty specimens were logged into the computer and the results obtained in form of output prints for each specimen. For each step of 5nm in wavelength values were given of

FIGURE 4.24

Chromaticity Diagram

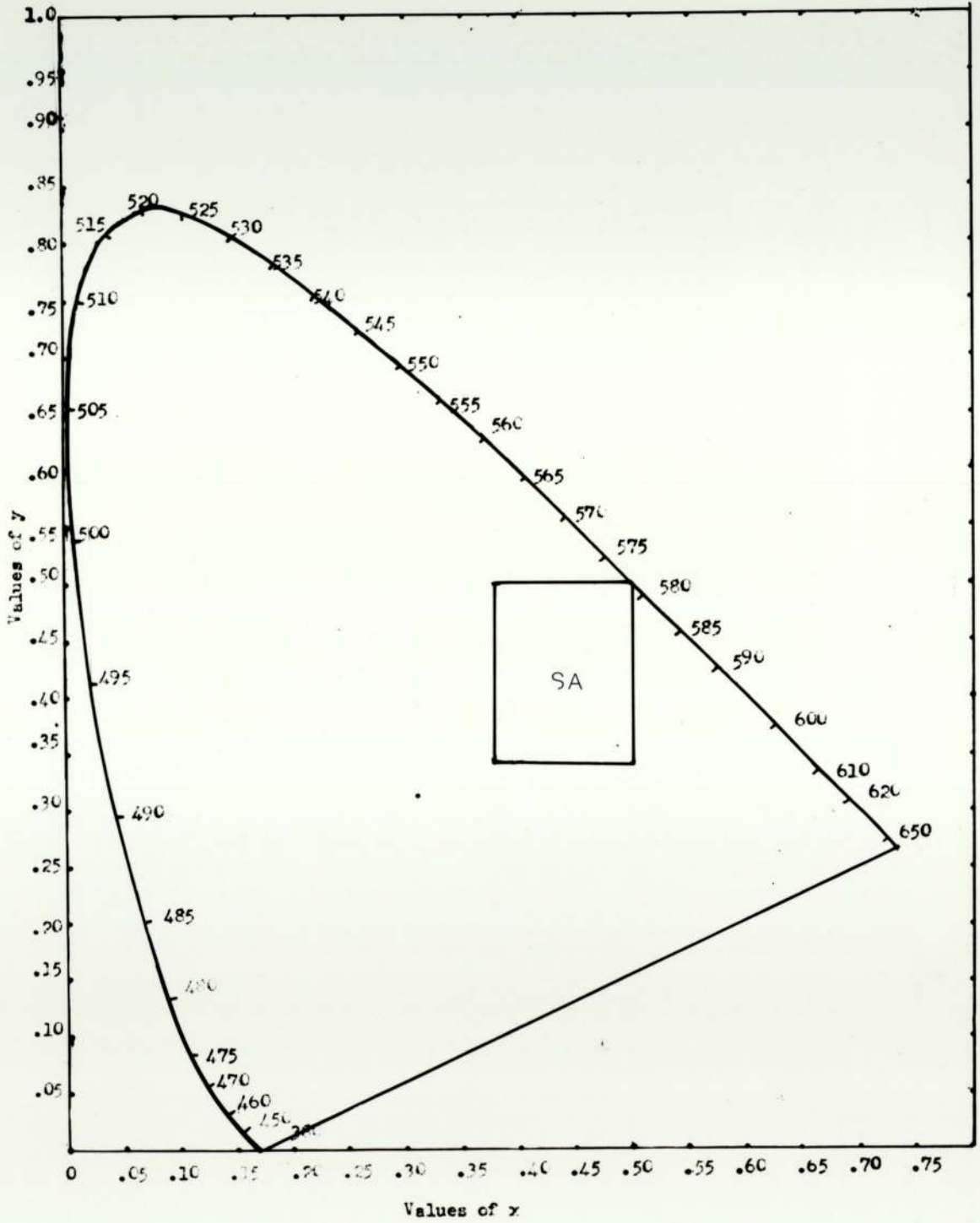
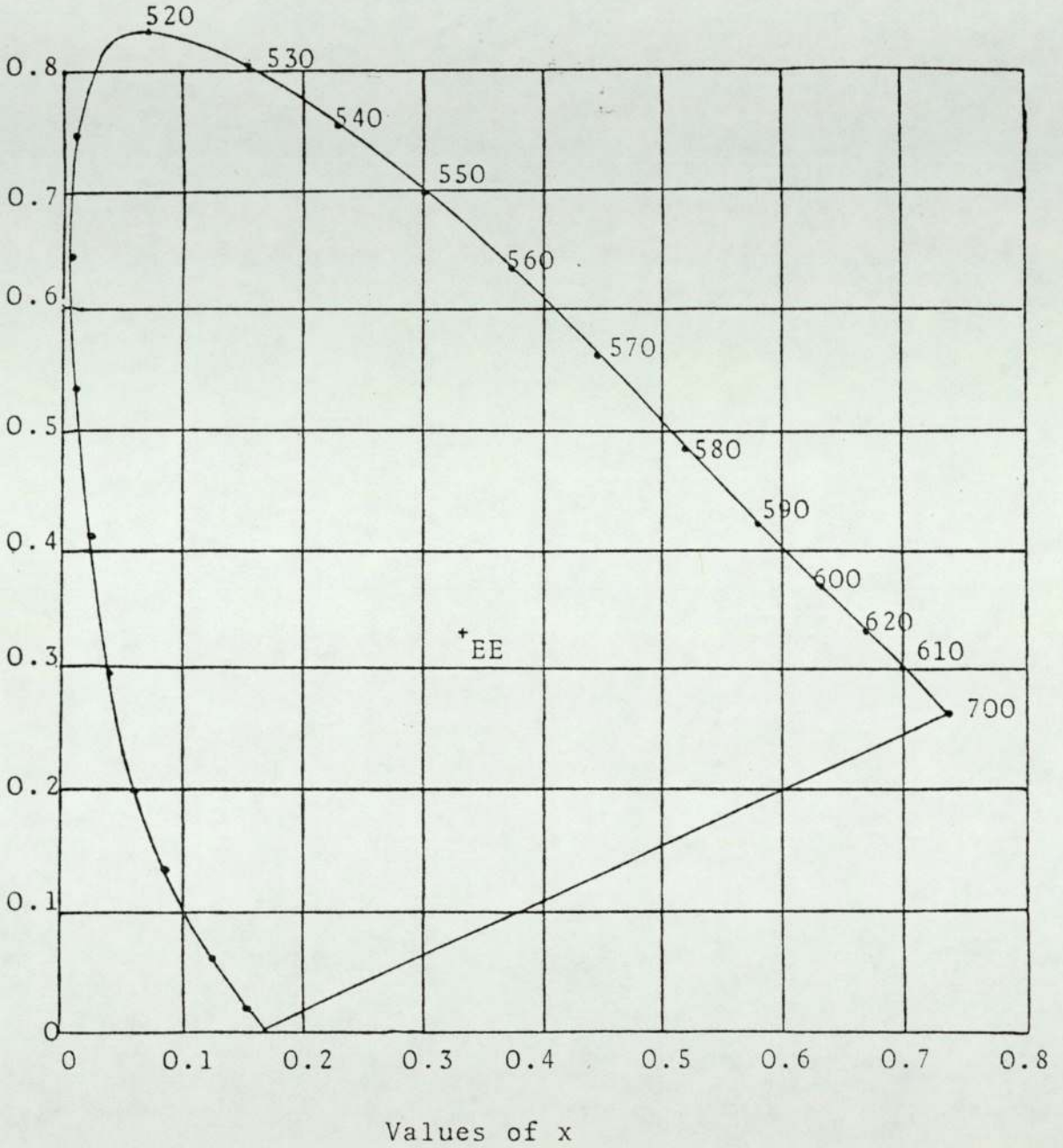
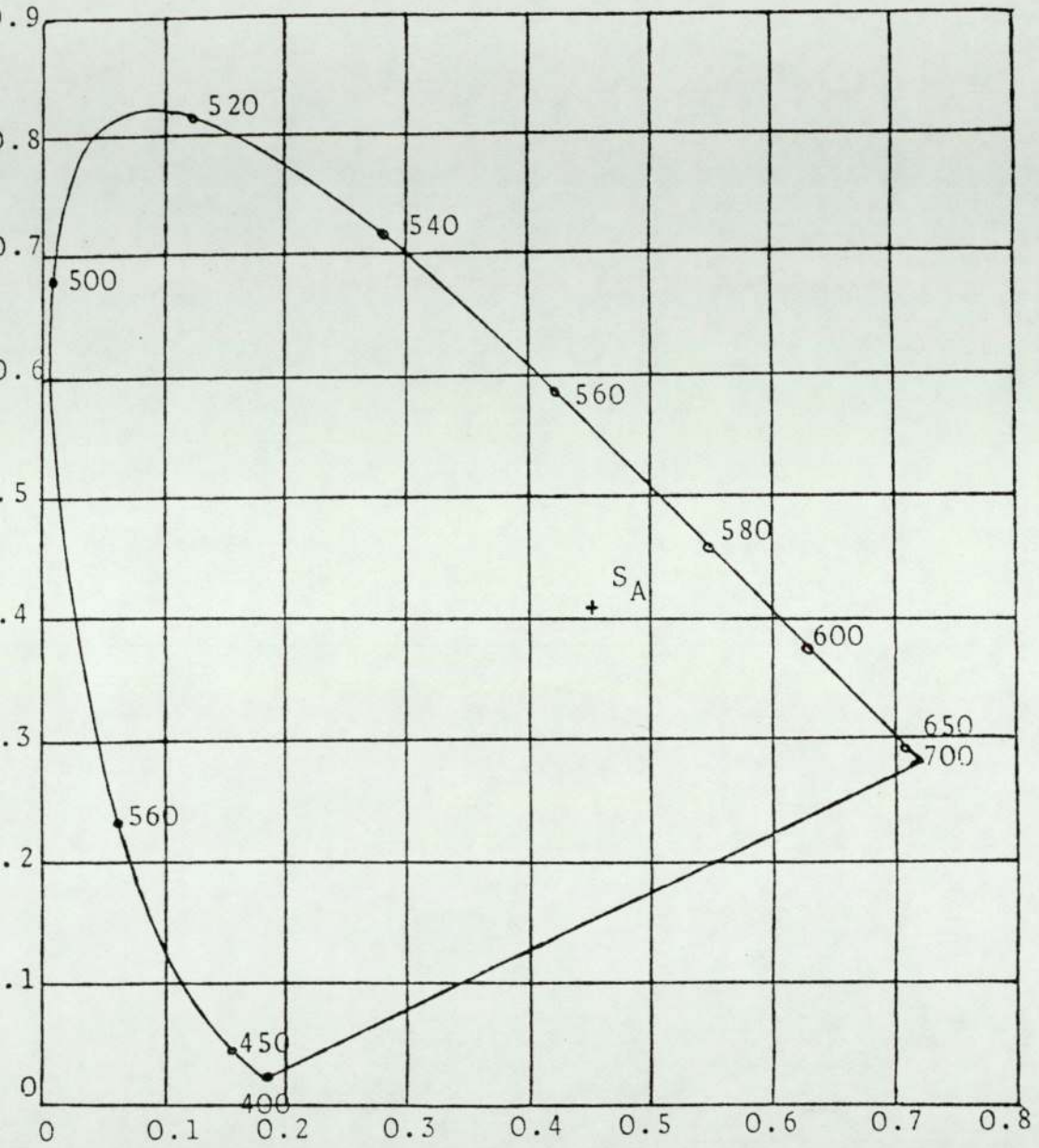


FIGURE 4.25



The CIE chromaticity chart for Equi-Energy (EE) conditions

FIGURE 4.26



Values of x

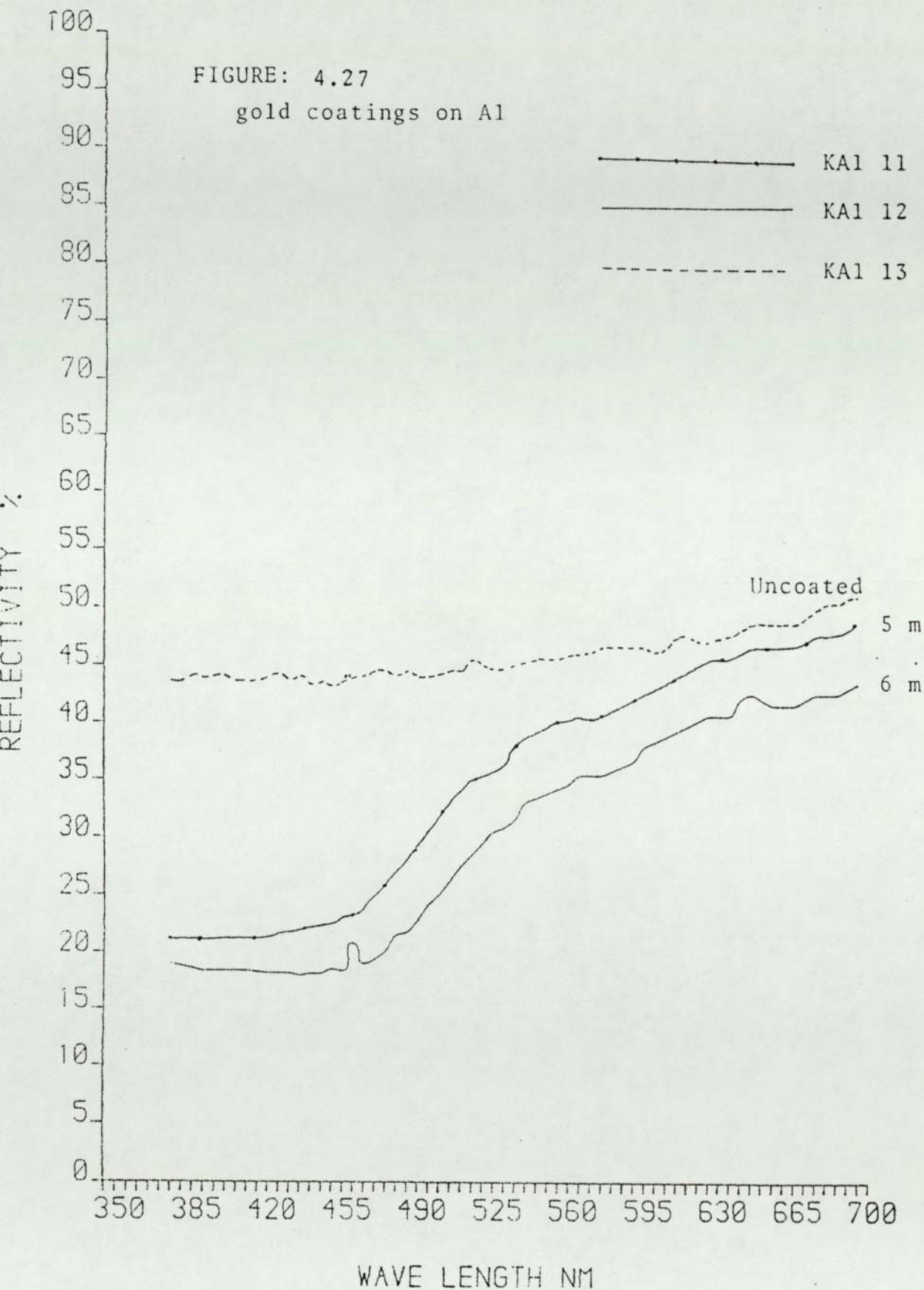
The CIE chromaticity chart for tungsten lamp (S_A) conditions

absorbance, reflectivity, the tristimulus values X, Y and Z and the colour co-ordinates x, y and z. The printed results for a blank and a coated specimen are shown in Appendix 10 and 11 respectively. The other output of the programme was a reflectivity curve (as in Figure 4.27). This shows the colour characteristics of the Al coatings.

4.5.7 The optical properties of thin gold coatings (Au coatings on glass cover slips) (Series E and F)

In order to determine the thickness and colour co-ordinates of thin gold coatings of different thicknesses, glass cover slips were used as a substrate. The colour co-ordinates of uncoated glass cover slips were determined and compared with the white standard and with a series of gold coatings sputtered for increasing times on similar glass cover slips. Two series of experiments (E and F) were carried out with similar operating conditions and for the same sputtering times. There were six discs of each stainless steel, aluminium and nickel, as well as the six glass cover slips coated for 2, 3, 4 (and a duplicate), 5 and 6 minutes. The above three substrate materials were used to observe their influence on the coating achieved for a same period. Each specimen was labelled to indicate the substrate material and coating time.

The average thickness of the glass cover slips was less than 0.005cm, but its effect on the colour co-ordinate was measureable. Therefore the colour of the gold coatings was measured in the two



Reflectivity curves of an aluminium substrate coated with gold for different length of time

positions A and B, one directly on the gold, the other through the glass, as shown in Figure 4.28. The colour co-ordinates of the glass cover slips coated with gold for different times were determined and plotted in Figure 4.29. The colour of the coatings is more yellow when determined in position B compared with position A (Figure 4.29). The behaviour of both the complete and broken lines (Figure 4.29) is similar. The colour co-ordinates of the two coatings coated for the longer time (series F, i.e. KG07 to KG12) are not as yellow as series E (i.e. KG01 to KG06).

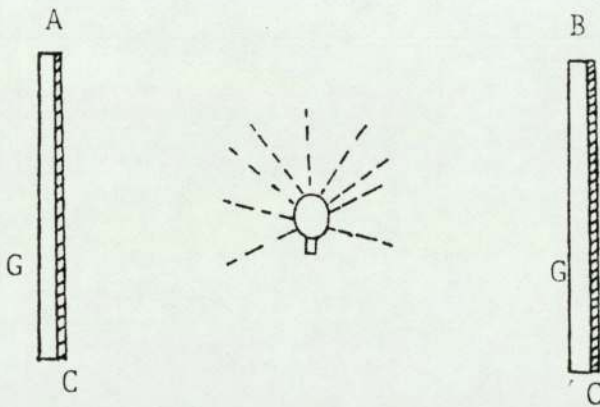
The reflectivity curves for the gold coatings in both series are shown in Figures 4.30 and 4.31. The reflectivity values of the curves are higher at the lower frequency of the light waves for the F series compared with the E series. This means that there is a more reddish influence in the gold colour in the F series than at the E series. One specimen i.e. KG06 in the E series of coatings shows a darkish influence on the colour, although the reflectivity is slightly higher at the yellowish and reddish part of the spectrum.

Photographs of the apparent surfaces of the coatings on the glass cover slips were taken at a magnification of 15 times using the overhead projection microscope. Figures 4.32 and 4.33 show the microphotographs of the four coatings.

4.5.8 Thickness of the gold coatings

Gold was deposited on glass, nickel, stainless steel and aluminium at the same time. The thickness of the gold coatings of the two

FIGURE 4.28

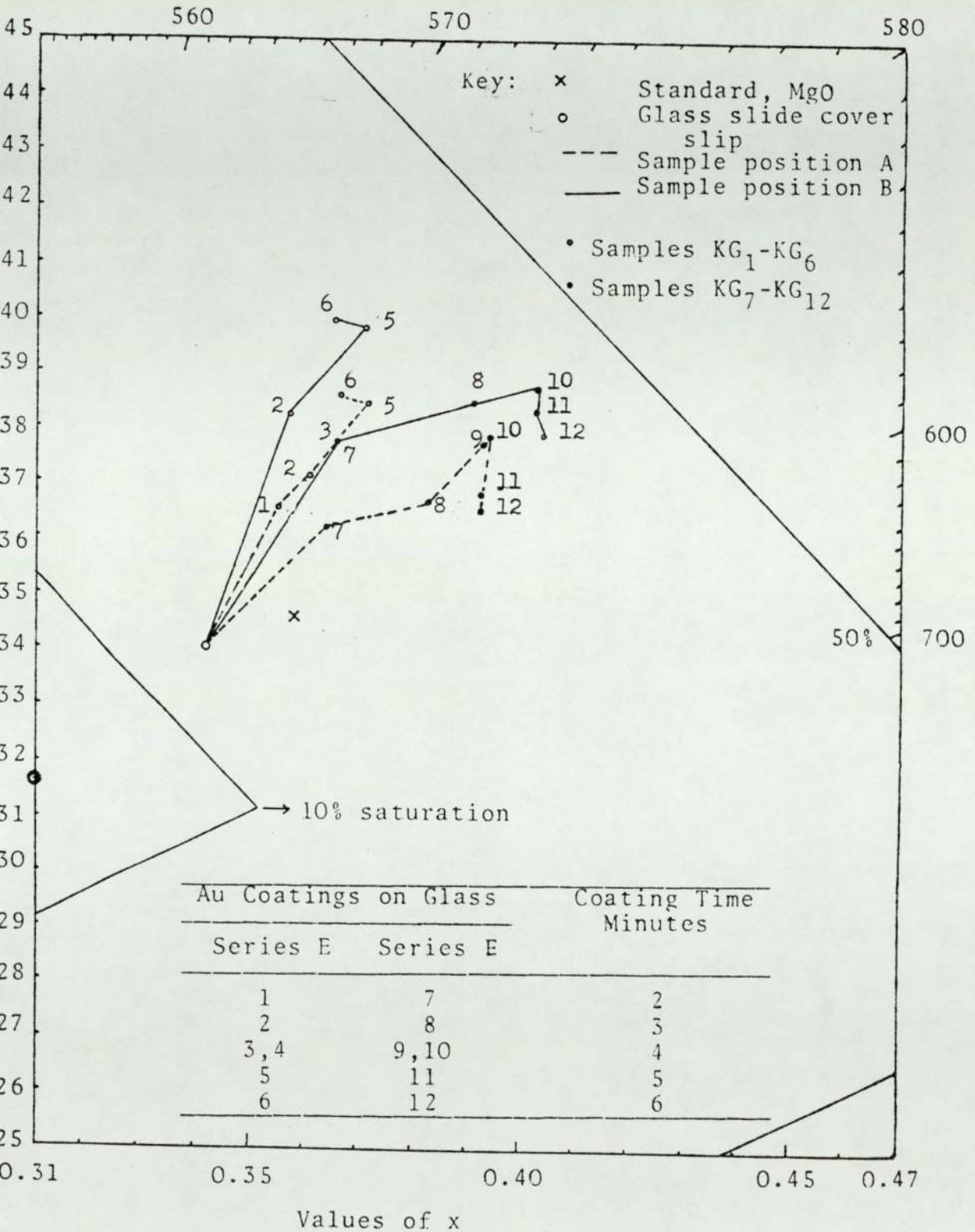


Positions of the coated glass cover slips

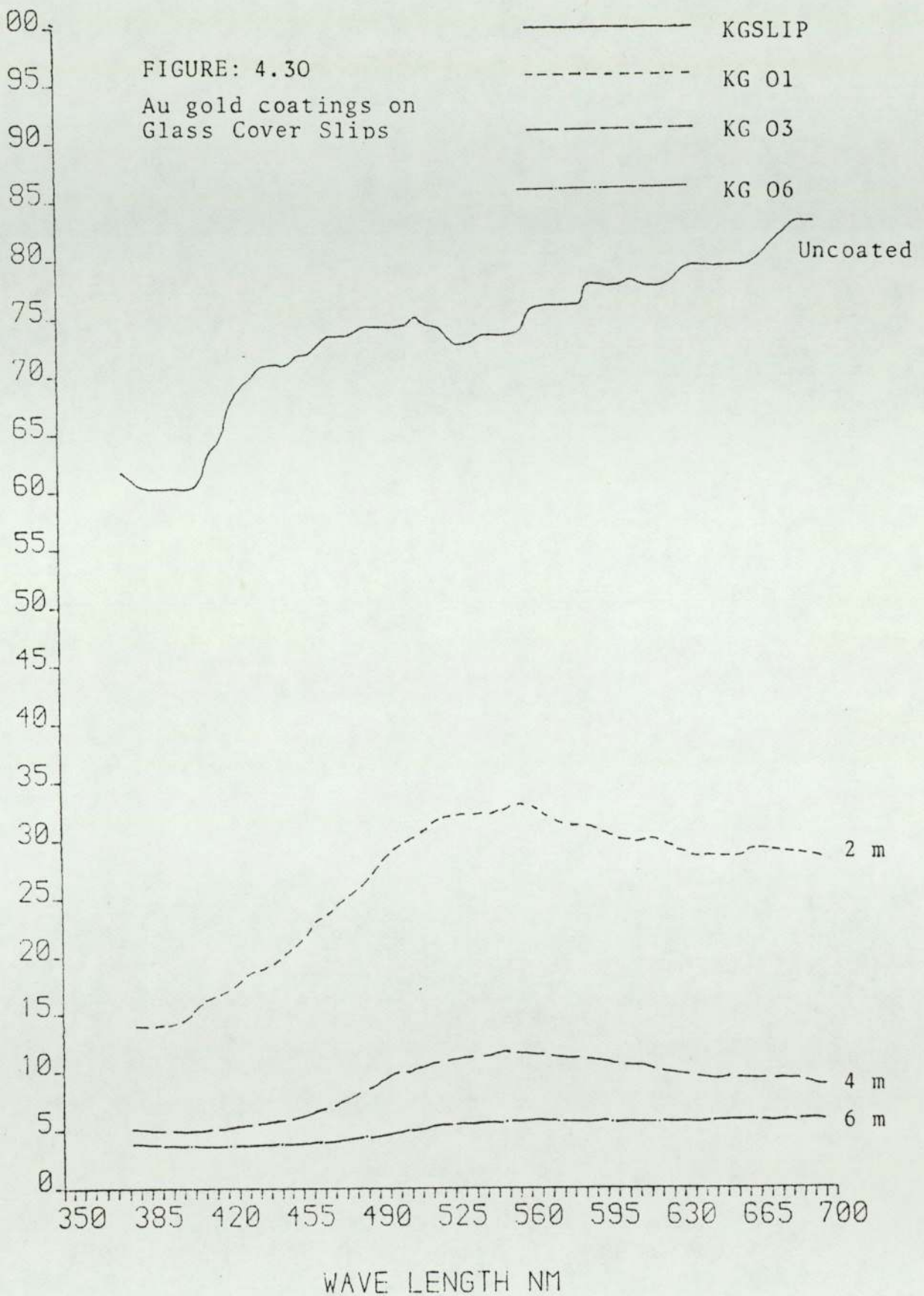
C = Gold coatings

G = Glass cover slips

FIGURE 4.29



Colour co-ordinates of gold coatings on glass cover slip

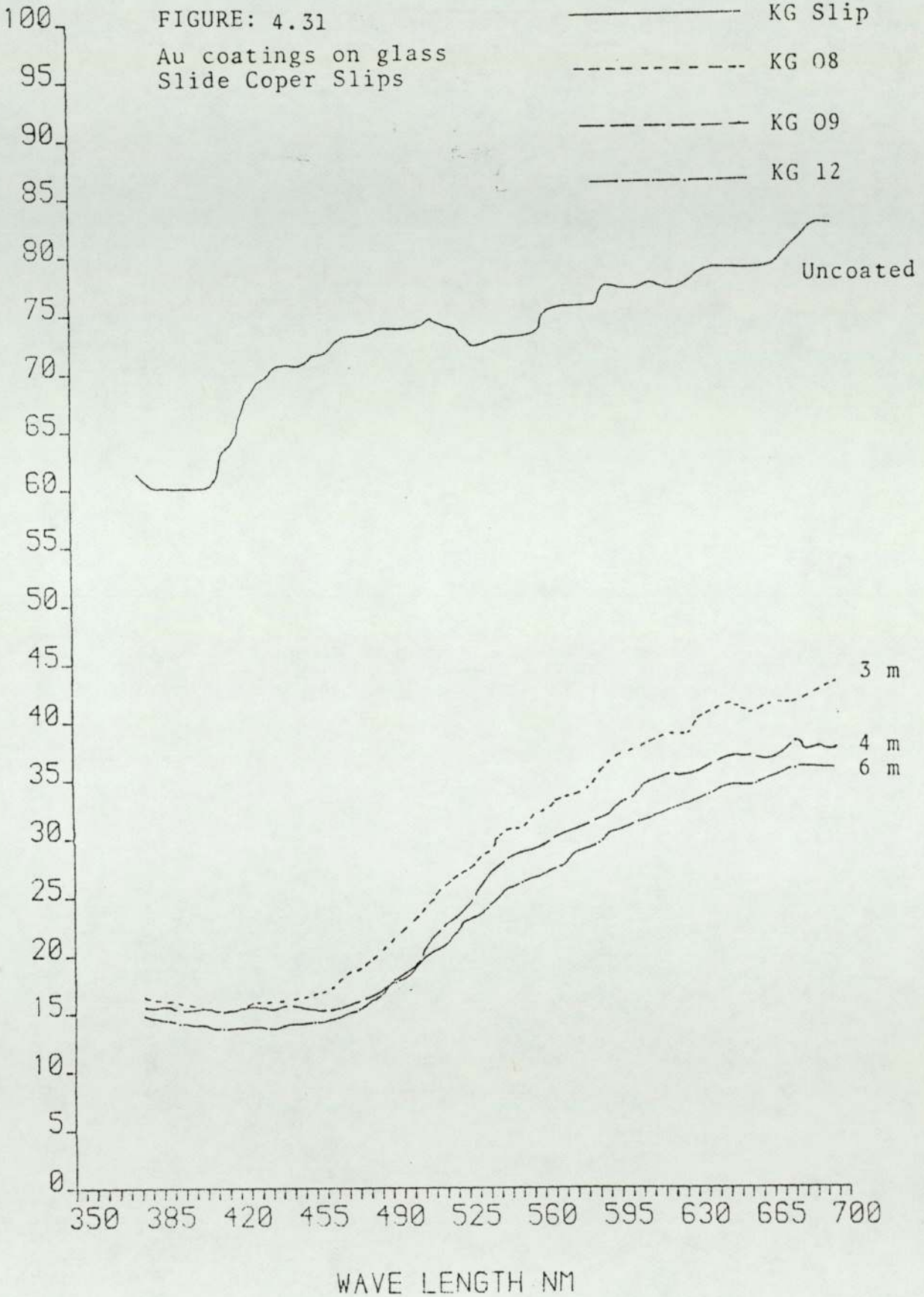


Reflectivity curves of a glass cover slip coated with gold for different length of time

FIGURE: 4.31

Au coatings on glass
Slide Coper Slips

- KG Slip
- KG 08
- KG 09
- KG 12



Reflectivity curves of a glass slip coated with gold for different length of time

Figure 4.32



Gold coating for 2 minutes of sputtering time on glass cover slip.

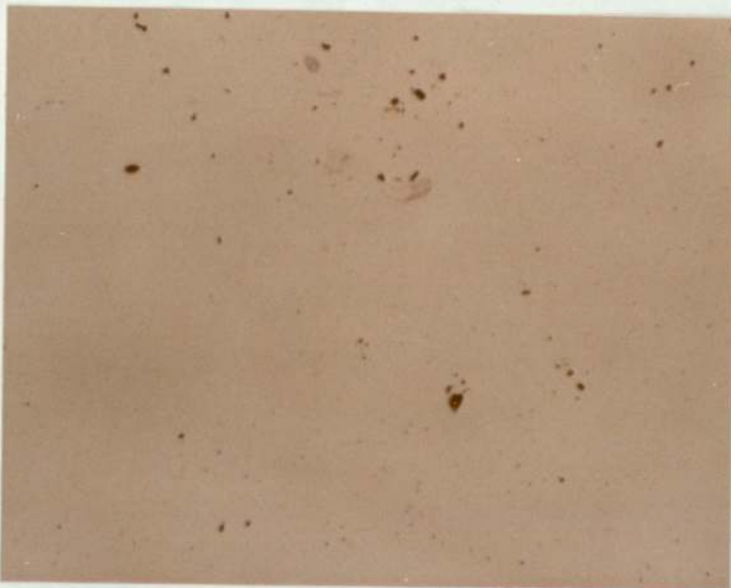


Gold coating for 3 minutes of sputtering time on glass cover slips.

Figure 4:33



Au coating for 4 minutes of sputtering time on glass cover slips.



AU coating for 5 minutes of sputtering time on glass cover slips.

series deposited on the glass cover slips were determined gravimetrically. The thicknesses and the colour co-ordinates (both at equi-energy and illuminant SA) are shown in Table 4.5 and 4.6. Gaps in the table are where a few of the specimens were damaged. The values of the thicknesses of the coatings obtained for different coating times for Series E and F are shown graphically in Figure 4.34. The figure indicates a linear relation between the thickness and coating time; the slopes differ and indicate the rate of deposition was different for the two series. The standard deviation on the measurements of mass of the glass cover slips was 6%; instrumental error was 9%; thus the uncertainty on the coating thickness is 11%.

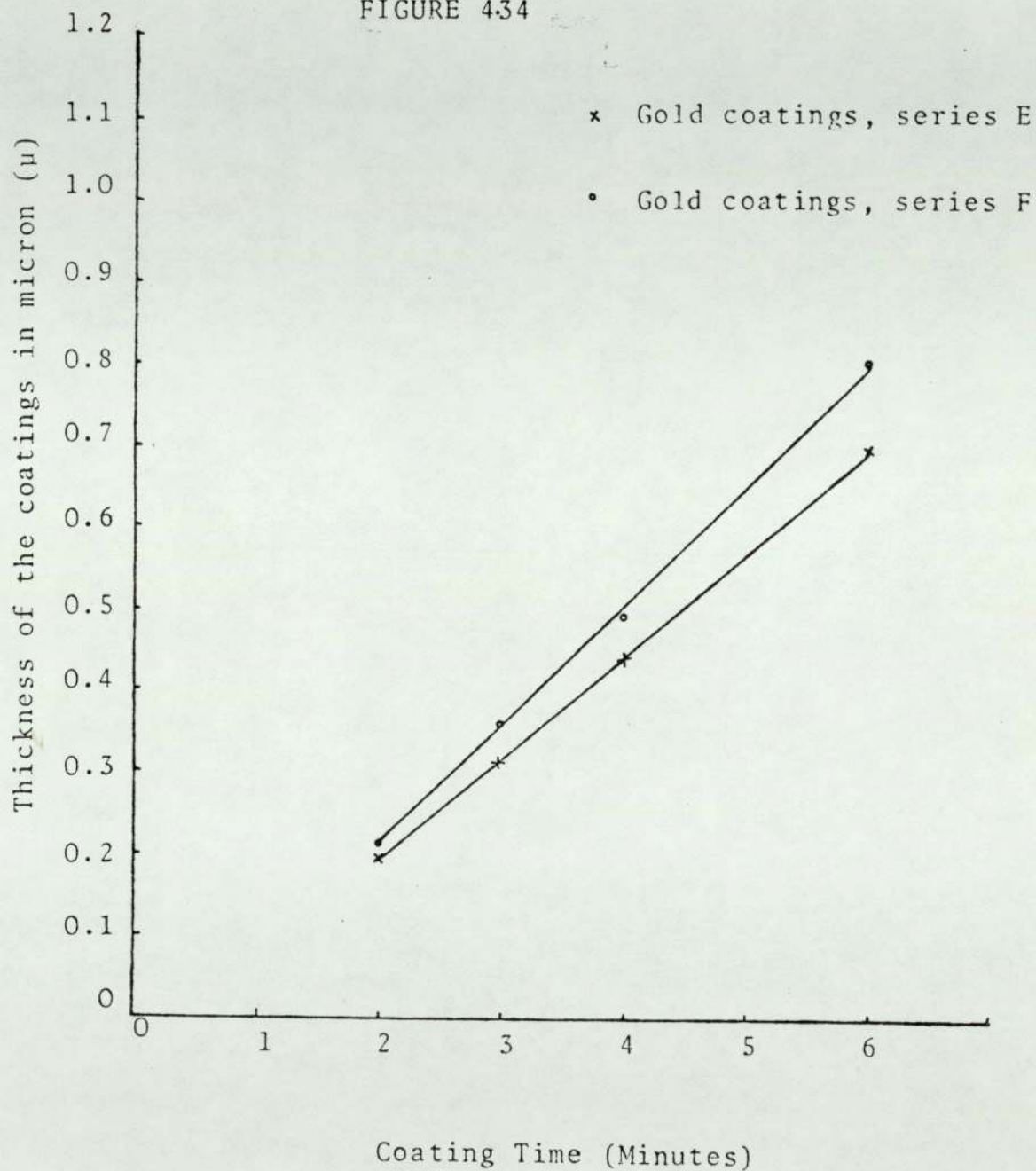
4.5.9 Influence of substrate composition on the colour of gold coatings

The colour co-ordinates of the gold coatings deposited on glass nickel, stainless steel and aluminium were determined at equi-energy EE, and plotted in Figures 4.35, 4.36 and 4.37. The reflectivity curves for the substrate materials and for each series of gold coated specimens were obtained from the computer output. These curves are shown in figures 4.38-4.43.

4.5.9.1 Influence of nickel

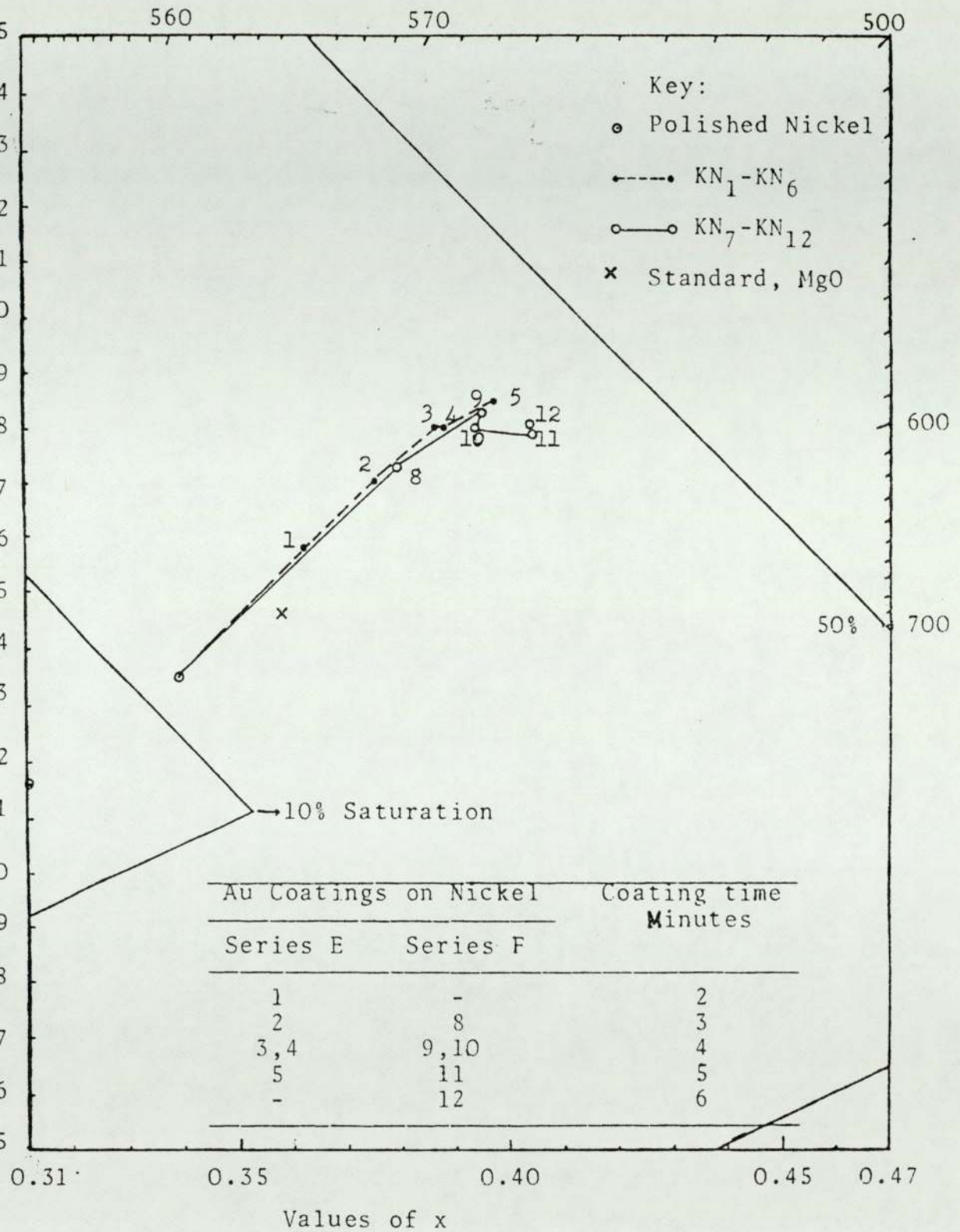
Figure 4.35 shows the colour co-ordinates of the gold coatings on nickel substrates for both series. Broken and unbroken lines have been drawn connecting the co-ordinates and show the increasingly yellowish hue with thickness of gold. The dominant wavelength is

FIGURE 434



Reproducibility of the Au coating for the same length of time

FIGURE 4.35



Colour co-ordinates of the gold coatings on polished Nickel

Au coatings series F

Thickness of Au coat- ings	Coatings on Glass		Coatings on Nickel		Coatings on Stainless Steel		Coatings on Aluminium										
	EE	SA	EE	SA	EE	SA	EE	SA									
									Time Minutes	Thick- ness μm	Time Minutes	Thick- ness μm	Time Minutes	Thick- ness μm	Time Minutes	Thick- ness μm	
Blank	Nil	0.342	0.454	0.408	.339	.335	.453	.405	.338	.337	.454	.405	.328	.327	.443	.404	
2m	0.23	.357	.382	.459	.42	.362	.358	.470	.421	-	.469	.415	.352	.352	.462	.413	
3m	0.37	.366	.399	.484	.414	.375	.370	.479	.420	.361	.356	.477	.416	.363	.365	.418	
4m	0.48	-	-	.487	.414	-	.487	.421	.372	.367	.487	.419	.381	.382	.481	.423	
5m	-	.372	.384	.495	.410	.388	.379	.488	.420	.386	.377	.481	.419	.391	.384	.489	.422
6m	0.81	.361	.370	.493	.418	.397	.385	.495	.421	.395	.384	-	-	-	-	-	-

between 580 and 583nm. Two points exceptionally have a reddish influence on colour. The brightness of the coatings is between 25% to 41%. The reflectivity curves in figures 4.38 and 4.39 show the detailed characteristics of the coatings. It can be concluded for the two specimens in Figure 4.39 that the higher reflectivity at the lower end of the energy spectrum produces the reddish influence on the coatings.

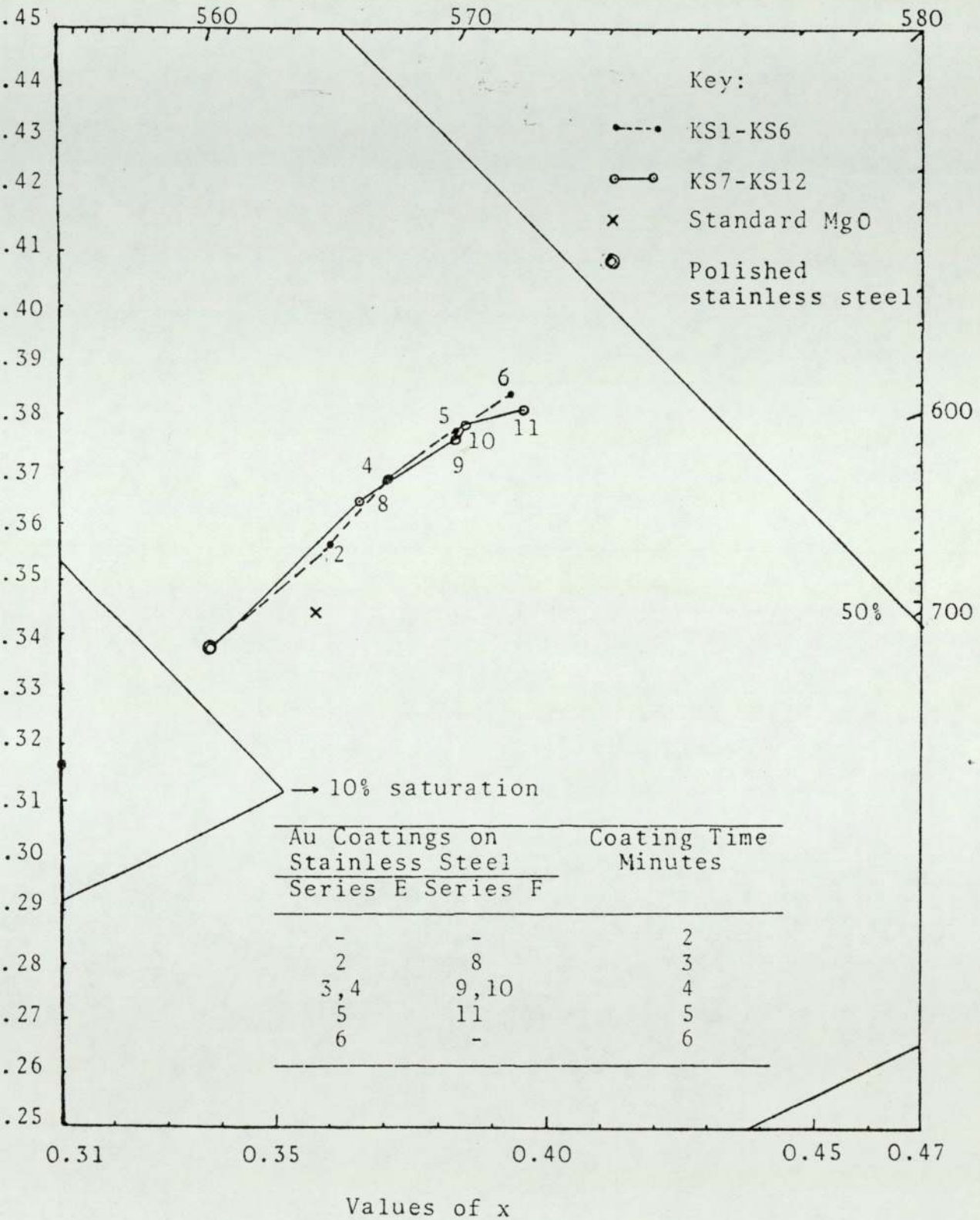
4.5.9.2 The influence of stainless steel

Figure 4.36 shows that the polished stainless steel substrate and the gold coated stainless steel have the similar colour co-ordinates to nickel and gold coated nickel (Figure 4.35). With stainless steel the substrate, the trend is an almost linear increase to the yellow colour with increasing thickness of gold. The same progressive change to yellow is observed in the reflectivity curves for all of the coatings on stainless steel (Figure 4.40 and 4.41).

4.5.9.3 Influence of aluminium

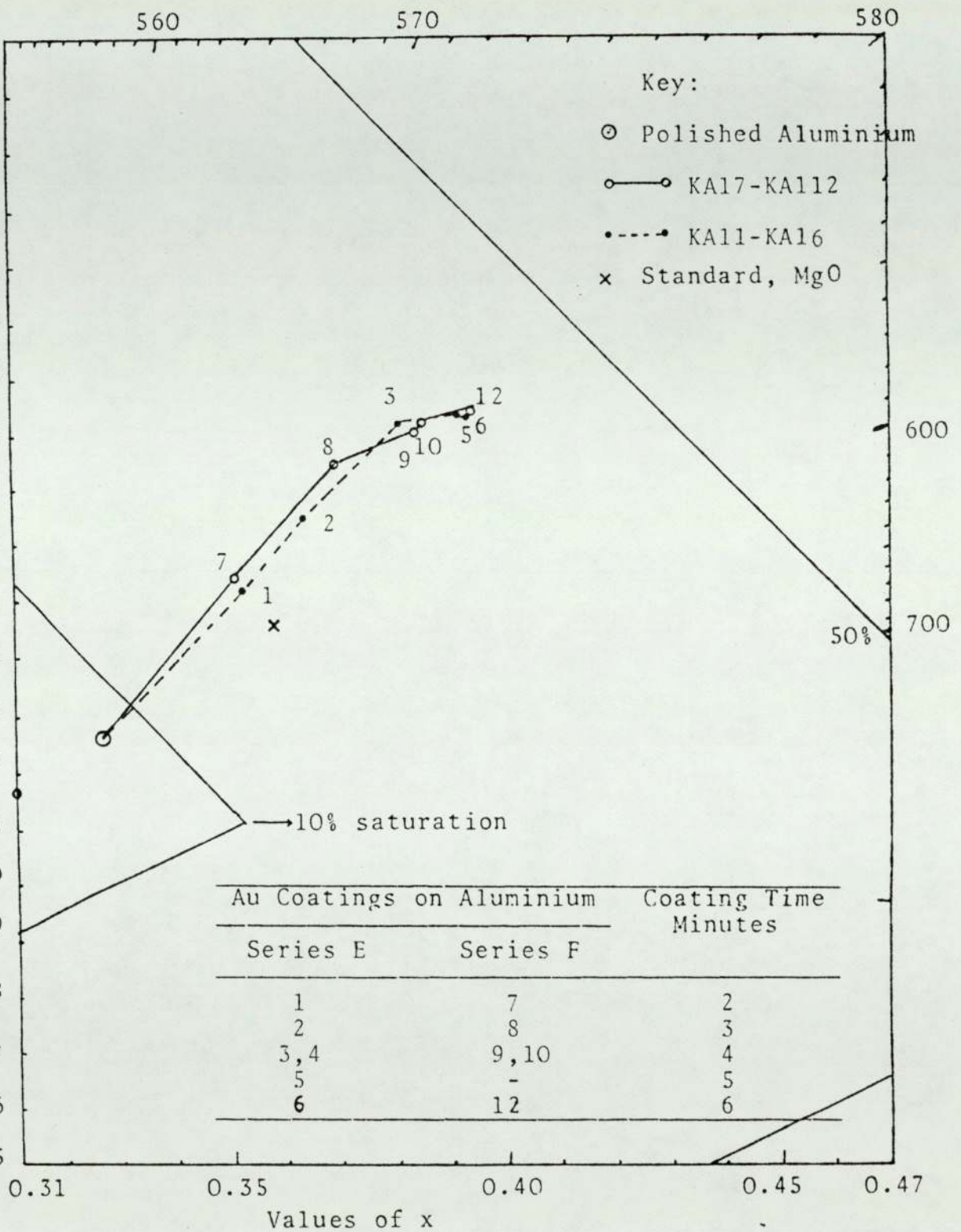
The colour co-ordinates for gold on aluminium for both series are plotted in Figure 4.37. The surface colour of aluminium is whiter (7% brightness) than nickel and stainless steel (15% brightness). The colour co-ordinates show an increasing trend to the yellowish hue with the dominant wavelength between 577nm and 579nm and the saturation/brightness of the coatings is between 21% and 40.5%.

FIGURE 4.36

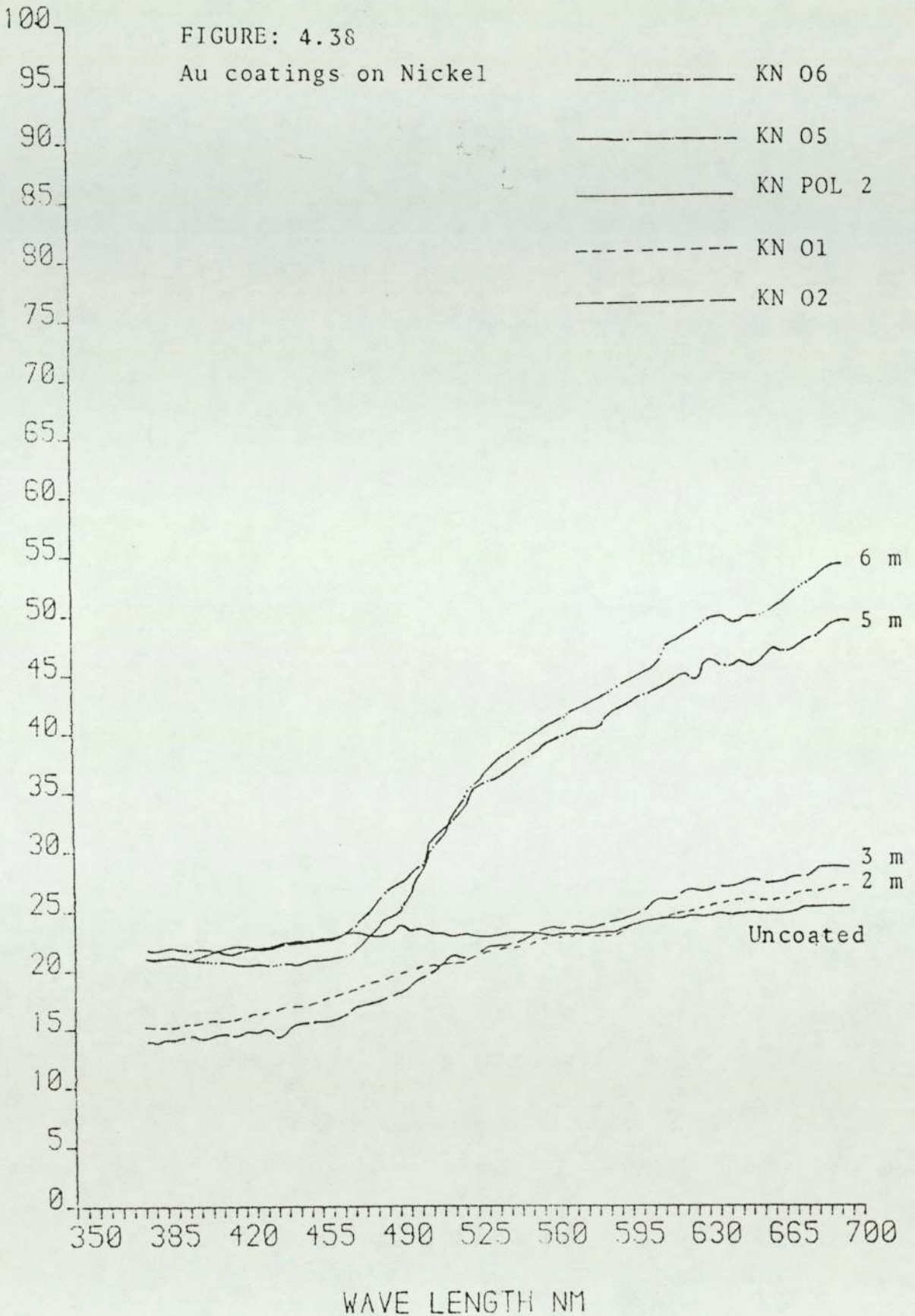


Colour co-ordinates of gold coatings on polished stainless steel

FIGURE 4.37



Colour co-ordinates of gold coatings on polished aluminium

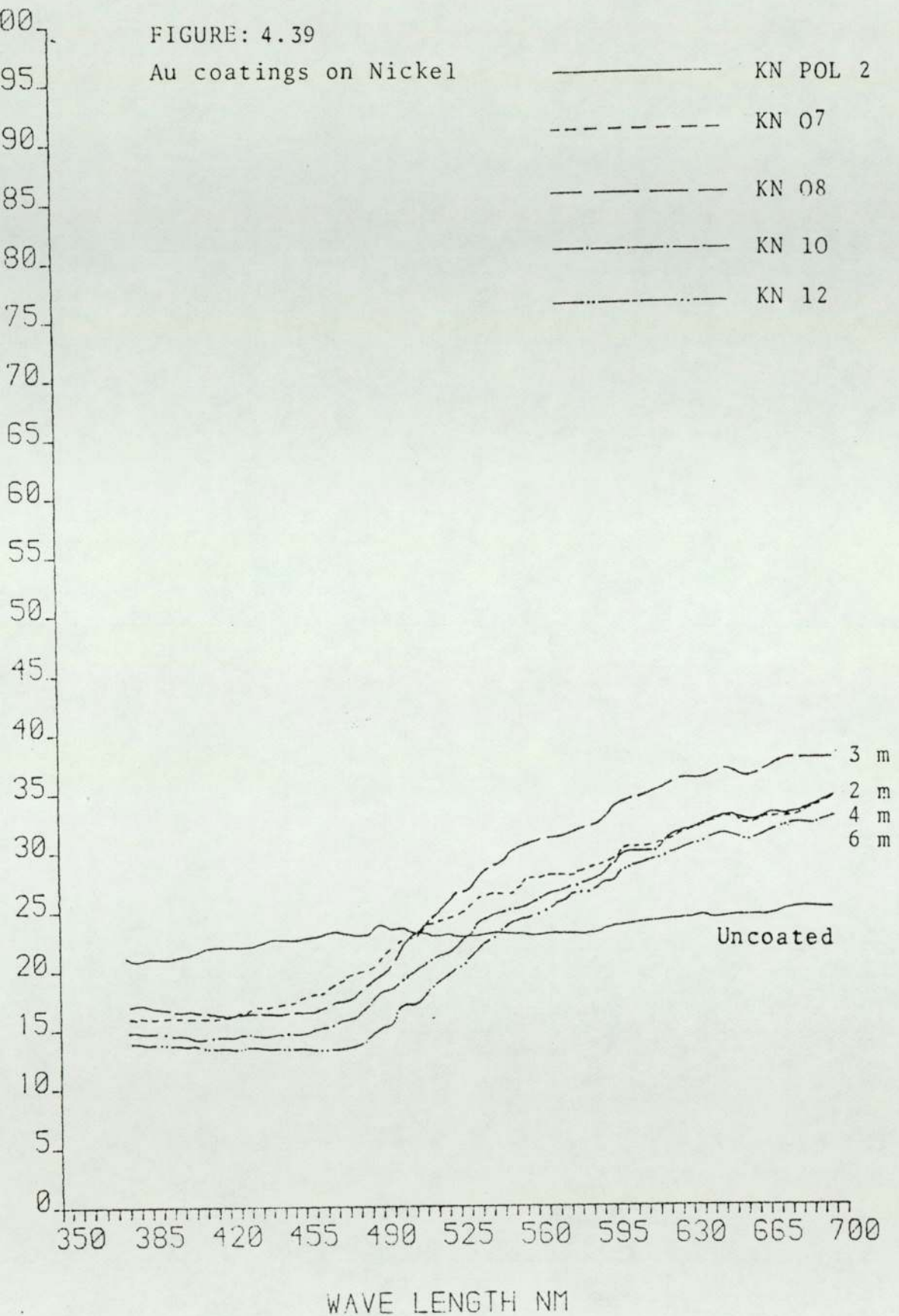


Reflectivity curves of a nickel substrate coated with gold for different length of time

FIGURE: 4.39

Au coatings on Nickel

- KN POL 2
- - - - KN 07
- · - · KN 08
- · - · KN 10
- · - · KN 12

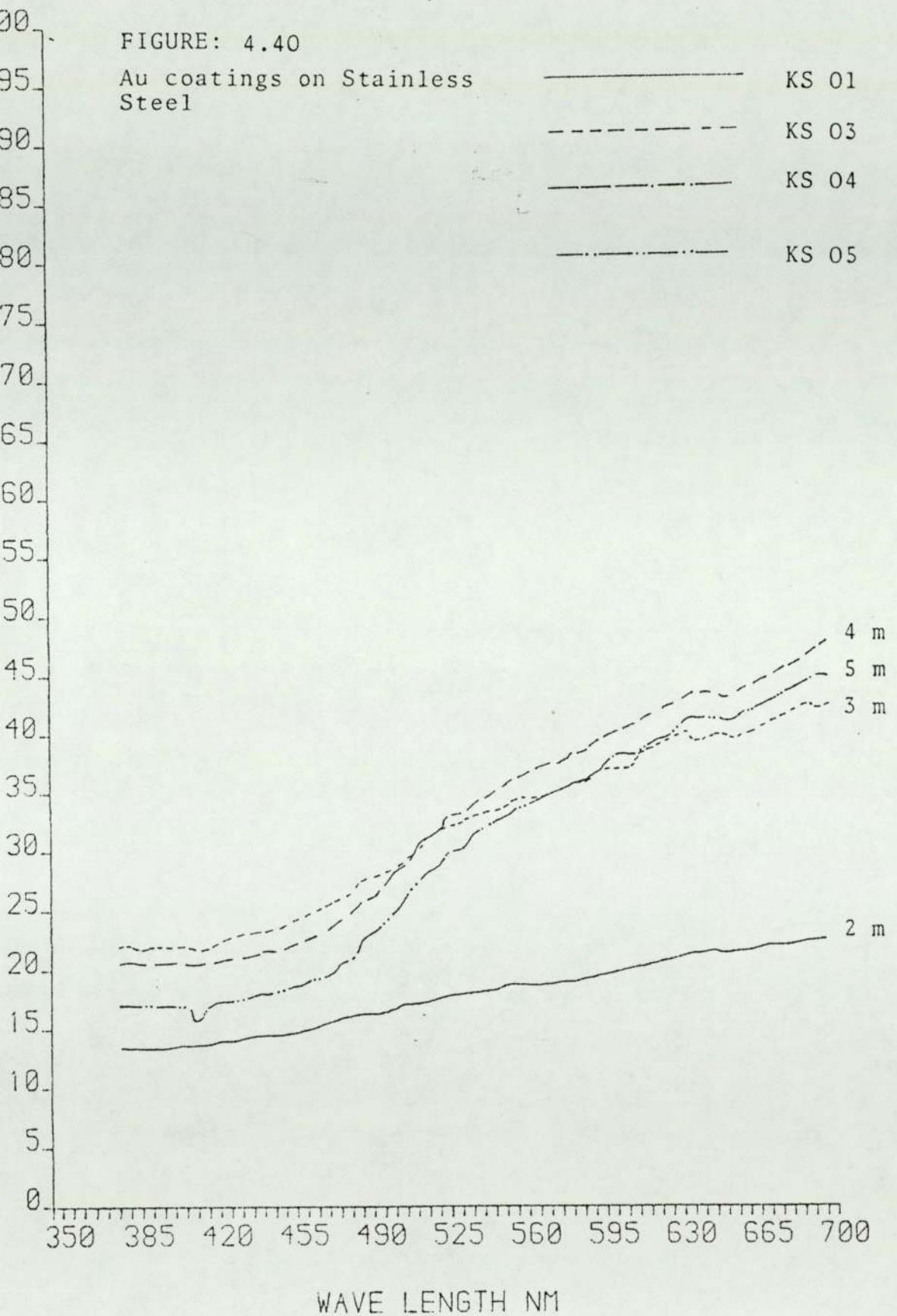


Reflectivity curves of a nickel substrate coated with gold for different length of time

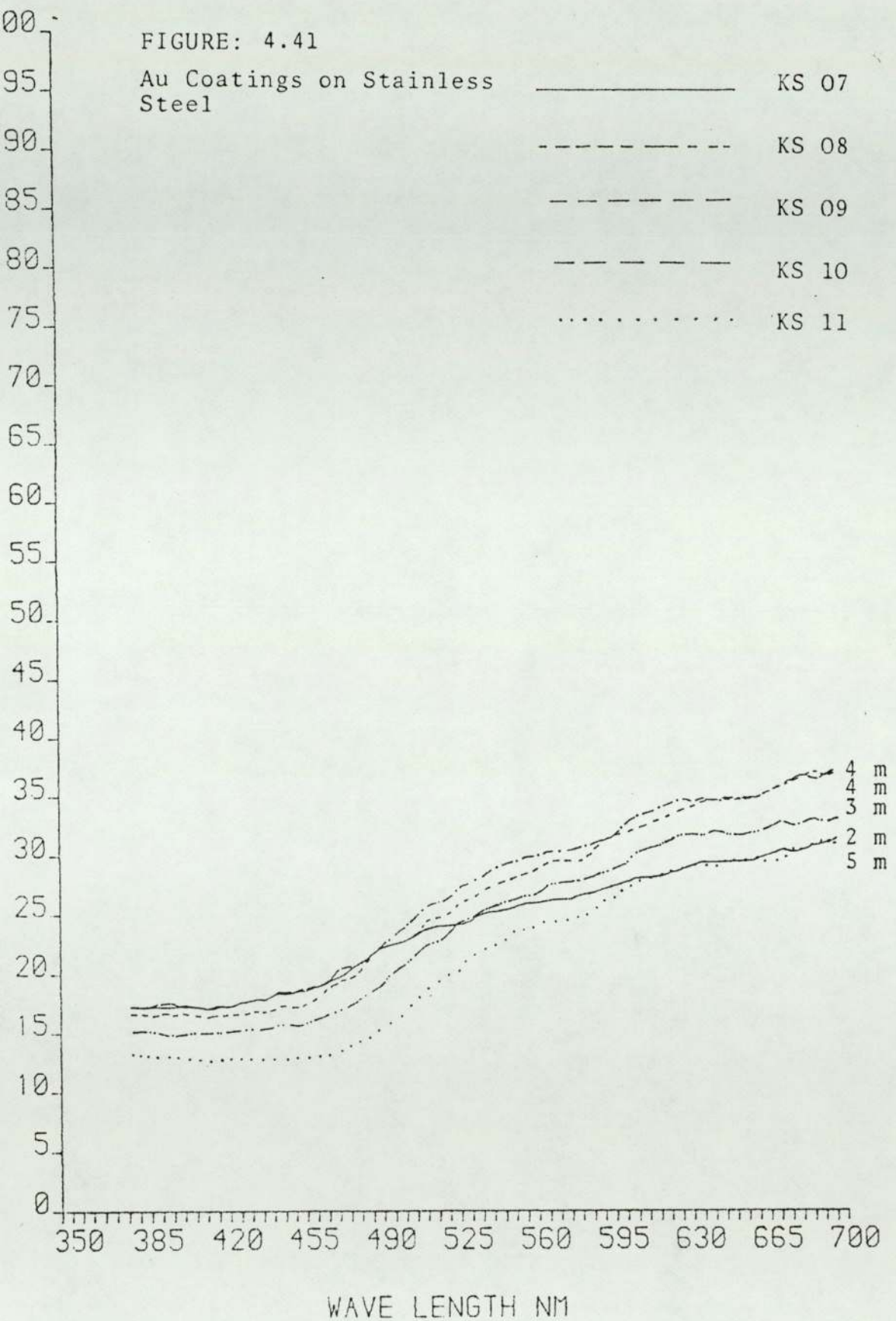
FIGURE: 4.40

Au coatings on Stainless Steel

- KS 01
- - - - - KS 03
- · - · - KS 04
- - - - - KS 05



Reflectivity curves of a stainless steel substrate coated with gold for different length of time



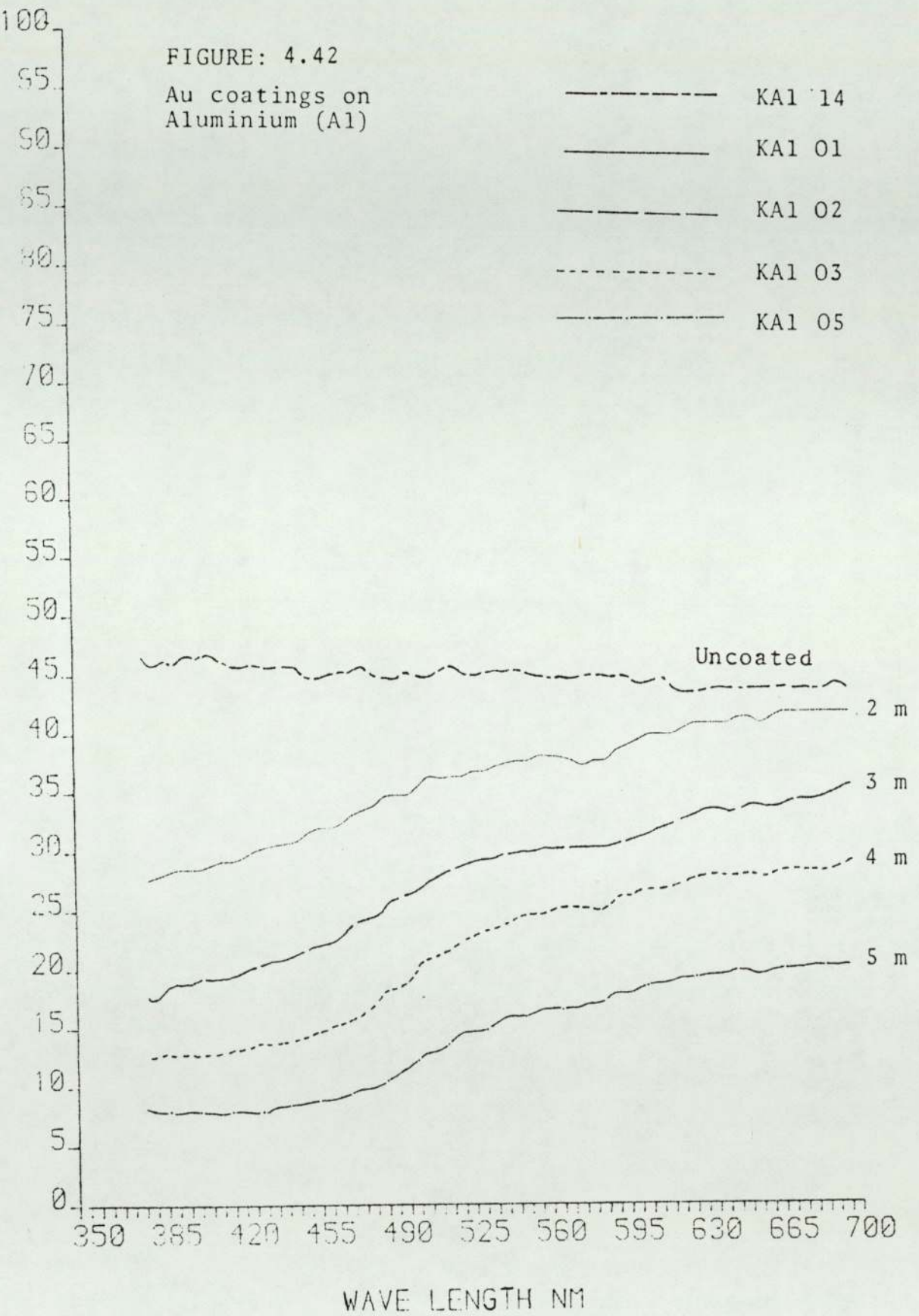
Reflectivity curves of a stainless steel substrate coated with gold for different length of time

The colour co-ordinates of the white standard (AnalaR MgO) are plotted as each diagram for comparison. The white standard has a 20% brightness at a dominant wavelength of 585nm.

The influence of surface roughness of the aluminium substrate on the colour of gold coatings was examined. The reflectivity curves of abraded aluminium specimens are shown in Figures 4.42 and 4.43. The curves show a slight green influence compared with bluish white polished aluminium.

FIGURE: 4.42
Au coatings on
Aluminium (Al)

- KA1 14
- _____ KA1 01
- KA1 02
- KA1 03
- KA1 05

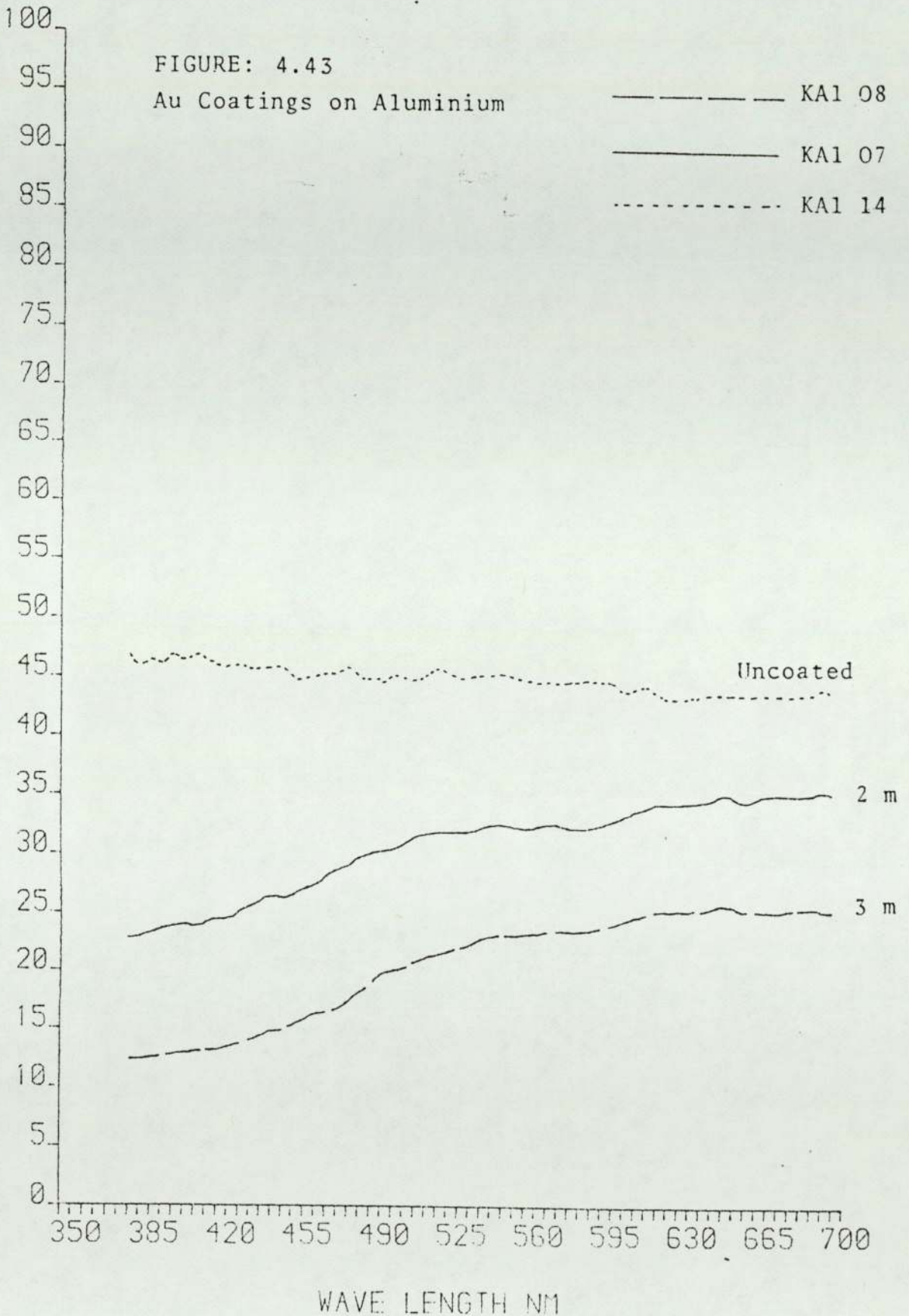


Reflectivity curves of an aluminium substrate coated with gold for different length of time

FIGURE: 4.43

Au Coatings on Aluminium

----- KA1 08
————— KA1 07
- - - - - KA1 14



Reflectivity curves of an aluminium substrate coated with gold for different length of time

Chapter 5

Discussion and Conclusions

5.1 Discussion

5.1.1 Thin coatings; techniques and methods

The techniques and methods used in this study were used to produce thin gold coatings based on recent developments published in the relevant literature. Various workers (52, 53) have reviewed coating techniques.

Sputtering takes less time, less room, less material, less energy and a lower initial investment than other processes. Spalvins (52) has shown the capabilities to form new layers of materials using ion-plating and sputtering. He has established great flexibility by forming graded composition interfaces. Bucklow (44) and Bessot (51) have also described various deposition techniques and discussed their merits and disadvantages.

Cathodic sputtering has been employed in the present study. Although the precise coating rate was undetermined, the sputtering rate seems to be higher in the present study, as estimated from the thickness coating time results than the rate reported by Bessot (51) which for gold was $5.4\mu\text{m}/\text{hour}$ or $0.09\mu\text{m}/\text{minute}$.

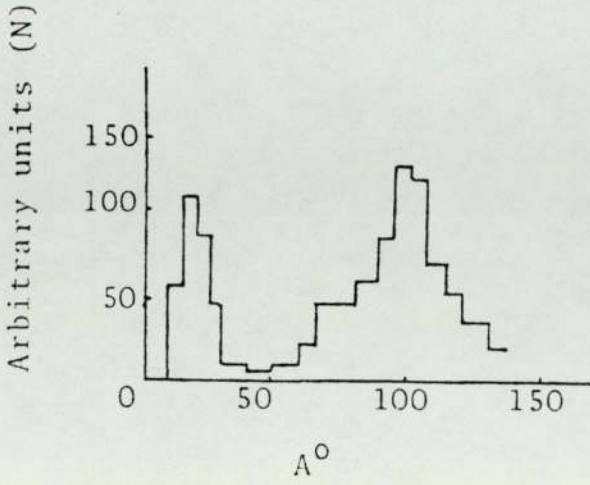
5.1.2 Thickness measurement

Although Ogburn et. al. (13) estimated uncertainty of about $0.06\mu\text{m}$ for the thickness measurement of the thin coatings using scanning electron microscopy at a magnification of 10K and Borziak et. al. (100) have reported the possibility of measuring thicknesses of $30\text{-}60\text{\AA}$ gold coatings, scatter of 26% was seen in the thickness measurements for gold coatings in the present study, using SEM photomicrographs. Gravimetric and electrical conduction methods were also adopted to measure the thicknesses of the gold coatings in the present study and a thickness of $0.064\mu\text{m}$ was measured with an uncertainty of 9%. P.G. Borziak et. al. (100) plotted histograms of initial island sizes and inter-island spacings (Figures 5.1 and 5.2) for the islands nucleated in the initial stages of forming coatings and showed inherent reasons for the inaccuracy of thickness measurement of thin coatings. The gravimetric method is considered to be the most convenient and useful with an accuracy of 11%. Brown (94) also selected this method for thickness evaluation.

5.1.3 Colour measurement

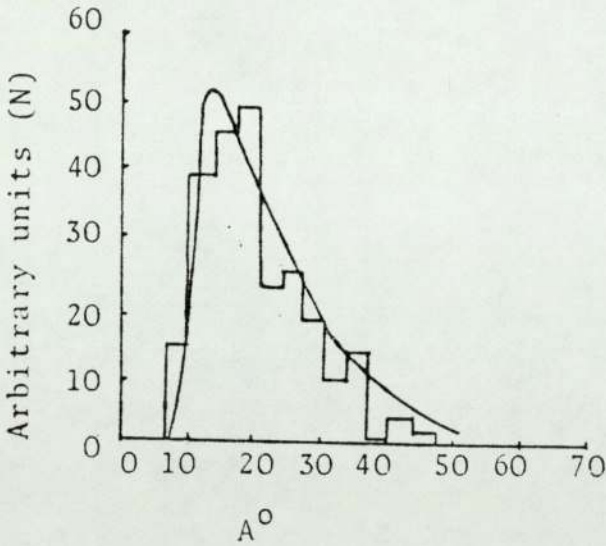
The intrinsic colour of thin gold coatings was determined employing glass cover slips. The gold coatings on such glass slips were also used to determine their thicknesses employing both gravimetric and electrical resistance methods. The influence of the substrate material was determined and compared using nickel, stainless steel and aluminium. The colour co-ordinates of the uncoated surfaces

FIGURE 5.1



Histogram of the Island size in a typical coating

FIGURE 5.2



Histogram of the inter-island spacing

were also determined and compared with the white standard which was AnalaR MgO. A comparison of results is made with other workers in Table 5.1. The colour co-ordinates for the coatings obtained for the maximum coating time on nickel in the present study are same as the values obtained by Gardam (2) for pure gold. It is seen that the colour co-ordinates for stainless steel are higher in the present study whereas the values for polished nickel are 1% lower than those of Gardam (2). Our values for polished aluminium are higher than his values obtained on evaporated coatings of aluminium. The values of Brown (94) for rolled aluminium are high compared with those of ours and those of Gardam (2), but the condition of the surface must be considered and these were not alike. Similarly the colour co-ordinates of the polished nickel of Brown (94) are higher than those of ours. Her values for the electroplated gold coating deposited in five seconds at a current density of 25 a.s.d. at a temperature of 65°C in $K Au (CN)_2$ both are lower than those of ours and Gardam (2). Reasons for the differences include differences in thickness distribution and surface condition of the substrate. Roberts et. al. (3) also determined the colour co-ordinates of gold (99.99%) and obtained lower values than all others reported. Considering the 11% scatter inherent in the coating method and the thickness measurements the results achieved in the coatings are reasonable and if the values of Gardam (2) are taken as standard for the colour co-ordinates of pure gold, then our values can be treated with confidence and show the trend of colour change with increasing waiting thickness.

Table 5.1

No.	Materials	Present study		Study by G.E. Gardam(2)		Study by G. Brown (94)	
		Colour Co-ordinates		Colour co-ordinates		Colour co-ordinates	
		x	y	x	y	x	y
1	Al polished sheet	0.328	0.327	-	-	-	-
2	Evaporated Al	-	-	0.332	0.331	-	-
3	Rolled Al film	0.333	0.335	-	-	0.344	0.342
4	Polished nickel	0.339	0.335	0.344	0.342	0.329	0.328
5	Gold (fine 99.99%)	0.378*	0.377*	0.394	0.385	-	-
6	Gold (coatings) on nickel	0.397	0.385	-	-	0.389	0.374
7	Gold (coatings) on glass	0.397	0.378	-	-	-	-
8	Electroplated (gold coatings)	-	-	-	-	0.389	0.374
9	Silver discs	-	-	0.337	0.336	0.321	0.321
10	Stainless steel	0.338	0.337	0.335	0.334	-	-

* Values of E.F.I. Robert et. al. (3)

5.2 Conclusions

- (1) A reproducibility of 89% can be achieved using the vacuum deposition techniques to produce thin coatings of gold. Strict control of the operating parameters, working conditions and the surface conditions of the substrate are essential.
- (2) The chromaticity co-ordinates (colour co-ordinates) of the coatings are very much dependent of the surface condition and composition of the substrate.
- (3) The average thickness of thin gold coatings is a difficult method and is most conveniently determined gravimetrically. The scanning electron microscope is useful in showing the heterogeneity of thin coatings.

5.3 Suggestions for further work

- (1) It has been shown that the colour of gold coatings thinner than $1\mu\text{m}$ depends on the surface roughness and composition of the substrate. A systematic study of the influence of substrate composition on colour of thin coatings is now needed to gain insight into the physical behaviour of light in films thinner than $1\mu\text{m}$.
- (2) To improve the reproducibility of sputtering the development of microprocessor control of the sputtering conditions is required.

(3) Colour measurement was carried out using a spectrophotometer and laboriously transferring data to a computer programme to calculate the colour co-ordinates. It is timely to develop microprocessor control for the entire process and produce an instrument capable of determining the colour co-ordinates and presenting the calculated co-ordinates as direct readings.

References - Part I

1. J.C. Maxwell Garnett
Colours in metal glasses and in metallic films.
J. Philosophical transaction, 1904, 203, 385.
2. G.E. Gardam
The colours of some metals and alloys, Trans. Inst.
of Met. Fin., 1966, 44, 186.
3. Errol F.I. Roberts and Keith M. Clarke
The colour characteristic of gold alloys
Gold Bulletin, 1979, 12, 9.
4. Peter Sigmund
Theory of sputtering (Ion sputtering yield of amorphous and
polycrystalline targets).
Phys. Rev. 1969, 184, 383.
Erreta, Phys. Review, 1969, 187, 768.
5. J.A. Thornton
Structure of evaporated films.
Annual review of Met. Science, 1977, 7, 239.
6. M.G. Hall and W.B. Hutchinson
Smooth surface metallography using scanning electron
microscope
The metallurgist, 1980, 12, 371.
7. Seager, K.E. and Rodies, J.
The colour of gold and its alloys, the mechanism of variation
in optical properties.
Gold Bulletin, 1979, 12, 10.
8. W.D. Wright
The measurement of colour
(Hilder, London) 4th ed. 1969.

9. C. Hardy
Handbook colorimetry
The MIT Press (Massachusetts Institute of Technology), 1966.
10. P.J. Bouma
Physical aspect of colour
Second edition, Philips Technical Library, 1971.
11. F.W. Clulow
Colour its principles and application
Foundation Press, London, 1972.
12. M. Robert Pinnel,
Diffusion related behaviour of gold in thin film systems.
Gold Bulletin, 1979, 12, 62.
13. F. Ogburn and D. Ballard
Thickness of gold coating measured with a calibrated SEM.
Plating and surface finishing, 1980, 67(4), 49.
14. E. Beraha
Colour metallography
American Society for metals, 1980, 133.
15. B.A. Philpott,
Design Engineering Handbook
Metals product journal Ltd., 1961.
16. Antonin Vasicek
Optical study of a thin absorbing film on a metal surface
Symposium Proceedings, Washington, 1963 (Mis. Publication 256)
17. J.M. Blakely
Surface physics of materials.
Vol.1, Academic Press, 1975.
18. K.H. Behrndt
Thin films
Seminar of the American Society for metals, 1963.

19. P.J. Boume
Physical aspects of colour
Philips Technical (sec. edition), 1971.
20. A. Mark
Growth of single crystal overgrowth on silicon substrate
J. Electrochem. Soc., 1960, 107, 568.
21. C.F. Powell I.E. Campbell and B.W. Gonser
Vapourplating
John Wiley & Sons (1955).
22. W.R. Grove
Phil. Trans., 1852, B142, 87.
23. J. Plucker
Pogg Ann, 1858, 103, 88.
24. G.K. Whener
'Physical sputtering'.
Proc. 5th Int. Conf. Ionic Phenomena in gases, Munich, 1961.
North Holland Pub. Co., Amsterdam, 1962, p.1141.
25. D. Rosenberg and G.K. Wehner.
Sputtering yields for low energy He^+ , Kr^+ , Xe^+ ion bombardment
J. Applied Phys., 1962, 33, 1842.
26. G.K. Whener
Sputtering by ion bombardment.
Adv. Electron Physics, 1955, 7, 239.
27. L. Holland
Vacuum deposition of thin films
John Wiley & Sons, New York, 1956.
28. H.S.W. Massey and E.H.S. Burhop
Electrons and ion impact phenomena.
Oxford Univ. Press, London, 1956.

29. E. Kay
Impact evaporation and thin film growth in a glow discharge.
Adv. Elect. Physics, 1962, 12, 245.
30. S.P. Wolskey
Sputtering mechanisms.
Trans. 10th Natl. vacuum symposium 1963 Mac. Co., New York, p.309.
31. M.H. Francombe
Preparation and properties of sputtered films.
Trans. 10th Natl. Vac. Symposium, 1963, Mac., New York, p.316.
32. N. Schwartz
Reactive sputtering.
Trans. 10th Natl. Vacuum Symp., 1963, Mac. Co., New York, p.325.
33. A.T. Vagnamyan and Z.A. Solva'eva
Technology of electrodeposition.
R. Draper Ltd., Teddington, 1961.
34. A. Brenner
Electrodeposition of alloys - principles and practice.
Vol.1, Academic Press, New York, 1963.
35. I.W. Wolf,
Electrodeposition of magnetic materials.
J. Appl. Phys, 1962, 33, 1152.
36. R. Nahrwold
Wied Ann, 1888, 31, 469.
37. R. Kundt
Wied Ann, 1888, 34, 469.
38. R. Pohl and P. Pringsheim.
Verhandle Deut Physik Ges, 1912, 14, 506.

39. K.H. Behrndt
The influence of the deposition parameters on the properties of evaporated thin ferromagnetic films.
Trans. 8th Nat. Vacuum Symp. 1961, Pergamon Press, London, 1962, 912.
40. K.H. Behrndt
The influence of the deposition conditions on growth and structure of evaporated films.
Vacuum, 1963, 13, 337.
41. P. Drude
Wildeman
Ann. Phys., 1889, 36, 884, 886.
42. British Standard Institute (B.S. 1611: 1953)
43. Commission Internationale de L'Eclairage (C.I.E.).
44. I.A. Bucklow
Surfacing journal.
Oct., 1977, 3, Physical vapour deposition techniques.
45. D.M. Mattox
Mechanisms of ion plating.
Proceeding Int. Conf. on Ion Plating and Allied Techniques, London, 1979.
46. Klaus H. Behrndt
Thickness uniformity on rotating substrates.
Trans. 10th Natl. Vacuum Sympos., 1963.
Macmillan Co., New York, 1963, 379.
47. W. Hallenthal
Thickness and temperature dependance of the coercive force of thin evaporated nickel films, measured by the change of magneto-resistance.
Z. Naturforsh, 1959, 14A, 772.

48. K.H. Behrndt,
Investigation of the coercive forces of Ni and Ni-Fe films
during evaporation.
J. Applied Physics, 1962, 33, 193.
49. J.W. Dini and H.R. Johnson
The properties of gold deposits produced by D.C. pulse and
asymmetric
Gold Bulletin, 1980, 13, 31.
50. J.W. Dini
Gold plating in the electronic industry.
Gold Bulletin, 1979, 12, 159.
51. J.J. Bessot
New vacuum deposition techniques.
Metal finishing, 1980, 78(3), 21.
52. T. Spalvins
Industrial potential uses and performance of sputtered and
ion plated films.
Metal finishing, 1980, 78(1), 17.
53. Why sputter when you can plate?
Plating and surface finishing, 1980, 67(6), 20.
54. Design and finishing capabilities.
Plating and surface finishing, 1980, 67(1), 14.
55. Nanotech, NQC1 (digital film thickness monitor)
Electrotechm, P1001, conductance monitor (deposition process
control).
56. S.P. 800D spectrophotometer manual p.1.1-1.3 and
S.P. 890 diffuse reflectance accessory, Sec. 14 accessories
14-16-1.
57. M.P. Givens
Optical properties of metals.
Solid State Physics, 1958, vi, 313.

58. O.S. Heavens
Thin film physics.
Methuen and Company Limited, 1970.
59. A. Blair
The electrodeposition of precious metals in the electronic industry.
Galvano Tech., 1978, 29(6), 97.
60. H. Silman, G. Isserlis and A.F. Averill
Finishing Publications Ltd., (Proc. Conf.),
28 High St., Teddington, Middlesex, U.K., 1978 (MET A 7907-720185), p.584.
61. M.M. Barker
P.P.G. Industries Inc., AES Coatings for gold solar collectors.
Proc. Conf. 1976 (MET A 7907-720184), 51.
62. E.W. Williams
Gold ion plating
Gold Bull., 1978, 11(2), 30.
63. B.B. Knapp
Research and decorative coatings
Plat. Surf. Finishing, 1978, 65(8), 24.
64. T. Spalvins
New application of sputtering and ion plating.
ASME paper, 1978, 77 - Dec. 21, 9.
65. F.L. McCrackin, E. Passaglia, R.R. Stromberg and H.L. Steinberg
Measurement of the thickness and reflective index of very thin films and the optical properties of surfaces by ellisometry.
J. Res. Nat. Bur. Std., 1963, 67A, 363.
66. B. Borie and C.J. Sparks Jr.
A determination of thin oxide film thickness by integrated intensity measurements.
Acta Cryst., 1961, 14, 569.

67. L. Missel and N.S. Platakis.
Wet and vacuum coating processes.
Met. finishing, 1978, 76(9), 65.
68. N. Platakis and N.L. Missel
A comparison of technology and products.
Met. Finish, 1978, 76(8), 56.
69. J.L.Hughes
Scale up problems in electron beam evaporation and sputtering.
J. Vac. Sci. Tech., 1978, 15(4), 1572.
70. J.A. Thornton
Recent development in sputtering.
Met. Finish, 1979, 77 (4), 45.
71. S. Betz
Alloy sputtering.
Surf. Sci., 1980, 92(1), 283.
72. L. Holland and S.K. Bateman
A low pressure evaporation plant for rapid operation.
Trans. 8th Natl. Vacuum Symp., 1961.
Pergamon Press, London, 1962, 1201.
73. L. Holland
A new apparatus for cathodic sputtering
Nature, 1956, 177, 1229.
74. M.P. Seah
Thin solid films, 1981, 81, 279.
75. S.A. Schwarz and C.R. Helms,
J. Vac. Sci. Technol., 1979, 16, 781.
76. S. Hofman
Surface interface anal., 1980, 2, 148.
77. R.E. Honig
Thin solid films, 1975, 31, 89.

78. K.E. Singer
Thin solid films, 1979, 57, 115.
79. J.E. Castle
Surf. Sci., 1977, 68, 583.
80. P.M. Hall, J.M. Morabito and J.M. Poate
Thin solid films, 1976, 33, 107.
81. P.M. Hall and J.M. Morabito
Surf. Sci., 1976, 54, 79.
82. M.P. Seah
J. Vac. Sci. Technol., 1980, 17, 16.
83. L.I. Moissel
Phys. Thin Films, 1966, 3, 61.
84. P.K. Rol, D. Onderlinden and J. Kistemaker
Trans. 3rd Int. Vacuum Congress, Stuttgart, 1965, Vol.I
Pergamon, Oxford, 1966, p.75.
85. G. Carter and J.S. Colligon
Ion bombardment of solids,
Heinemann, London, 1968.
86. G.K. Whener, in A.W. Czanderna (ed.)
Methods of surface analysis.
Elsevier, New York, 1975, p.5.
87. H. Oechsner
J. Appl. Physics, 1975, 8, 185.
88. N. Laegreid and G.K. Whener
J. Appl. Phys, 1961, 32, 365.
89. D. Rosenberg and G.K. Whener
J. Appl. Phys., 1962, 33, 1842.
90. C.H. Weijsenfeld
Philips Res. Rep., Suppl., 1967, 2.

91. A.L. Southern, W.R. Willis and M.T. Robinson
J. Appl. Phys., 1963, 34, 153.
92. F. Keywell
Phys. Rev., 1955, 97, 1611.
93. K.L. Chopra
Thin film phenomena
McGraw-Hill, New York, 1969.
94. G. Brown
The influence of composition on the optical properties of
electrodeposited gold.
Ph.D. thesis, Univ. of Aston in Birmingham, 1980.
95. J.E. Morris and T.J. Coutts
Thin solid films, 1977, 47, 3.
96. W.C. Granville and E.J. Jacobson
J. Opt. Soc. Am., 1944, 34, 382.
97. D.J. Nickerson
J. Opt. Soc. Am., 1940, 30, 575.
98. C.J. Gorter
Physica, 1951, 17, 777.
99. D.P. Seraphim
Electronic properties of thin films.
Thin films, American Society for Metals, 1963, 19-20, 135.
100. P.G. Berziak, Y.U.A. Kalyupin, L.A. Rudakovskaya and R.D.
Fedorovich.
Thin solid films, 1981, 81, 137.
101. G.A. Candela, K.F. Galloway and Y.M. Kiv.
Thin solid films, 1981, 82, 183.
102. J.Vook,
Journal of Crystal growth, Netherlands 31975 Pt., 353.

Part Two

Thin coatings: hardness measurement and micro-indentation techniques

Chapter 6

Introduction

Hardness is a term having a different meaning to different people. It is 'resistance to penetration', to a metallurgist, 'resistance to wear' to a lubrication engineer, 'a measure of flow stress' to a design engineer, 'resistance to scratching' to a mineralogist and 'resistance to cutting' to a machinist. Although these several actions appear to differ greatly in character, they are all related to the 'plastic flow stress' of the material.

There are various hardness test procedures. These include: static indentation tests, scratch tests, cutting tests, ploughing tests, rebound tests, damping tests, abrasion tests and erosion tests. The values of hardness obtained by different methods are to some extent related to each other. A few of the hardness test methods are described in chapter seven.

In the present study of micro-indentation testing, phenomenological characteristics of micro-indentation behaviour are outlined in chapter eight; the load dependence of hardness is also discussed. The modifications to the micro-manipulator and the design of an indenter and holder for micro-indentation testing are described in chapter nine.

A method of making very sharp pointed tungsten tips was developed for the production of microindenters. The micro-indenters

produced were evaluated on aluminium and brass specimens.

The reproducibility in making these tips was examined and various other factors in preparing the micro-indenters were investigated.

The reproducibility of micro-indentations made with the modified micro-indenter was also assessed. The tester was tested after being installed within the stereoscan SEM (66). It was compared with the Vickers (65) micro-hardness tester on aluminium and brass specimens.

Conclusions and suggestions for future work are given in chapter ten.

Chapter 7

Methods of hardness testing and micro-indentation

7.1 Introduction

The hardness of a metal is one of its properties and one that can be compared with the hardness of well known standard hard materials. Serious attempts were made to produce a comparative scale of hardness values of materials as early as 1722 with a series of minerals (5) in a scratch test.

The hardness of a metal is related to the other properties of the metal. Since it is not a single property but a complex integration of properties it is useful in assessing the influence of chemical and structural heterogeneities, diffusion gradient, precipitates, eutectics, dendrites and grain boundaries. Due to the link between the mechanical properties and the hardness of the materials coupled with the ease and convenience of hardness testing, the measurement of hardness is widely used in science and industry.

The measure of hardness of a metal by indentation is similar to that of man's sense of softness or hardness on pressing or squeezing a material. Indentation of a material like clay or a solid metal deforms the material and leaves a permanent impression. The size of the indentation left on the specimen is a measure of its hardness.

7.2 Methods of hardness testing

There are various methods to produce differently shaped indentations for hardness testing, but whatever the shape, the indentations are geometrically similar to that of the indenters. Various indenters of differing shapes have been considered. They were used to investigate the relationship between indentation size and the hardness of the material. The following tests with differently shaped indenters have been developed and are in current use:

- (1) cone indentation tests.
- (2) the Rockwell test - 120° diamond cone.
- (3) Ball indentation tests.
- (4) Pyramid indentation tests.
- (5) Micro-indentation tests.

7.2.1 Cone indentation tests

A standardised cone indentation test is one of the attractive ways of measuring hardness. With a very small load on a flat surfaced specimen plastic flow is produced by the indent. Ludwick (14) used sharp steel and diamond cones having an included angle of 90° , with a very large load on iron. Devries in 1911, also carried out several cone tests and measured the movement of the indenter from the original surface during the application of the load.

The phenomena of elastic recovery and ridging in the specimen were

also considered. For soft metals like copper, aluminium, zinc and lead, the elastic recovery of the indentation impression (after the release of load) results in a change of size and shape of the impression. This property has also been studied by many authors (50,51).

Buckle (50) studied pyramid indenters and concluded that the diagonals of the indentation do not suffer from recovery effects and therefore do represent the indentation under load. Dlubek (51) studied the recovery and recrystallisation of plastically deformed $\alpha + \beta$ brass by the position annihilation technique and obtained detailed information about the recovery process for a two phase alloy. The important practical consideration so deduced was that the depth measurements of recovered indentations are much more unreliable than the width (diagonal or diameter in the case of a ball indentation test) measurement. The effects of the cone angle and friction have also been studied (52, 53, 54, 55) and led to the conclusion that 90° cone indenters were chosen to be used for comparative purposes.

7.2.2 The Rockwell test - 120° diamond cone

In about 1920 Rockwell introduced a direct reading tester which was further developed when Wilson produced his polished spherical conical diamond indenter. This had an included angle of 120° and a tangential spherical tip of 0.40mm diameter. The test consisted of applying a preliminary load $F_0=10\text{Kg}$, setting the dial depth gauge to zero and applying an additional load $F_1=140\text{Kg}$ for a

definite time. After releasing the load, it was noticed that the dial movement of the machine showed the elastic recovery of the indentation, which was dependant on the Young's modulus of the specimen. The hardness is a number, called the Rockwell number and is read off directly as:

$$\text{Rockwell hardness (HRC)} = 100 - e \text{ ————— } 7.1$$

where e is the permanent increase of the initial depth in mm.

7.2.3 The pyramid indentation test

In the pyramid indentation test the metal flow is not as regular or uniform as in the cone or ball indentation tests because of the sharp edges of the pyramid indenter.

The diagonal distance between the corners of the square indentation are measured with the aid of a microscope and the mean of the diagonals of the recovered indentation is used to calculate the hardness using either of the two following relations:

$$(1) \text{ Pyramid hardness (mean pressure HP)} = \frac{\text{load}}{\text{projected area}} = \frac{2F}{d^2} \text{ ————— } 7.2$$

$$(2) \text{ Vickers hardness (HV)} = \frac{\text{load}}{\text{cavity area}} = \frac{2F \sin \psi/2}{d^2} = \frac{1.854F}{d^2} \text{ (7.3)}$$

$$\text{when } \psi = 136^\circ$$

If h_0 = depth of the unrecovered indentation, the $d = h_0 \cdot 2\sqrt{2} \tan \psi/2$

$$d = 7h_0 \text{ when } \psi = 136^\circ \text{ ————— } 7.4.$$

Therefore the relation between the Vickers hardness and pyramid

hardness is: HV = 0.9272 HP

The test method is outlined in B.S. 427: 1961 (9) and a standard table for various materials has been produced.

Many materials flow or creep under stress and loading for some period is usually specified until equilibrium is reached. This period may be up to 2 minutes. Hardness testing specifications should specify the minimum load and duration of the load.

Experimental results show that the expression $F = ad^{2.0}$ — 7.5 is valid for the pyramid indenter except for very small indentations (12). The elastic recovery of the diagonals of the pyramid indenter appears to be practically negligible (50) and since the area is calculated from the diagonals (Expression 7.5) the hardness value is independent of the recovery of the material.

Very small pyramids are now employed in low load hardness testers. This technique is now the basis of micro-indentation hardness testing.

7.2.4 Ball indentation tests

Brinell used hard steel ball-bearings as indenters. The load on the indenter was maintained for 15-30 seconds and after the removal of the indenter the diameter of the recovered permanent impression was measured with the aid of a microscope and gauge. He used a relation to calculate the hardness using the mean of the diameters across 90° , such that the

$$\text{Brinell hardness (HB)} = \frac{2F}{\pi D^2 (1 - \sqrt{1 - (d/D)^2})} \quad \text{7.6}$$

Since $d/D = \sin \varphi/2$

$$\text{HB} = \frac{2F}{\pi D^2 (1 - \cos \varphi/2)}$$

$$\text{HB} = \frac{F}{\pi D h_0}$$

Mayer (56) calculated the hardness value using a single relation:

$$\text{Mayer hardness} = \frac{4F}{\pi d^2} \quad \text{7.7}$$

$$= \frac{F}{D^2} \frac{4}{\pi \sin^2 \varphi/2}$$

where for a load F with a ball of diameter D , d is the diameter of the ball indentation at a surface, so the indentation ratio is d/D and the angle of indentation (φ) and h_0 is the initial depth of the indentation.

Brinell hardness tests show a variation in hardness values with load. Brinell attempted to reduce this variation to a minimum and specifications were produced with a certain range of standard loads for a given ball diameter on metals of various hardnesses.

7.2.5 Micro-indentation testing

Scratch hardness testing with diamond scribes were used to investigate metallographic structures during the early years.

The accuracy of the results obtained were comparable with Brinell, Rockwell and Vickers indentation tests.

The success of the Vickers diamond indenter prompted Lips and Sack (57) to use diamond at low loads. A new field of micro-indentation developed, resulting in the Knoop (58) apparatus being equipped with a diamond indenter. Knoop measured micro-indentations obtained with low loads up to a few grams. Mott (15) reviewed the subject in detail, but the main area of difficulty was the logarithmic relationship between the load and indent size. Buckle (50) examined the problems and concluded that the classical theories were no longer applicable to interpretation of the results when the size of the indentation was near to the size of micro-constituents. He put forward the following suggestions for classifying indent size and load.(Table 7.1)

Gone and his co-workers (60, 61) conducted studies on the indentation of metals using extremely fine indenters and very low loads. These indentation studies have been carried out inside a scanning electron microscope to enable observation of the penetration of the indenter into the surface of the specimen. They have shown that in the presence of surface contamination, penetration does not occur until high pressures are developed. Tabor (63) has suggested that the surface contamination has a lubricating effect rather than strengthening. Micro-indentation inside a SEM is a useful technique for the study of the nucleation of dislocations in crystals.

Table 7.1

	DESCRIPTION	LOADS	INDENT DIAGONAL
(a)	Standard or mean hardness	above 3Kg	above 3mm
(b)	Low-load hardness	200g-3Kg	300 μ
(c)	Micro-hardness	1-200g max.	30-50 μ

Chapter 8

Theory of micro-indentation and micro-hardness testing

8.1 Basics of micro-indentation hardness testing

Indentation hardness is proportional to the resistance of a specimen to the penetration of a non-deformable indenter under a given load. It is generally expressed in terms of the ratio of the load P (applied force) to the surface area A of the indentation. The area of the indentation is dependant on the slope of the indenter and is calculated from the characteristic length measured under the microscope.

Hardness is generally given by:

$$H = K(P/A) \text{ in Kg/mm}^2 \text{ ——— 8 (1)}$$

where K is a constant depending upon the shape and the material of the indenter. The Vickers hardness (tetragonal pyramid) corresponding to an impression of diameter (diagonal) d is given as $H = 1854.4 (P/d^2)$ in Kg/mm^2 ——— 8 (2) where P is expressed in grams and d in microns.

In the case of micro-indentations, hardness testing is dependant on the applied force, which is in accordance with an empirical rule expressed in the term of the diagonal of the indentation:

$$P = ad^n \text{ ——— 8 (3)}$$

This relation is known as Meyer's formula and n is called the Meyer Index.

Combining equations 8(2) and 8(3):

$$H = a \cdot d^{n-2} \quad \text{---} \quad 8(4)$$

Since n is dependant on the load P , the formula is unsuitable for standardisation(14). However the variation of the mean value of n can be interpreted empirically using the experimental results, thereby making equation 8(3) approximately satisfactory. The results obtained under controlled conditions are presented either by plotting the curves of $\log P = F(\log d)$ —8(5) or the curves of $H = F(\log D)$ —8 (6).

The curves which represent the characteristics of the measured data, provide a rational interpretation of the indentation and load relationship.

It is generally understood that the value of the micro-hardness increases with decreasing load (14, 15, 16) and is independent of instrumental error or surface preparation.

This aspect of micro-indentation has been the subject of considerable controversial discussion. Mott (15) has suggested that the indentation hardness of a given material will be a constant above a critical size of impression, and a steady increase in hardness value will occur as the load is decreased.

Orowan (17) has given a theoretical justification based on his model of work hardening. Buckle (14) has suggested that due to

the presence of 'coherent regions' in the material, an increase in indentation hardness is observed at decreasing loads, but when the size of the indentation falls below the size of these coherent regions, there is no further increase in hardness. Yoshino (16) has proposed that the increment of the hardness with decreasing of load is due to heterogeneity of the deformation produced by the penetration of the indenter into the material, and so to have heterogeneous impressions.

Gane (18) et. al. have suggested that the observed load dependence of micro-indentation hardness is due to an increase in the stress necessary to operate the dislocation sources. Therefore the stress required to operate a dislocation source is dependant on the work hardening. The flow of stress of the material sampled by the indenter is then a sum of the work hardening and source hardening. It is therefore apparent that the indentation hardness is load dependant. It is associated with the movement of dislocation introduced by the indenter. This can be visualised from the punching mechanism. Freidel (19) deduced an expression by taking into account the detailed mechanism at the micro-indentation. According to him, the micro-indentation creates an impression by introducing loops of prismatic dislocations, with the sum of energy of the dislocation loops created, including their Peierls-Nabarro energy ΔW , and the surface energy γ_s

If the load or applied force F which is applied to a rigid flat-ended punch of diameter D produces an impression in a surface of depth b , where b_0 is the Burgers Vector, the load is then:

$$F = \frac{\mu b^2}{4K} \ln \frac{D}{b_0} \pi D (\Delta W + \gamma_s) \text{---} 8(7)$$

where:

μ = shear modulus.

K = bulk modulus.

The contact pressure σ that maintains the dislocation loop is given

by $\sigma = \frac{4F}{\pi D^2}$

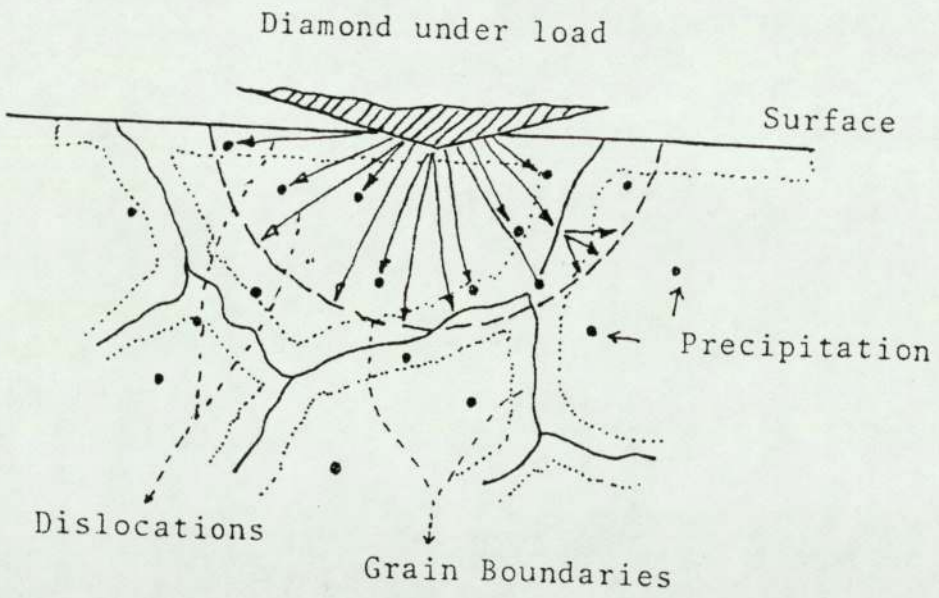
8.2 Related features of micro-hardness testing

Resistance to the movement of dislocations, which determines the hardness of the material due to pinning and blocking, arises from the following lattice defects: (1) grain boundaries, (2) vacancies, (3) solute atoms, (4) precipitates and other imperfections as shown in Figure 8.1.

The elastic recovery that an impression undergoes after the indenter is withdrawn from the material is another feature which makes micro-hardness testing a complex operation.

When the indenter is pressed against the metal, there is firstly an elastic front of deformation which moves below the indenter, followed by a curved zone of plastic deformation. Experimental results (20, 21) indicate that the deformation mechanism by a pyramid indenter leaves a uniform radial compression. This is the boundary between the zone of plastic deformation (work hardened) and the zone of the material to be stressed to the yield point. This remains

FIGURE 8.1



Micro Indentation Phenomena

rigid but it is approximately a hemisphere and virtually unaffected by the detailed shape of the impression itself.

On withdrawing the indenter, the impression undergoes an elastic recovery, and the unrecovered part of the impression is comprised of the material plastically deformed with a local hardening gradient and zone of influence around the impression. This zone is generally assumed to have a radius of action, equal to 10-15 times the depth of the indenter penetration (14, 22).

Many experimental results indicate that a considerable elastic recovery of an impression takes place in the opposite direction to the indentation, whereas it is negligible in the direction of the diagonal of the impression (14, 15, 23, 50).

8.3 Precautions and experimental conditions for micro-indentation

The micro-indentation test is very much dependant on the conditions under which the material is tested.

8.3.1

A. The use of the proper load on the indenter in the hardness investigation is crucial. Many attempts have failed (14, 15) to give reliable and interpretable results because of the improper selection of loads. Large loads very often are not suitable for the micro-indentation test since they cause the effect of impurities and other imperfections of the lattice to be noticed (24, 25). Very small loads require the strict control of experimental conditions (18).

The results of M. Brounovic et. al. (24) for iron containing 0.002 atomic % tungsten shows a considerable variation of micro hardness because of the increment of grain-boundary hardening at low indenter loads (Figure 8.2.).

8.3.2

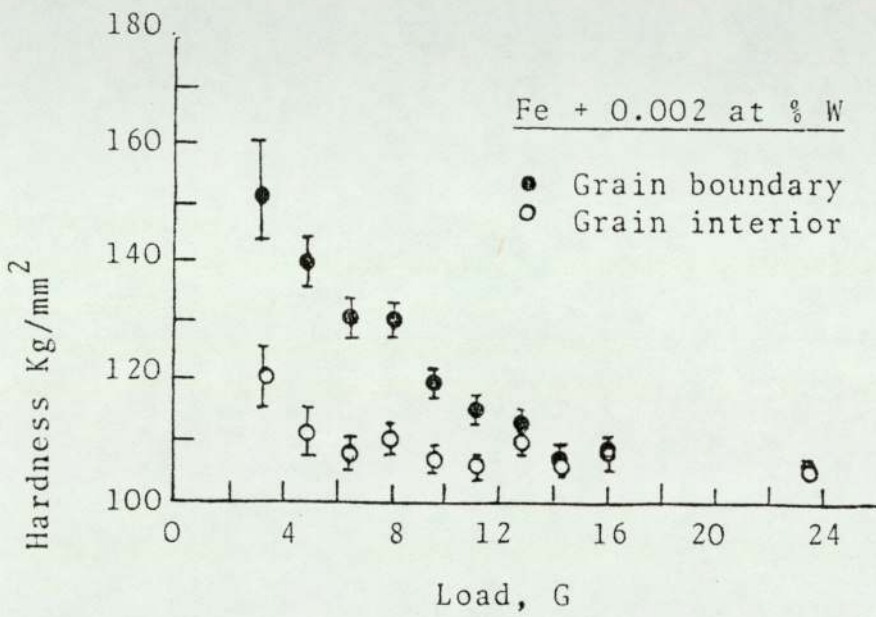
B. Surface preparation is another very important aspect in micro-indentation testing. Coarse machining and polishing of the specimen surface produce large errors in micro-hardness measurements and consequently make the results invalid (14, 15, 16, 25). Therefore in order to eliminate any undesirable influence due to work hardening, great care and consideration are taken in preparing the specimen surface. Electro-polishing is an important technique to prepare a good surface, but surface micro-hardness is also dependant on polishing time.

8.3.3

C. The effect of grain boundaries is a very important contributing factor in the measurement of the micro-hardness. Even though the concentration of defects and impurity segregation affect micro-indentation, segregation of solute atoms at the grain boundary can increase the micro-hardness 10 to 50% compared with that of the grain interior. The hardening region appears to extend several microns from the boundary into the interior of the grain.

This phenomena occurs in a wide variety of materials. Ferene (27) has detected an increase of about 15% in hardness at grain boundaries in fully annealed pure iron when using a load of 5 grams. It has

FIGURE 8.2



Variation of microindentation hardening value with indenter load for Fe + 0.002% tungsten

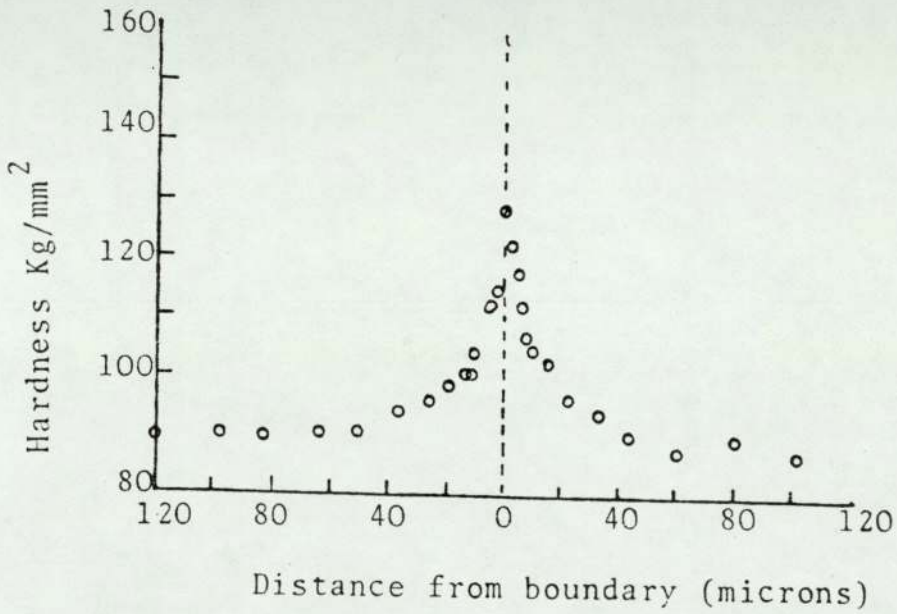
been concluded that the impurity segregation at grain boundaries is responsible for this increased hardness. Westbrook and Wood (28) have shown a hardness profile increasing about 40% which extends 50 microns on either side of the boundary (Figure 8.3), on a high purity α -Fe prepared by Ainslie et. al. (29). Further studies on hardness measurements show that the addition of W, Mo and Mn up to certain limits under certain conditions have no effect on the hardness of such metal systems.

In the case of non-ferrous metal systems, Westbrook and Aust (31) have studied zone-refined lead containing minute concentrations of Au, Ag, Sn and In, and have found that the addition of even very small amounts of these solutes produces a considerably harder grain boundary region than the adjacent grain interior. On further increase of solute concentration the grain boundary hardness increases, but there is no systematic variation in the hardness of the interior of the grain. Thus there is a systematic increment of boundary hardening on the inclusion of impurities in non-ferrous metal systems, depending upon the nature of the solutes or impurities (32) and the heat treatment condition of the alloys (33).

8.3.4

D. Grain size is also an important factor affecting the mechanical properties of the metals. Hardness is dependant on the grain size; as the grain size increases the hardness decreases. This phenomenon was demonstrated on brass by Basset and Davis (34) as early as 1919. Later W.J. Babyok (35), P.C. Jindal (36, 37), R.M. Douthwaite (38) and K. Farrel (39) demonstrated the same on brass, but no theoretical

FIGURE 8.3



Microindentation hardness profile of a grain boundary in a sulphur-segregated iron

model has been developed for the effect on grain size on hardness. However, several attempts have been made to correlate the hardness (H) of a material with its unidirectional stress-strain characteristics.

Hall (40) has proposed and shown the dependance of hardness (H) of polycrystalline material on the size of the grain (L) as follows:

$$H = H_0 + K_H L^{-1/2} \text{---} 8(8)$$

where H_0 and K_H are the experimental constants.

Several investigators (41, 42, 44) have measured this dependance and Mohrhiem (43) has shown a semi-logarithmic relation between grain size and Brinell hardness, such that

$$H = H_0 + K_H \log (L) \text{---} 8(9)$$

where H_0 is a constant, and K_H is the slope.

He has also shown the semi-logarithmic relationship between grain size and ultimate tensile strength for pure iron, using the data of Edwards and Pfeil (45). Great care must be taken however in using any relation between the grain size and the hardness of a polycrystalline material because the influence of the grain boundaries will be dominant when the indent overlaps grain boundaries.

Chapter 9

Techniques and Results

9.1 Introduction

The techniques of microindentation and microhardness testing and their accompanying test results are described in this chapter.

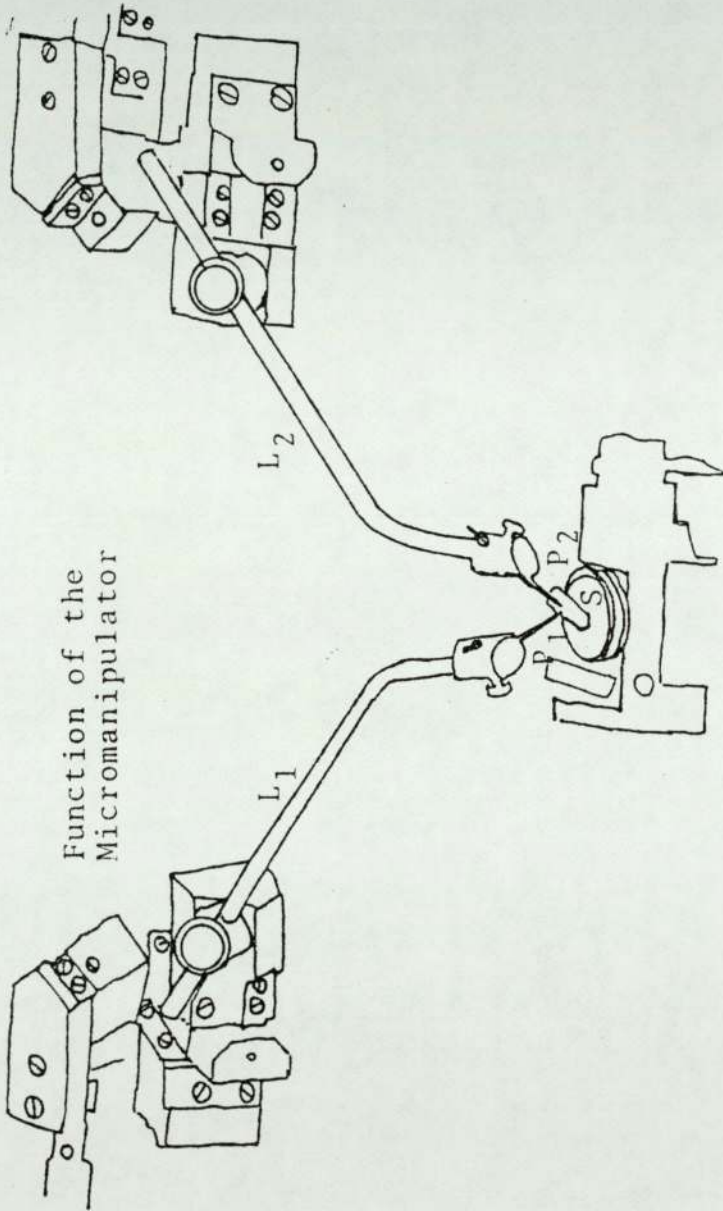
It is arranged as follows:

1. The micro-indentation tester
2. The preparation of tungsten micro-indenters.
3. Vickers (65) micro-hardness tests.
4. Micro-indentation testing using the modified micro-manipulator system with the tungsten micro-indenters.

9.2 Modification of stereoscan SEM micromanipulators for micro-indentation testing

9.2.1 The function of the SEM micromanipulator

An attempt has been made to use the stereoscan micromanipulator (64, 66) as a microindentation tester by modifying the manipulator's arm and the probe holder. The conventional function of the micromanipulators is to probe specific areas of specimens within the SEM as shown in Figure 9.1.



Function of the
Micromanipulator

L₁, L₂ = Micromanipulator's levers

P₁, P₂ = Micro Probes

S = Mounted Specimen

9.2.2 The modifications

The lever arm on the right hand side of the equipment was modified for use as a microhardness tester as illustrated in Figure 9.2.

The micromanipulator incorporates the load (W), the holder (H) and a holder tightener (S) with a snap in load pin (P) for the holder.

A new holder lever (L) was designed to replace the micromanipulator lever (L_1). The indenter (I) which was either the micromanipulator's probe needle or the electropolished tungsten microindenter was mounted in the holder (H) and held firm by tightening the holder tightener (S).

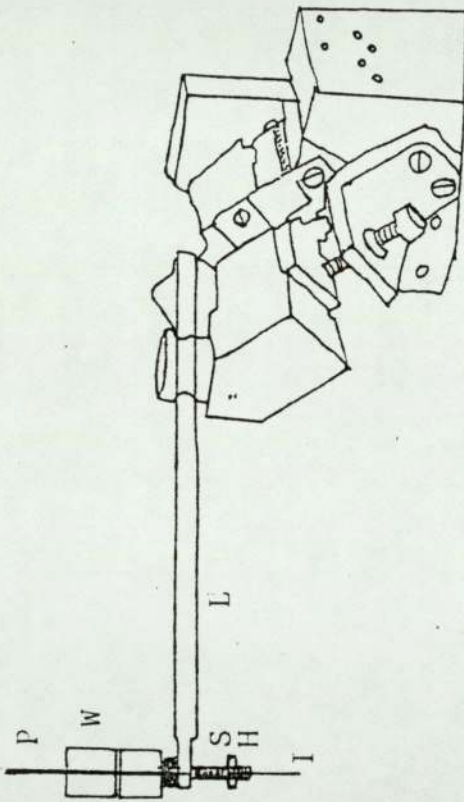
Two modified micromanipulator levers are shown in Figure 9.3 along with their holders and the holder tightener. Difficulty in mounting the load around the original (fixed) load pin (Figure 9.3A) was overcome by designing a new snap-in load pin. There was very little play, the holder moved up and down freely without frictional resistance, and loads from a minimum of 1 gram to a maximum of five grams could be used to indent materials. The movement of the lever in all the directions is controlled by the micromanipulator, ensuring indentation at a required location on the specimen. Centrally drilled brass blocks were made of different size to provide a range of loads*for the indenter and the tungster microindenters are shown in Figure 9.4.

9.2.3 The microindenter holder

The microindenter holder was made from a solid brass screw of 1.5cm

* (W1 - W5) the weights are mentioned in Table 9.6

Modified micromanipulator lever as
Microhardness tester



L = Modified lever for microindenter

P = Pin holder for weights

W = Loads for Indentations

H = Indenter Holder

S = Screw to tighten the Indenter in the Holder

I = Tungsten tip as Microindenter

FIGURE 9.3

The Holders for the Microindenter

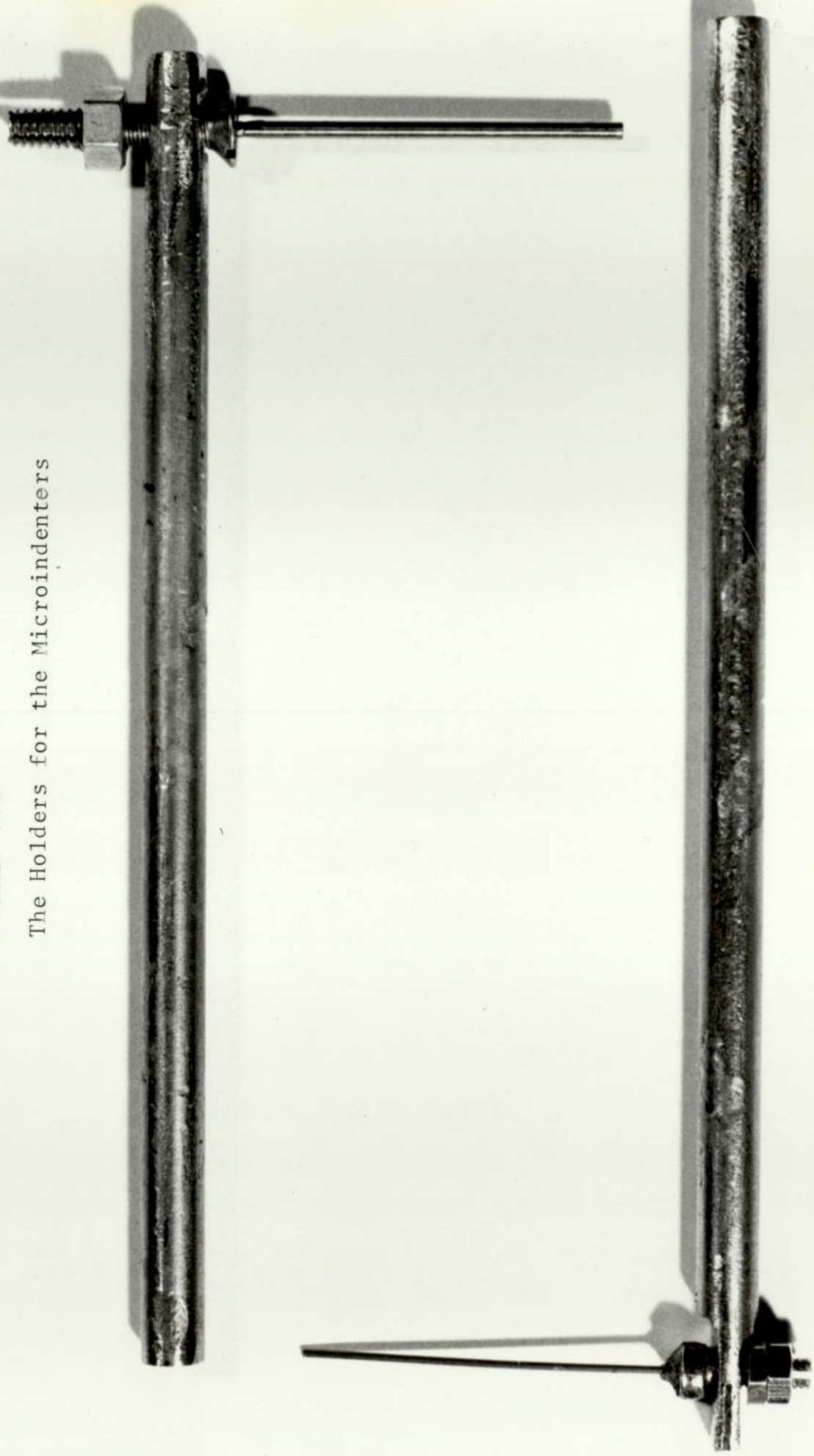


FIGURE 9.4

Microprobes and the Loads used for microindentations



in length and 1mm in thickness cut vertically from the bottom to the top up to 1cm in height. The cut of the cross section is shown in Figure 9.5. The top of the screw was drilled to hold the load pin. This indenter holder could be used to mount the micro-indenters of a minimum thickness of 0.1mm to a maximum thickness of 0.5mm in diameter. The cutter used was a 0.1mm thick diamond wheel and the 1cm deep cut ensured vertical and firm mounting of the microindenters.

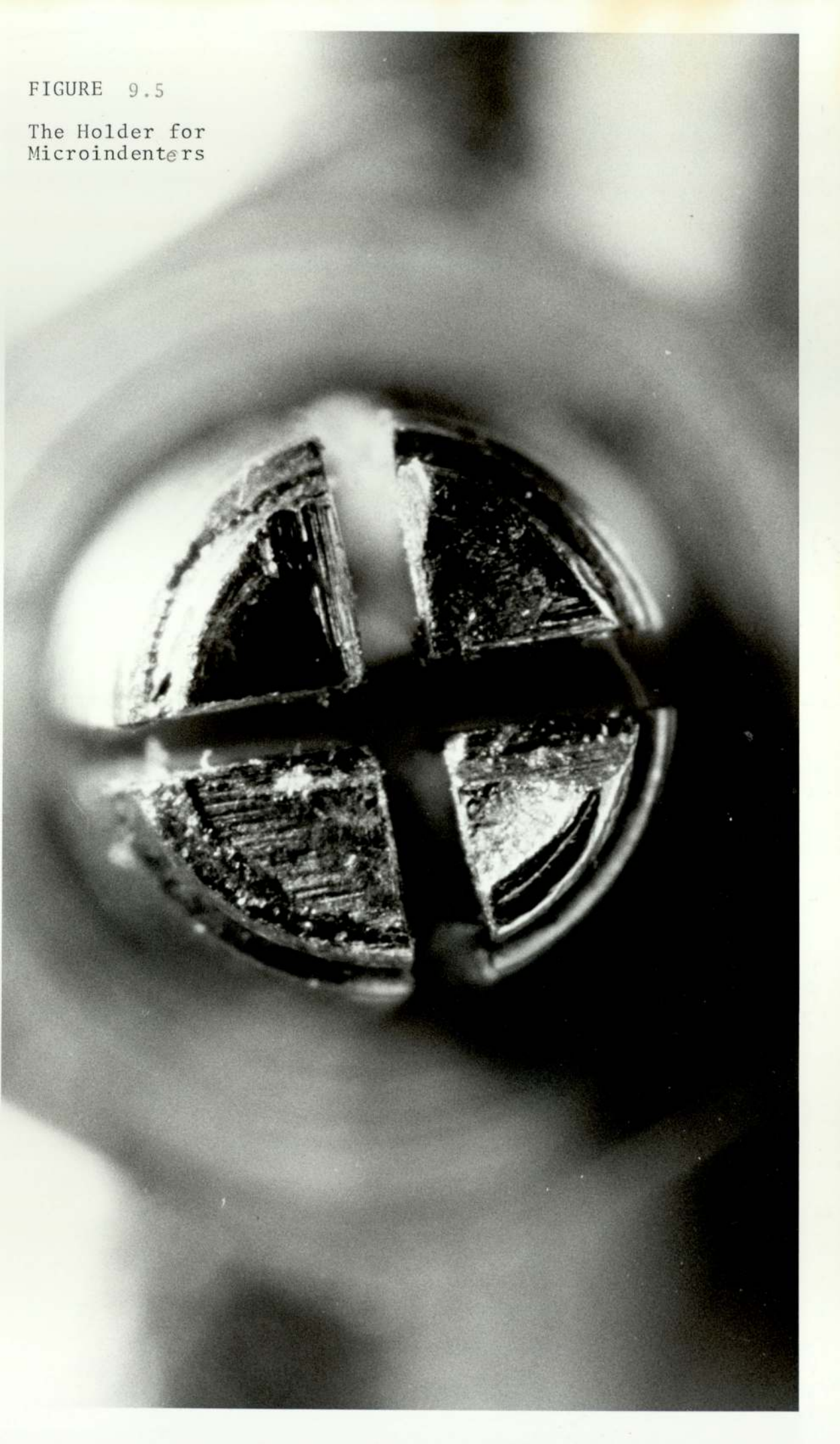
9.2.4 Procedure for using the microindentation tester

The micromanipulator was used to control movement in the horizontal plane and position the indenter at specific sites. Vertical movement was used to indent at the required site on the specimen, either by lowering the arm lever or by raising the specimen stage. Careful attention to the following points is very important to ensure a satisfactory indentation:

1. The microindentation tester lever must be in a horizontal plane.
2. The microindentation holder must be in a vertical plane.
3. The microindenters must be carefully mounted. Loose or unaligned mounting may cause an irreproducible change in the shape of the microindentation.
4. The load pin must be fixed in the holder.
5. To avoid any relative movements of the load blocks, no more than two load blocks should be used to indent the specimen at any one time.

FIGURE 9.5

The Holder for
Microindenters



9.3 The indenters for microindentation

9.3.1 The tungsten micromanipulator needles

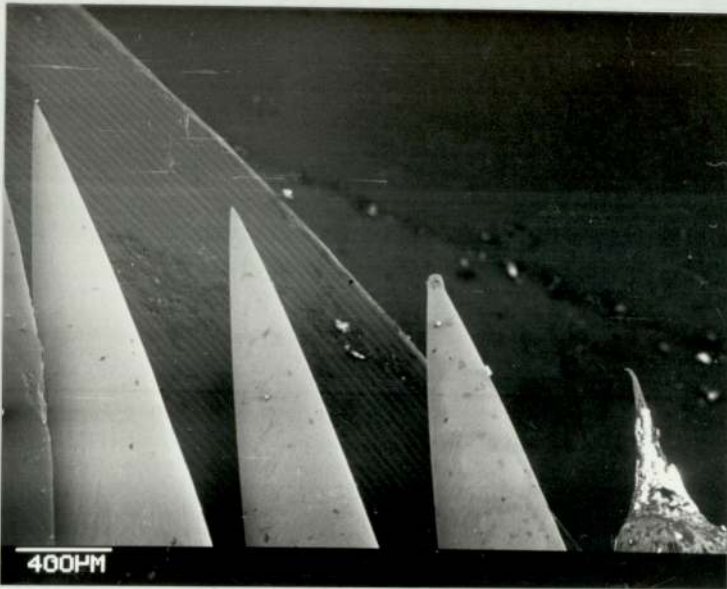
Initially, attempts were made to use the tungsten needles (supplied with the SEM micromanipulator for its probe) as the microindenter. The needles were available in two sizes - $3\mu\text{m}$ and $5\mu\text{m}$ tip diameter. Indentations were made with both sizes of needle. Figure 9.6 shows photomicrographs of the needle tips and Figure 9.7 and Figure 9.8 show microindentations made with the needles.

The indentations made using indenter holder A (Figure 9.3) proved unsatisfactory because of the relative motion between the lever hole and the microindenter holder. The indentation load was five grams and the average diagonal of the indentations was $42\mu\text{m}$. The indentation load was decreased from 5 grams to 2 grams and the size of the indentation correspondingly decreased to $25\mu\text{m}$ (Figure 9.8). These indentations were made on an aluminium specimen. The indentations indicated the necessity for improving the operational design of the holder and the use of thinner microindenters.

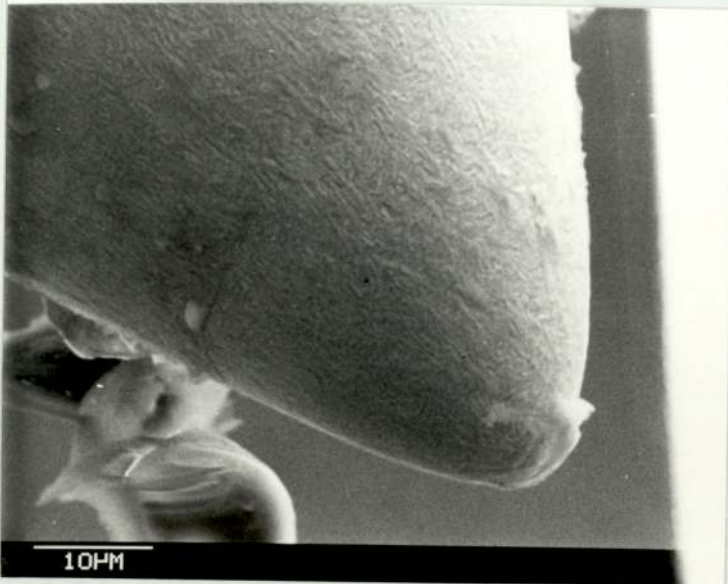
9.3.2 The choice of suitable microindenters

A survey was done to choose a suitable microindenter better than the tungsten micromanipulator needles. Vickers Limited (3) and Relion (4) diamond tool makers were contacted about possible fabrication of a diamond microindenter to be used with the modified micromanipulator. The use of the diamond tip of a commercial gramo-

Figure 9.6



Micromanipulator's probe needles.



The diameter of the tip of the probe needle.

Figure 9.7



The microindentations with the micromanipulators probe needles at 5 gram indentation load on aluminium.

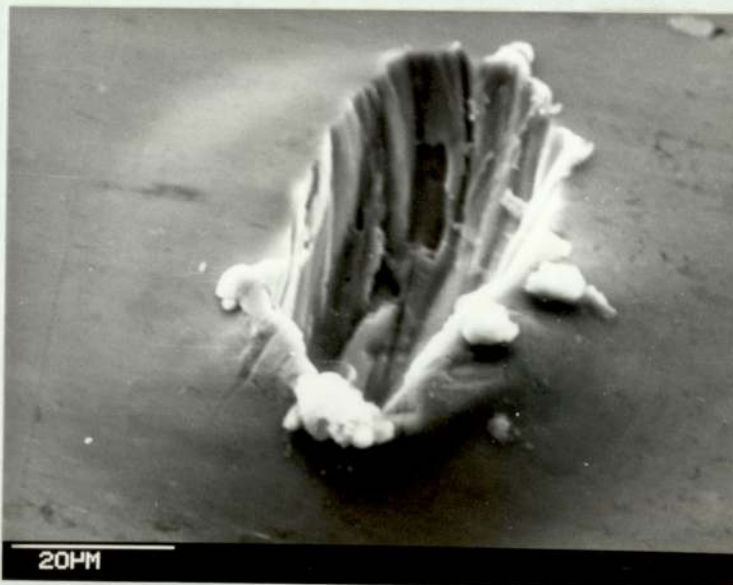
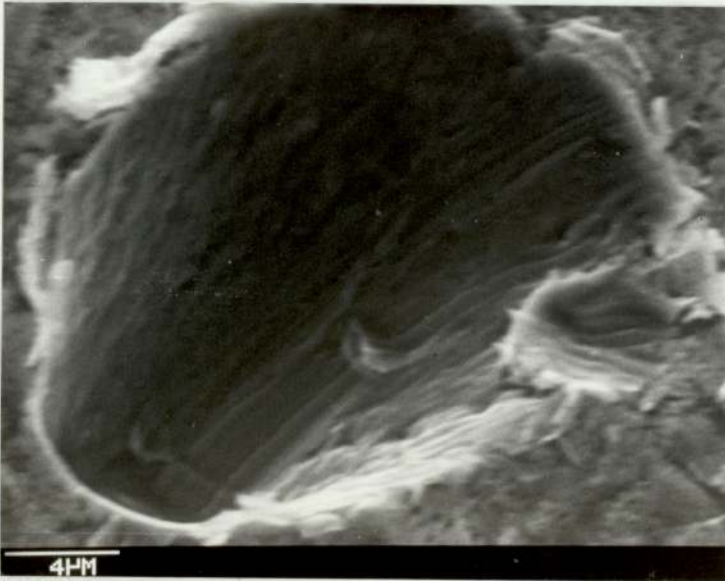


Figure 9.8



The microindentations made with the micromanipulator's probe needle at 3 gram indentation load on aluminium.



phone stylus (1, 2) was also considered as a microindenter.

The problem in both cases was the diameter of the tip which was too large. Even modern styli, which are more durable (sapphire or diamond tipped needles) than the old traditional steel or chrome-plated needles were found unsuitable for use as microindenters.

9.3.3 Electro-polished tungsten microindenters

The preparation of tungsten field emission (FE) tips by controlled electropolishing of tungsten wire using an automatic switch has been reported (6). The diameter of the tips were claimed to be about 0.1 μ m. It was therefore decided to make an electro-polishing unit, suitable modified, for the production of microindenters.

9.3.4 The preparation of tungsten tips

In a simple electropolishing system (6), a polishing electrolyte and a steady flow of electric current are required. The current is passed through the cathode to an anode, which is the specimen being polished, via an electropolishing liquid for a certain period of time.

For a very small current passing through a thin tungsten wire dipped in a 2Molar sodium Hydroxide (Na OH) solution, electro-polishing produces a fine sharp tip. The diameter of the specimen tip dependant on the polishing time and the handling of the specimen when taking it out of the solution. If the latter is done manually it is very difficult to produce tungsten tips which are fine

enough, i.e. $0.1\mu\text{m}$ in diameter. The tungsten wire electro-polishes preferentially at the electrolyte meniscus and a point is reached where the end falls off the wire with sudden increase of resistance of the polishing set up. Human observation of the drop of the polishing current on a milliammeter and switching off manually is too slow. The fine tip present at the instant of breakage is blunted by continuing action for a few milliseconds. Therefore an automatic switch is required in the circuit (as shown in Figure 9.9).

9.3.4.1 The functioning of the automatic switch

The polishing current is arranged to pass through a magnetic relay switch which is energised by a power supply. This supply is itself switched between two voltage states according to a control signal derived from the resistance change due to the breakage of the tip in the solution.

This automatic control of switching the circuit is a type of 'Schmitt Trigger' or cathode coupled bistable circuit which feeds the relay switch via an output transistor.

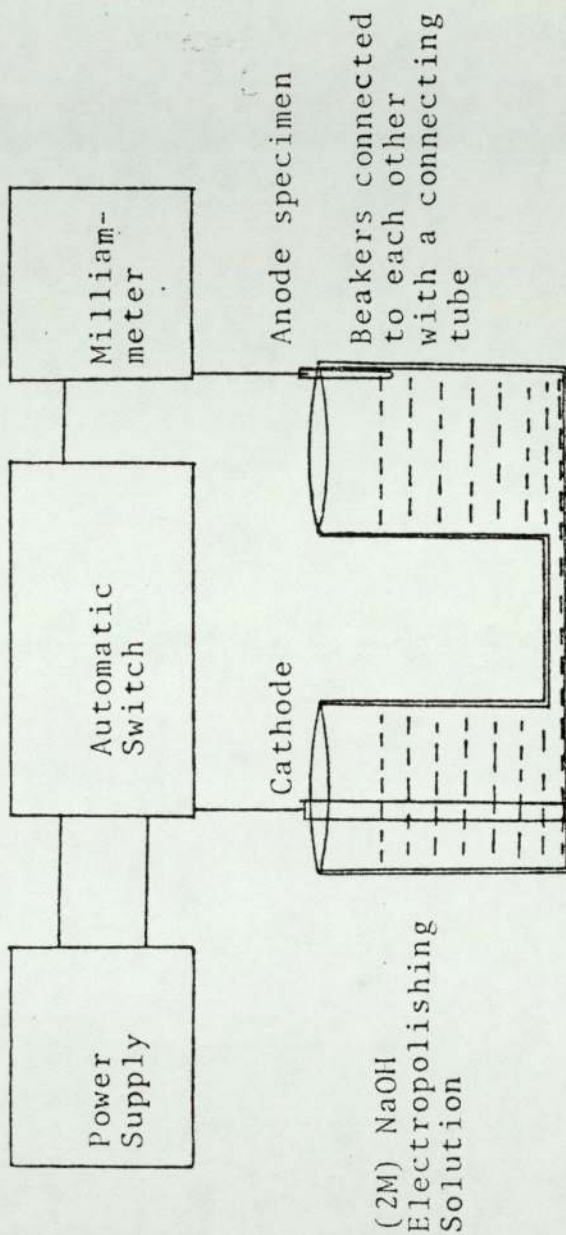
9.3.4.2 The characteristics of the circuit

A few preliminary experiments revealed the following circuit characteristics for the automatic switch (Figure 9.10).

For tungsten wire of a diameter 0.1mm dipped 4mm below the meniscus

FIGURE 9.9

BASIC PRINCIPLES OF THE ELECTROPOLISHING CIRCUIT TO PREPARE THE TUNGSTEN MICROINDENTERS



CIRCUIT DIAGRAM OF THE AUTOMATIC SWITCH

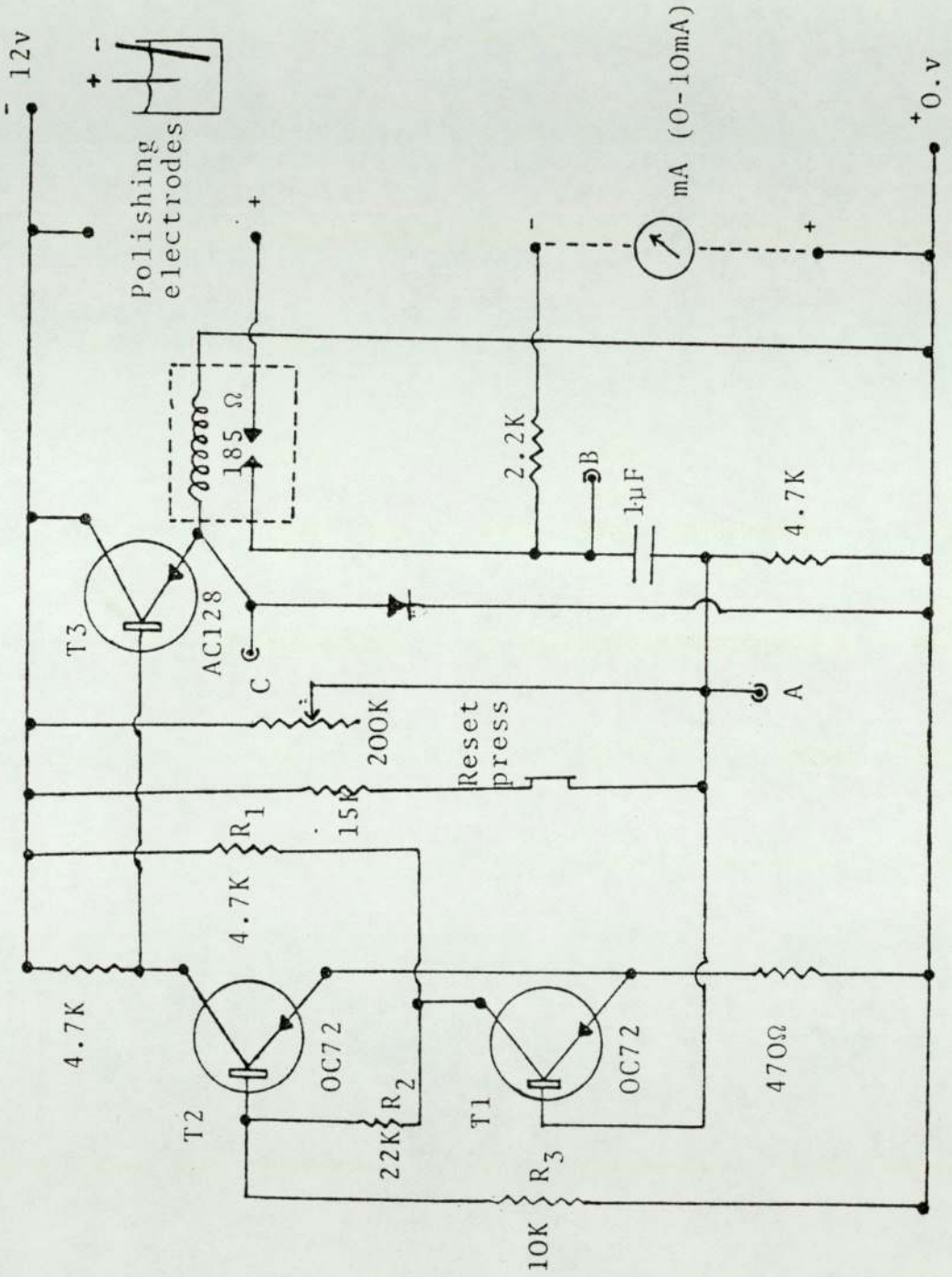


FIGURE 9.10

of 2M NaOH solution, the polishing current is initially about 4mA at 12V. It rapidly falls to about 2mA and then slowly to about 1mA (or less) before the breakage occurs. The rate of decrease speeds up considerably just before breakage. This behaviour markedly influences the operation of the automatic trigger. At breakage, the current drops from 1mA to 70 μ A. The resistance of the polishing circuit therefore rises from 3k Ω at the start to 12k Ω near the end and then suddenly to 170k Ω . The detailed features are given in Appendix 12.

9.3.5 Preparation of the polishing solution

The molecular weight of NaOH is 40 gram. 80 grams of the compound were mixed with distilled water to give 1 litre of 2M NaOH. The mixing must be carried out with care because the reaction is exothurmal. After cooling, some of the solution was transferred to two beakers connected with a tube as shown in Figure 9.9. Lids for the beakers must be used when the solution is not being used for polishing. Each time the indenters were prepared, a new solution was made and used.

9.3.6 The tungsten microindentors

Tungsten wire of different diameters (0.5mm, 0.45mm, 0.40mm, 0.25mm and 0.1mm) were selected and pieces of equal length (1.5cm) were cut. The dip length of the wire piece used as an anode was approximately 2-3mm for all diameters. Dipping tungsten specimens more than 4mm in the solution caused damage to the polished tip and made it somewhat blunt. The polishing time for each tungsten

specimen was noted. The time varied from specimen to specimen and was greater, the thicker the specimen and, the longer the dip length.

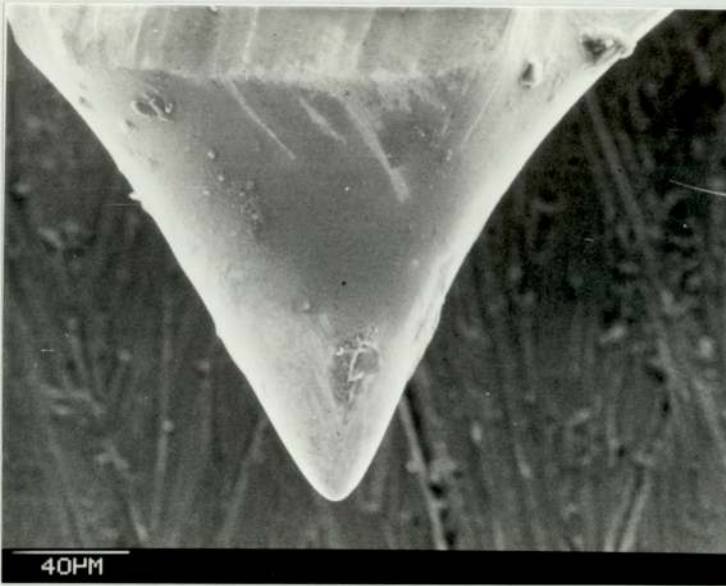
9.3.7 The tungsten microindenters

The automatic switch based on the circuit shown in Figure 9.10 was modified for a lower value resistor at the base and was employed in the electropolishing unit shown in Figure 9.9. Initially a current 4.5mA flows through the polishing solution with a P.D. of 12 volts when the thickness of the polishing tungsten wire is 0.45mm. The initial current is the same for all diameters of tungsten wire used. Five tungsten wire (series A) of different thicknesses were electropolished and used as microindenters. Details of thickness and polishing time are given in Table 9.1 and SEM micrographs showing the tip shapes produced are showing in figures 9.11 to 9.13.

The polishing current was changed to 3.35mA on placing a resistor of $1k\Omega$ in series with the circuit for tungsten wire of thickness 0.1mm. The polishing time was 7 minutes. The shape of the indenter tip was conical, but because of its length and thickness the indenter was insufficiently stiff and rigid, therefore tungsten wire of 0.45mm thick and 1.5cm long (KB_1 to KB_{16}) with a few of 1cm long (KC_1 to KC_4) were cut, and were dipped 2-3mm in the solution during polishing to observe the effects on the shape of the polished tips after the breakage of the polished material in the solution. These microindenters (series B and C) are listed in Table 9.2. The

Figure 9.11

A conical shaped tungsten microindenter.



A ball shaped tungsten microindenter.

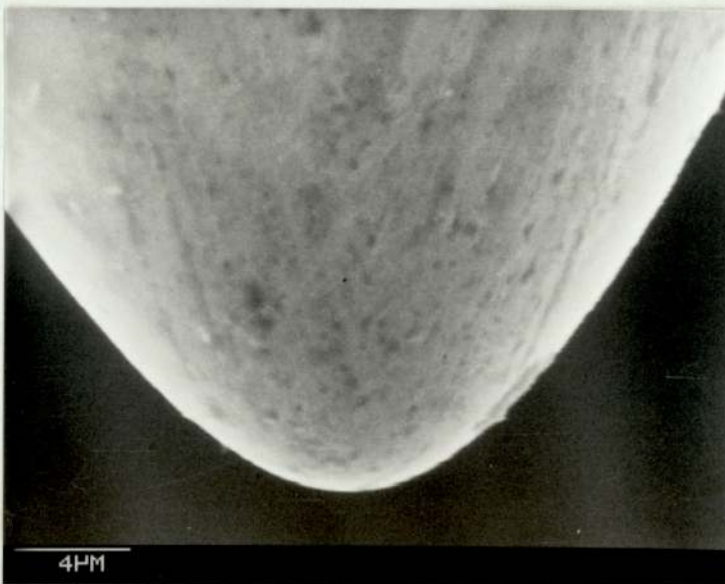
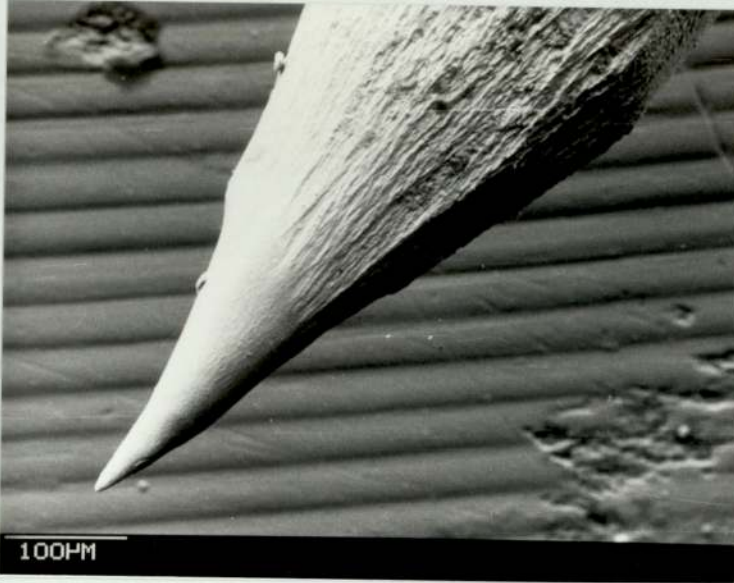


Figure 9.12



Microindenters polished from the tungsten wire
of various thickness.



Figure 9.13



Microindenters polished from the tungsten wire of various thickness.

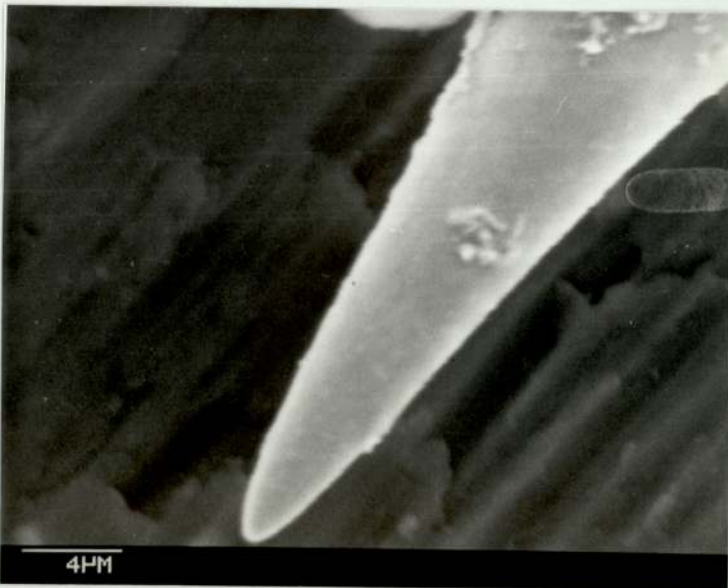


Table 9.1 (Series A)

No.	Diameter of Tungsten wire	Electropolishing time taken	Shape of the tip
1	0.1mm	4 minutes	cone shaped
2	0.25mm	30 minutes	"
3	0.25mm	30 minutes	"
4	0.45mm	150 minutes	Ball shaped
5	0.5mm	180 minutes	"

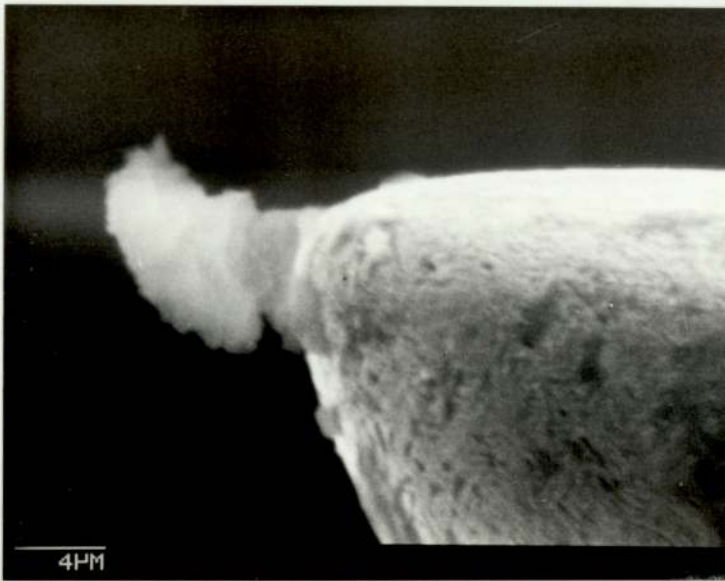
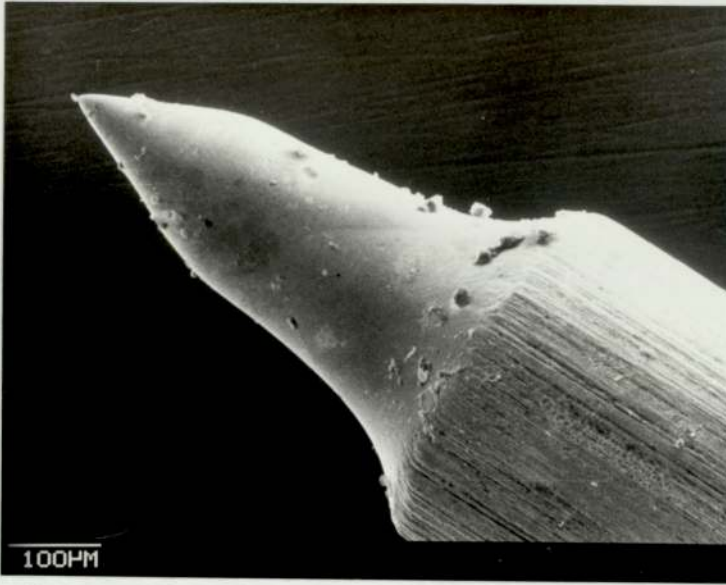
The table shows the specimen code number, the diameter of the tip in microns (μm) and the shape of each of the microindenters.

Each microindenter was examined in the SEM (Figure 3.12) and photomicrographs of most of them are displayed in Figures 9.14 to 9.20.

The results shown in Table 9.2 indicate that the preparation of microindenters is not completely reproducible. The tungsten wire should be cut with a proper wire cutter. It was also concluded that a laboratory height control unit should be used for controlling tungsten wire dip length in the polishing solution and for lowering beakers after the breakage of the polished tip. During electropolishing the adjustable height control was put on a metallic laboratory stand which in turn was placed on a heavy metallic block on a 2cm thick, dense foam sheet to minimise vibrational noise arrangement of the polishing unit (shown in Figure 9.21) was designed to produce tips of reproducible size and shape.

Five of the tungsten wires (Series E) of the same length and diameter as in series B were dipped 4mm in the solution using a Gallenkamp adjustable height control and electropolished. The microindenters so produced were examined in the SEM; microphotographs are shown in Figures 9.22 and 9.23. The results are tabulated in Table 9.3. The results indicate an improvement in the reproducibility (86%) of the tip sizes of the microindenters.

Figure 9.14

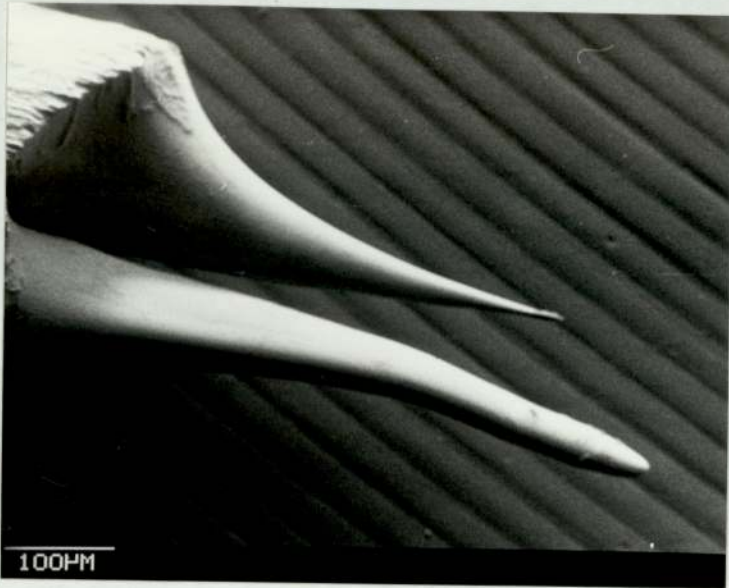


Tungsten microindenters of Series B.

Figure 9.14



Figure 9.15



Tungsten microindenters of Series B.



Figure 9.15

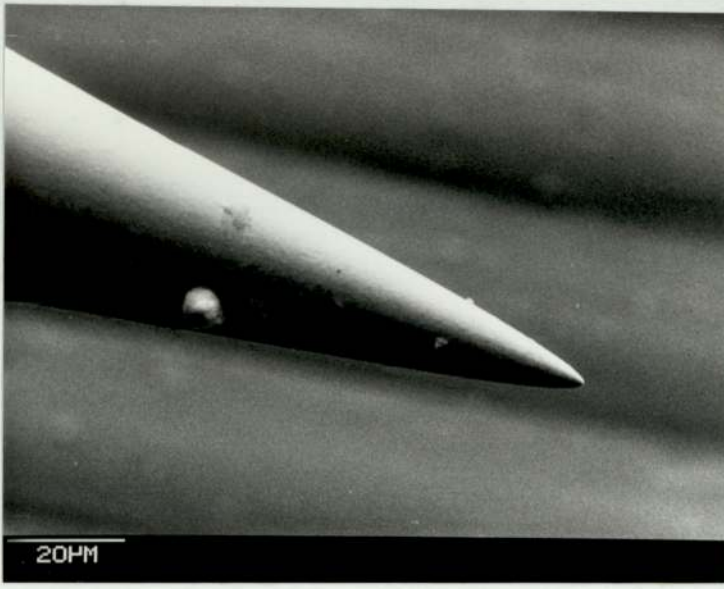
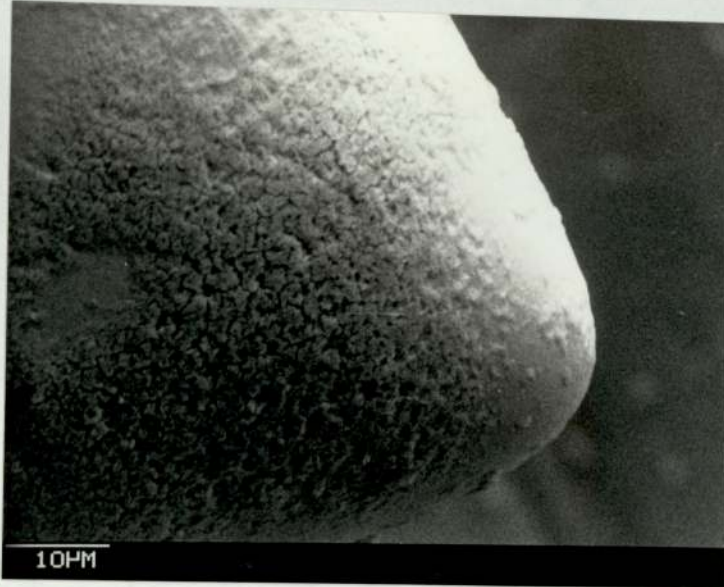
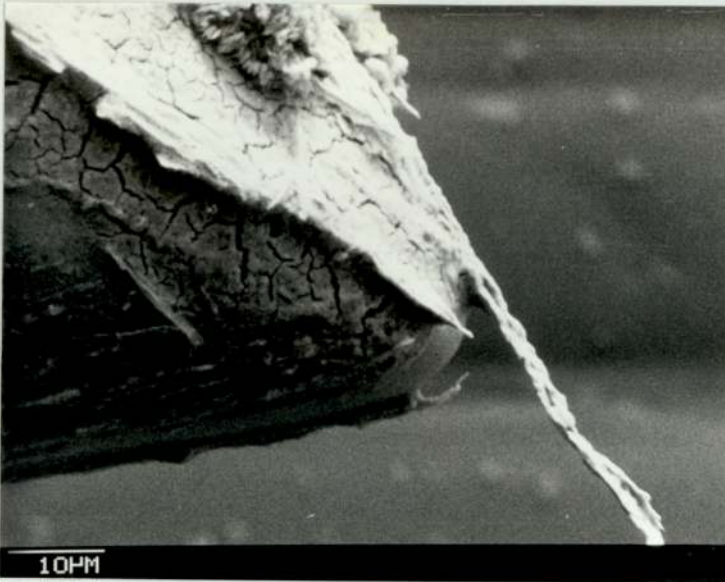


Figure 9.16



Tungsten microindenters of Series B.

Figure 9.17



Tungsten microindenters of Series B.

Figure 9.18



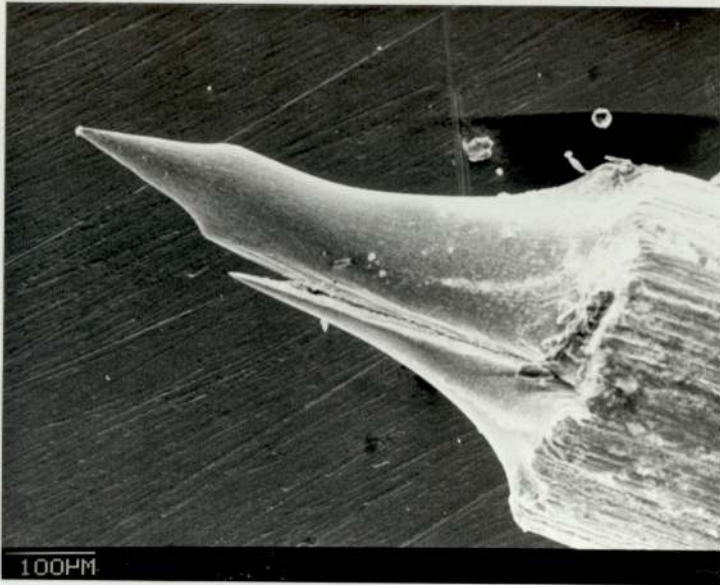
Tungsten microindenters of Series B.

Figure 9.19



Tungsten microindenters of Series B.

Figure 9.20



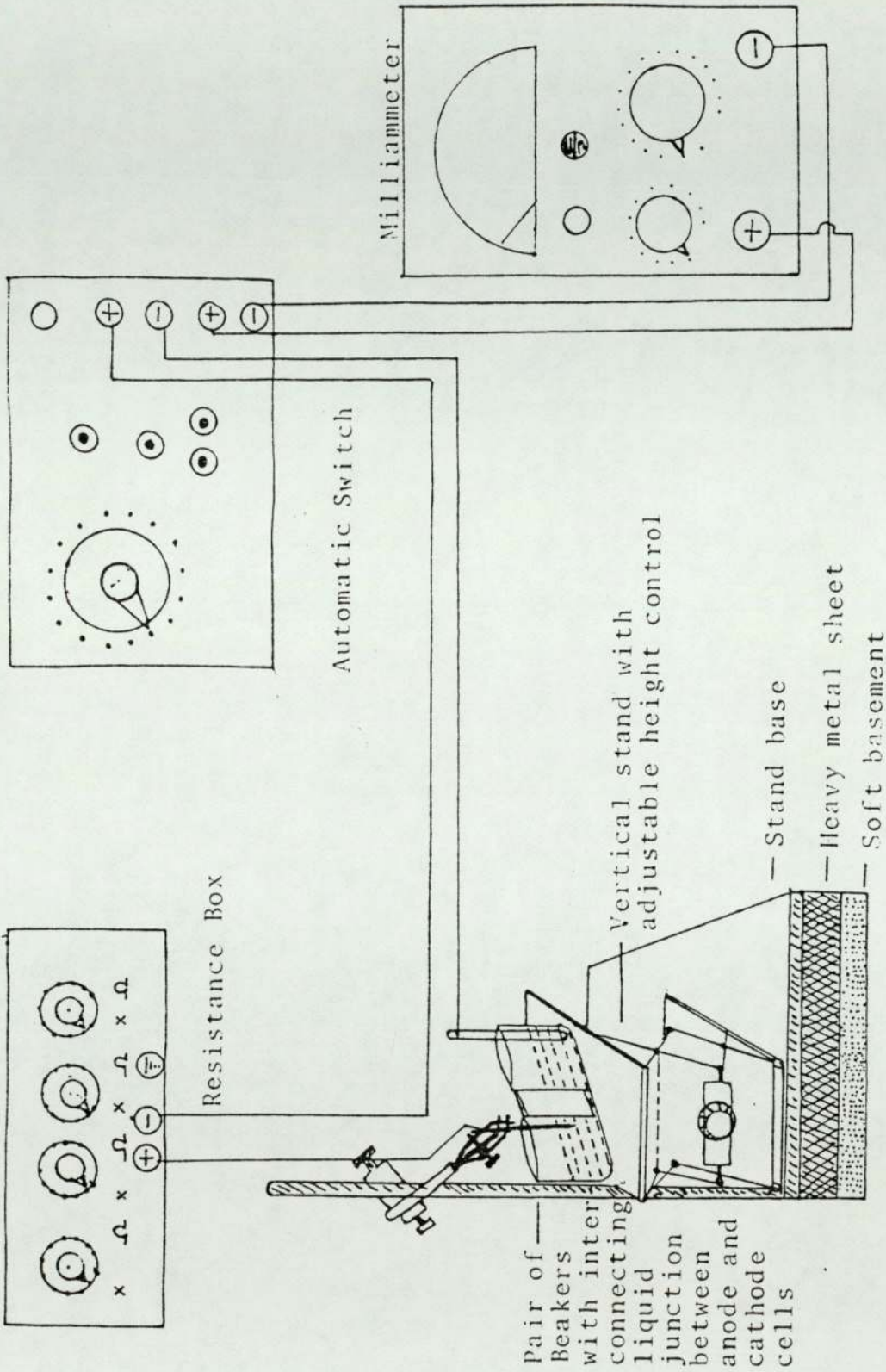
Tungsten microindenters of Series B.

Table 9.2 (Series B and C)

No.	Code No.	Diameter in μm	Depth immersed mm	Polishing time in minutes	Indenter shape
1	KB ₁	5.5	3.0	150	Conic shaped with a metallic burr.
2	KB ₂	4.21	3.0	167	Conic shaped with two pins
3	KB ₃	1.6	3.0	148	Conic shaped, good polished
4	KB ₈	6.92	2.5	170	Trunk shaped with two pins
5	KB ₉	10.0	2.0	155	Ball shaped, excellent polished
6	KB ₁₁	4.0	2.5	143	Conical ball shape, oxidized burr.
7	KB ₁₂	spoiled	3.0	-	Left in polishing solution after breakage.
8	KB ₁₃	3.45	2.0	140	Ball shaped, oxidized layer
9	KB ₁₄	-	2.5	165	Two pins of conical shape
10	KB ₁₆	0.87	3.0	150	Long conical shape with good polishing.
11	KC ₃	6.2	2.5	152	Conical flat shape, surface unfinished.
12	KC ₄	3.5	3.0	163	Conical ball shape, surface unfinished.

Table 9.3 (Series E)

No.	Code No.	Diameter μm	Mean Dia + error μm	Etching time Minutes	Mean time + error -	Indenter angle and shape
1	KE ₁	0.89		180		40° conical, good shape
2	KE ₂	0.92	0.96+0.13	188	186+ 4	38° conical with a little burr
3	KE ₃	1.19	14%	190	2%	42° conical with a burr
4	KE ₄	0.94		182		35° conical, good polished
5	KE ₅	0.90		180		42° conical, good polished



Equipment for making tungsten indenters

Figure 9.22

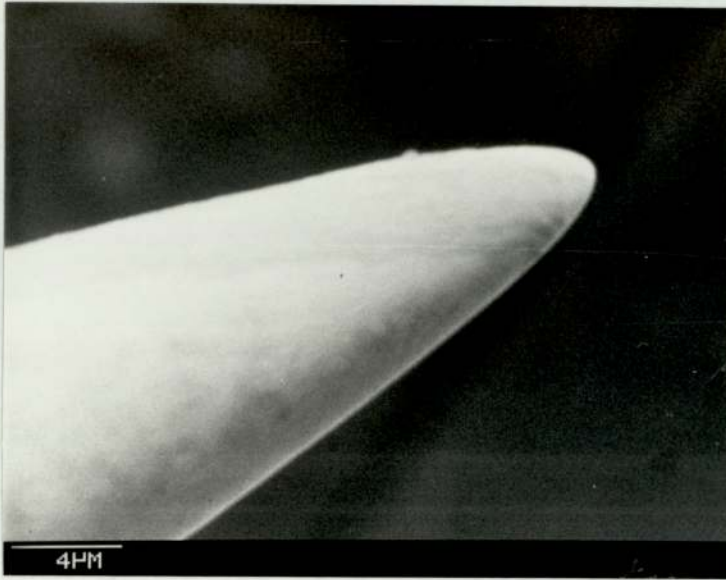


Figure 9.22



Tungsten microindenters of Series E.

Figure 9.23



Tungsten microindenters of Series E.



The incorporation of a $1k\Omega$ resistor in the circuit ensures production of a conical shape of tip of similar angle with a lower current and a higher polishing time than that of series B and series C.

Some of the microindenters (e.g. B_1 , B_2 , B_3 , C_3 , C_4 and E_3 , E_4) were used to indent aluminium and 60/40 brass specimens detailed in Appendix 13. After use the microindenters were re-examined in the SEM. One of them (B_2) was damaged during indenting (Figure 9.24). Others (e.g. C_3/B_15 and C_4) remained undamaged as shown in Figure 9.25.

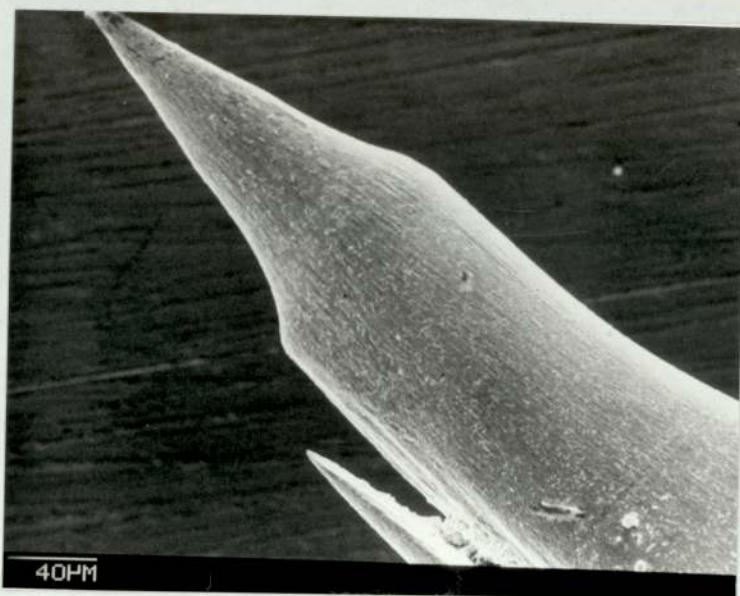
9.4 Microhardness testing using a Vickers microhardness tester

Pretreated (Appendix 13) 60/40 brass specimens KBI-2 and KBI-4 and polished aluminium were used for assessing the microindenters produced in the present work and comparing the results with those obtained with a standard Vickers microhardness tester.

9.4.1 Microhardness testing

Microhardness testers use comparatively low loads. They are delicate instruments requiring a high degree of precision, both in the application of load and in the measurement of the indentation produced. It is essential, therefore, to know the exact load applied to avoid friction in the loading system. In addition, the instrument used to measure the indentation must be accurately calibrated. A D. M41 Vickers microhardness tester as shown in

Figure 9.24



Used microindenters of Series B.



Figure 9.25



Used microindenters of Series C.

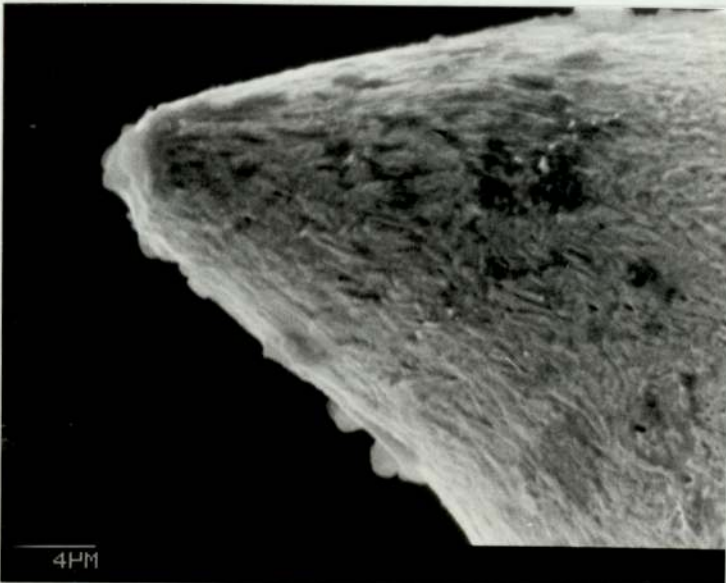


Figure 9.26 was used in this study for comparison with the micro-indentations made the tungsten microindenters discussed in previous sections. The assembly and experimental procedure are detailed in Appendix 14. Low loads were applied in order to observe the hardness of comparatively small regions.

9.4.2 Results of microhardness tests

The results of microhardness tests on both 60/40 brass and aluminium specimens are shown in Table 9.4. The photomicrographs of the indented brass are displayed in Figure 9.27 for loads of 20 grams and 5 grams. The smallest load used was 5 grams and attempts were made to indent each of the two phases in the brass specimen separately wherever possible. However the size of the two phases was sometimes smaller than the size of the microindenter.

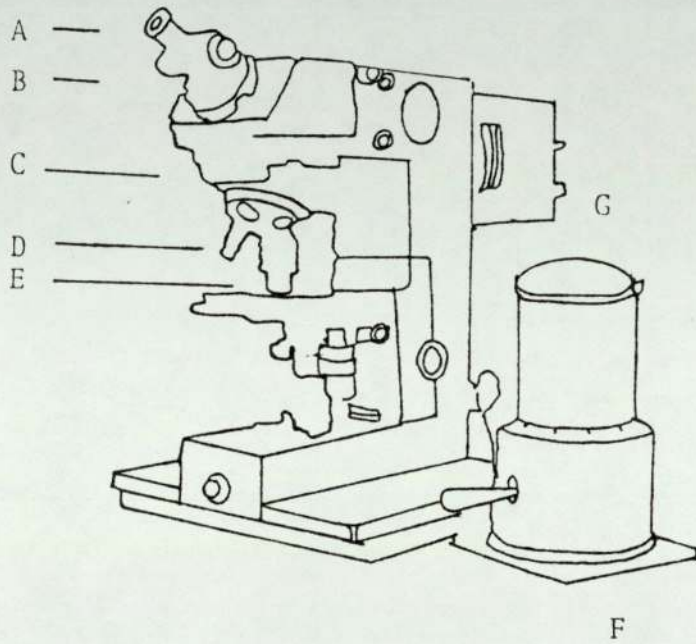
9.5 Microindentation tests on 60/40 brass and aluminium using the modified micromanipulator tungsten microindenters

The two brass specimens and the aluminium specimen used in the previous microindentation hardness tests were indented using the modified micromanipulator and tungsten microindenters. Since the size of the phases of 60/40 brass was smaller than the tip size of the tungsten microindenters, individual phases could not be indented separately. Preliminary microindentations were made outside the SEM. The specimen holder was used to hold the aluminium and a small workshop vice was employed to grip the specimen to be indented. The experiments were designed to test the modified system with the tungsten microindenters to be used as a microhardness test mounted in SEM specimen chamber.

Table 9.4

No.	Specimen	Load	Phase	File-Micrometer divisions primary magnification 75x	Hardness VH	Average Hardness VH	Photomicrographic Diagonal μ
1	KBI-2	10	B	80.5	161	160	-
					159		
					196		
					207		
					169		
					155		
					197		
					205		
					169		
					200		
2	KBI-4	5	B	55.5	186	169	-
					209		
					172		
					166		
					160		
					131		
					81		
					64		
					72		
					72		
3	KAI-2	5	B	46.0	197	145	-
					205		
					169		
					200		
					186		
					209		
					172		
					166		
					160		
					131		
81							
64							
72							
72							
				Average 27			
				Average 13.1			

FIGURE 9.26



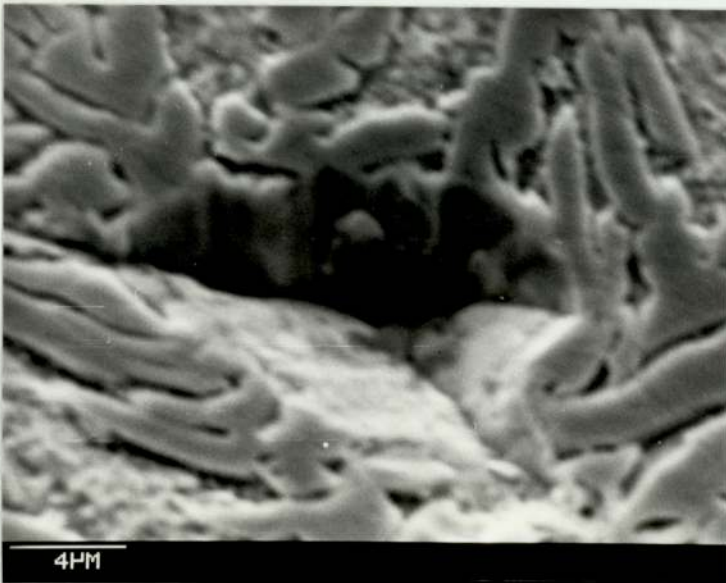
DM41 Microhardness tester

- A = Filar eye piece micrometer
- B = Graduated tube
- C = Centering mount
- D = Reading objective
- E = Indenter objective
- F = Anti-vibration platform
- G = Transmitter

Figure 9.27



Microindentations made with the Vicker's
microhardness tester.



9.5.1 Reproducibility of the microindenters

Four microindentations were made using the nominal 3gram load on the brass specimen at various points. Similarly two indentations were made on aluminium with the nominal 1gram load. The tungsten microindenters (KB_3^*) and KC_4^* were tried out on brass and aluminium respectively and the indented sites were marked and examined in the SEM. The photomicrographs which are displayed in Figures 9.28, 9.29 and 9.30 show the indentation depths and diameters. Figures 9.28 and 9.29 indicate the profile of the microindenter KB_3^* shown in Figure 9.15.

Microindenter KB_3 is more conical than KB_1 which is shown in Figure 9.14. The diameter of each microindentation was measured at four positions, the mean value and standard deviation calculated for all four microindentations and the percentage error calculated as detailed in Table 9.5.

The results in Table 9.5 show a reproducibility of 87% for micro-indentations made with the modified micromanipulator and tungsten microindenter. The photomicrographs of the microindentations (Figures 9.28 and 9.29) on brass show the indenter scratched the surface either before or after indentations. This phenomenon may occur if the length of the indenter is excessive.

9.5.2 Calibration of the indentation diameter and load

The two specimens detailed in Table 9.5 were also used to calibrate the microindentation system with different loads (applied force).

* Code details given in Table 9.2.

Figure 9.28

Microindentations made on brass.

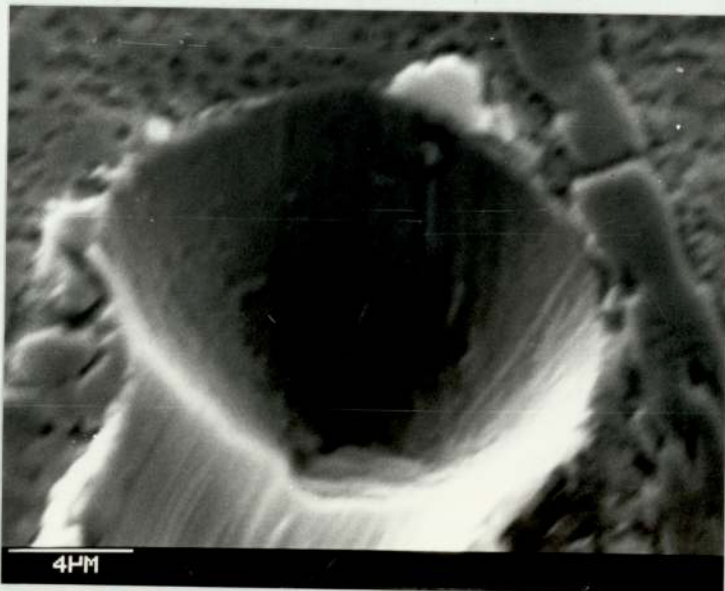


Figure 9.29

Microindentations made on brass.

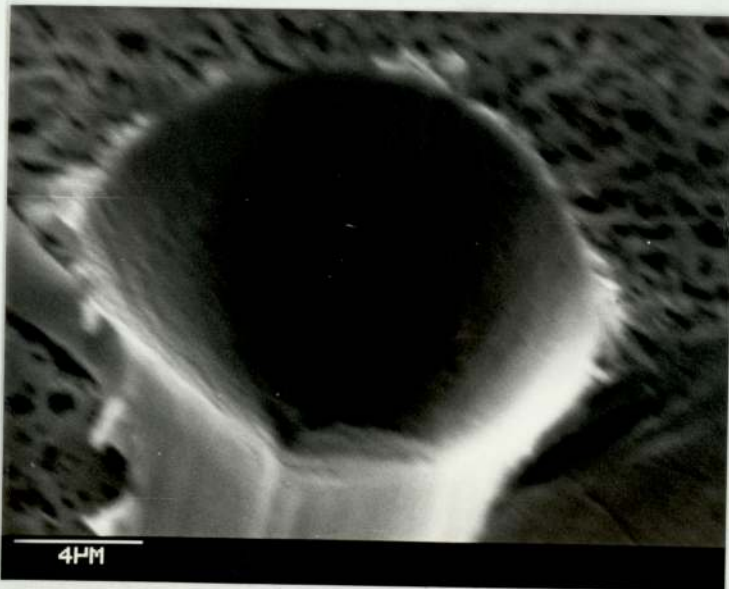


Figure 9.30

Microindentations made on aluminium.



Table 9.5

Specimen	Microindenter	Total load gram	Indenta- tion	Diameter μm	Mean diameter of each indentation (μ)	Average mean + standard - deviations
Brass KBI-2	B ₃	3.139	A	14.93	12.40 + 1.81 15%	
				11.73		
with KB ₃	B ₃	"	B	12.27		
				10.67		
Tungsten microin- denter	B ₃	"	C	14.93	13.13 + 1.43 11%	12.72 + 1.66 13%
				11.47		
				13.33		
				12.80		
	B ₃	"	D	10.13	12.13 + 2.35 19%	
				13.60		
				14.67		
				10.13		
Aluminium KAI-2 with KC ₄	C ₄	1.874	A	14.93	13.20 + 1.35 10%	
				12.00		
				13.60		
				12.27		
tungsten micro- indenter	C ₄	"	B	25.00	21.07 + 2.94 14%	21.43 + 2.62 12%
				18.57		
				22.14		
				21.43		

The brass specimen was indented with the loads W_1 , W_2 and W_3^* and the aluminium was indented with the loads W_1 , W_3 , W_4 and W_5^* . The indented sites were marked on both of the specimens and SEM photomicrographs (Figures 9.31, 9.32 and 9.33) obtained. The diameter of each microindentation was measured in four positions and the mean value and standard deviation calculated.

The values (tabulated in Table 9.6A) were used to evaluate the values for 2g to 4g loads as shown in Table 9.6B. Linear regression analysis was carried out to evaluate these values. The weight of the microindenter holder was one gram and was added to the weight of the load blocks to derive the total load (force) applied which also included the weight of the tungsten microindenter.

The weight of 1.5cm long and 0.45cm thick tungsten wire was 0.0023 grams. The weight of 1cm of the same wire was 1.56×10^{-3} g which was included in the total load applied to indent a specimen, but the weight of the lost polished material during the electro-polishing process was neglected.

The results in Table 9.6 indicate a maximum error of 16% in estimating the size of microindentations in the brass specimen. The estimated error in measuring the indentation in aluminium was 9%. These figures show a maximum uncertainty of $\pm 16\%$ on the microindentation produced with the modified system. This indicates $\pm 14\%$

* Details of loads given in Table 9.6

Figure 9.31

Microindentations made with different load on brass.

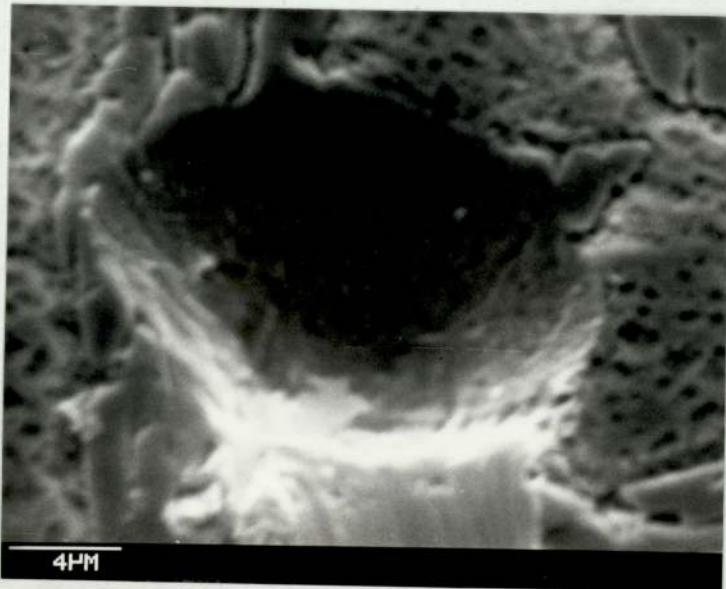


Figure 9.31

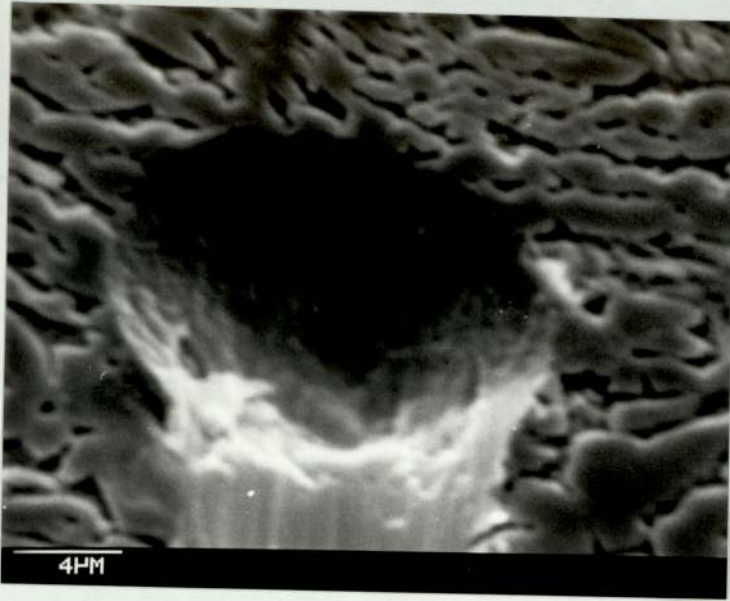


Figure 9.32

Microindentations made with different load on aluminium

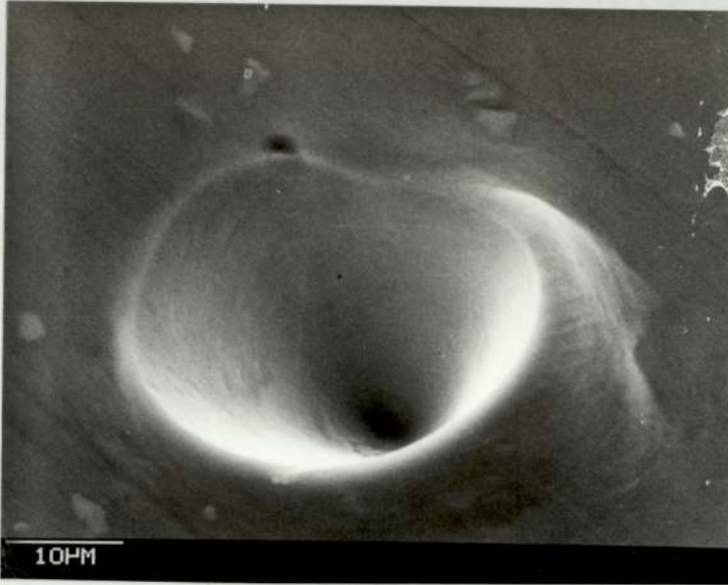


Figure 9.33

Microindentations made at different load on aluminium

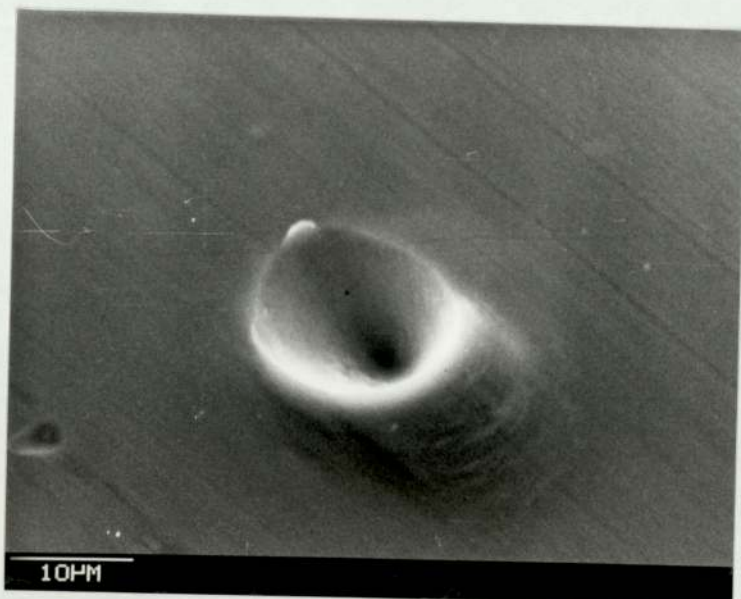


Table 9.6A

Specimen	Load No.	Total Load g	Indentation position	Diameter in μ	Mean diameter in $(\mu) +$ standard deviation
Brass KBI-2 Indenter KB ₁	W1 2.681g	3.683	A	18.19	15.33 \pm 2.46 16%
			B	13.43	
			C	16.57	
			D	13.14	
	W2 2.762g	3.765	A	16.00	13.83 \pm 1.59 12%
			B	13.71	
			C	13.41	
			D	12.18	
	W3 2.137g	3.139	A	15.38	13.39 \pm 2.08 16%
			B	10.46	
			C	13.85	
			D	13.85	
Aluminium KA1-2 Indenter KC ₄	W1 2.681g	3.683	A	13.60	12.33 \pm 1.14 9%
			B	10.93	
			C	12.00	
			D	12.80	
	W3 2.137g	3.139	A	12.27	11.47 \pm 0.69 6%
			B	10.67	
			C	11.20	
			D	11.73	
	W4 1.604g	2.606	A	13.00	11.73 \pm 1.05 9%
			B	10.44	
			C	11.60	
			D	11.89	
W5 0.874g	1.876	A	6.48	6.35 \pm 0.27 4%	
		B	6.13		
		C	6.13		
		D	6.67		

Table 9.6B

Specimen	Load (applied force) gram	Evaluated constants	Extrapolated/Interpolated values using the mean values (μ)
Brass KBI-2	3.00g	$m = 1.73$	13.26
	3.25g	$c = 8.07$	13.69
	3.50g		14.13
	3.75g		14.56
	4.00g		14.99
Aluminium KA1-2	1.59	$m = 3.11$	6.35
	2.09	$c = 1.68$	7.90
	2.59		9.46
	3.09		11.43
	3.59		12.57
	4.09		14.12

scatter obtained on microindentation with the same load. On subtracting this error quadratically, $\pm 8\%$ error was estimated for microindentation produced with different loads. By comparison $\pm 2\%$ error is given for reading the Filar micrometer divisions with the Vickers (65) microhardness testing equipment.

Since the maximum load used with the modified system and tungsten microindenters was lower than that of the minimum with the Vickers equipment, the microhardness values for the microindentations with the modified system could not be compared directly but by extrapolation.

9.5.3 Microindentations with special features

Several microindentation tests were carried out with the modified system on aluminium and brass. Some of the microindentations, selected for their special features, are discussed below.

9.5.3.1 Series C (Table 9.2) Microindenters

The microindenters from series C were found to have shapes particularly suitable for indentation. These microindenters, because of their suitable length (1cm), could be mounted in the indenter holder with their tips just protruding. Fine pointed tweezers were used to mount the microindenters in the holder. The microindentations made with two of these microindenters (viz. KC_3 and KC_4) was perfectly shaped with no sign of undesired lateral movement.

9.5.3.2 Microindentations on aluminium

SEM photomicrographs of the microindentations made with micro-indenter KC_4 are displayed in Figure 9.34. Plastic flow of material may be visualised with upward extrusion in the surface near the ridge (this is known as the ridging effect).

The ridging effect may also be seen in photomicrographs of other indentations reported earlier in this study. The elastic recovery of the material after the release of the microindenter results in a change of size and shape of the impression. For aluminium, 5 to 20% recovery in the depth direction has been reported (50).

9.5.3.3 Microindentations on brass

SEM photomicrographs of the microindentations made with the micro-indenter KC_3 are displayed in Figure 9.35. The indentations on brass show very little recovery of the metal after indentation. It is also observed that the ridging effect round the impressions is noticeably lower than those on aluminium. The size and shape of the indenters KC_3 and KC_4 were different; there must be more extrusion on the edges of indentation after the release of the more conical shaped microindenter.

Figure 9.34

Some selected microindentations on aluminium

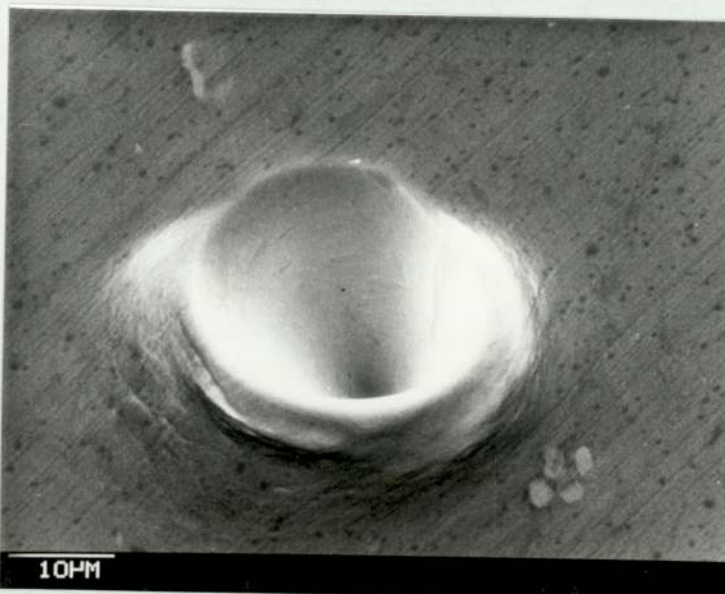


Figure 9.34



Figure 9.35

Some selected microindentations on brass

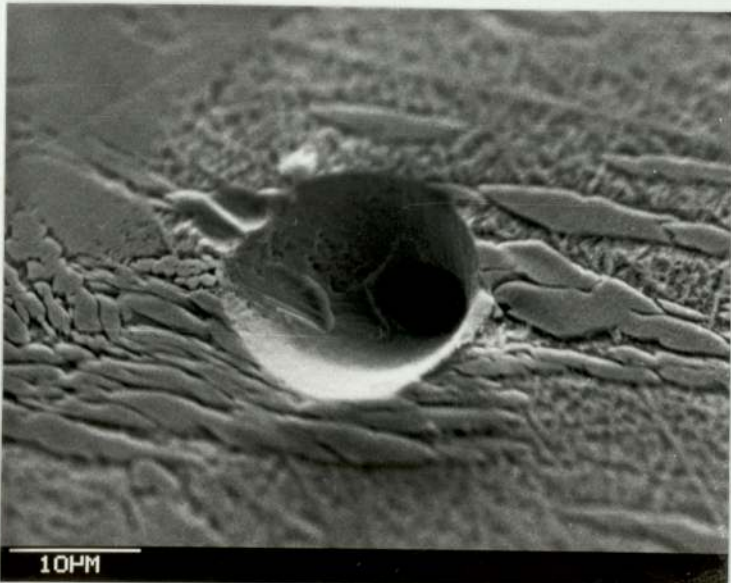
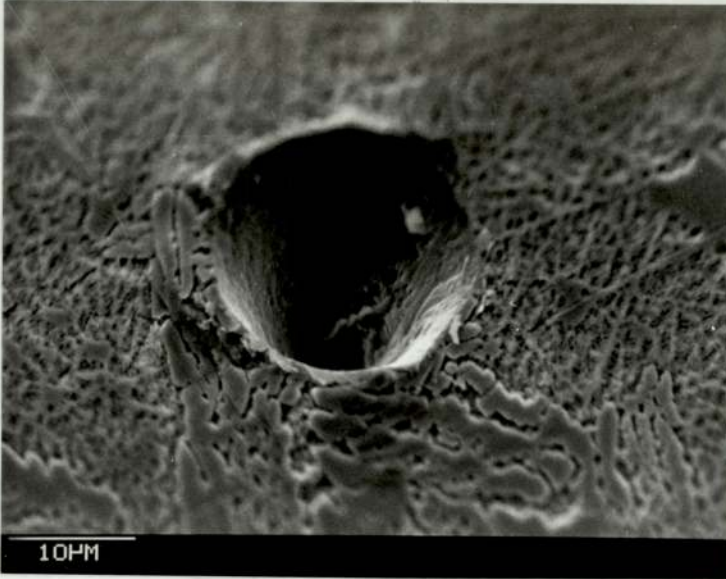
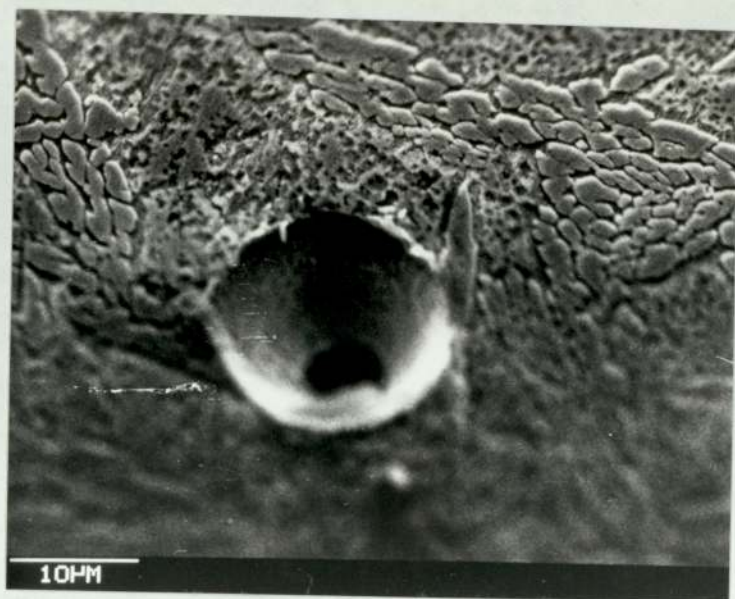


Figure 9.35



Chapter 10

Discussion and Conclusions

The results obtained in the present study and the associated techniques of microindentation and microhardness testing are of a rather more practical than theoretical nature. The development of a stereoscan micromanipulator for a microindentation hardness testing and the manufacture of tungsten microindenters employing an electropolishing circuit with modified automatic switch are the main contributions to the science of microindentation and microhardness testing.

Although most of the microindentations were made on aluminium and brass, these techniques may be applied to other materials including coatings of $40\mu\text{m}$ or more in thickness. The size of the tungsten microindenter tip was reduced to $0.5\mu\text{m}$ in diameter from a 0.45mm thick wire. Finer tips of such microindenters are so fragile that they break or get damaged during preparation or handling. Indenters with tip sizes of diameter 0.1 and 0.25μ could not be handled for mounting. Even the microindenters made of 0.45mm diameter tungsten wire with tips $1\mu\text{m}$ or less in diameter (series E, Table 9.4) were damaged during indentation. The SEM photomicrograph of a damaged indenter is shown in Figure 9.36.

The reproducibility of 86% in the preparation of the microindenters may further be increased by minimising vibration, draughts and any movement in the laboratory. Microindenters with tips of about 0.1

Figure 9.36

A damaged microindenter



to 0.5 μ m diameter can be coated with carbon of a few nanometers in thickness. Such carbon coated microindenters can be hardened by heat treatment to diffuse the carbon into the tungsten to give tungsten carbide tips. These tips are harder than tungsten tips. The ductile tungsten supports the tungsten carbide coating and prevents the tips being too brittle to use. The tips are fragile and require very careful handling.

Microindentations made using the tungsten microindenters in the modified system are observed to be 84% reproducible. The use of machined brass blocks to change the load on microindenters of various diameters was 92% accurate.

Scratch damage from lateral movement of the indenters which was observed with the microindentations made with the microindenters 1.5cm in length (series B), was minimised by the use of short microindenters 1cm long (series C). The length of the micro-indenter can be shortened using a tungsten wire cutter with care, while holding the tip side without damaging the fine tip.

The basic features of the microindentations show that the system can be further developed into a reliable microhardness tester to investigate the science of microindentations and microhardness inside and outside a scanning electron microscope. However it is essential to calibrate and assess the modified system at loads of above 4 grams since the lowest load used in the Vickers microhardness test is only 5 grams.

In the light of the above discussion of the results the following future work is suggested:

1. The tungsten microindenters should be prepared in a draught-free and vibration-free environment.
2. To avoid atmospheric contamination during microindentation, the testing should be carried out in a vacuum.
3. The microindenter should be calibrated and assessed by comparison with standard microhardness test equipment like the Vickers microhardness instrument.

References - Part II

1. What's the point??
Popular Hi-Fi, 1979, 79, 116.
2. Specifications of the stylus models M95ED, M95EJ and N95ED-EJ
Shure electronics Ltd., Eccleston Road, Maidstone, ME15 6AU
3. Private communication with Vickers Ltd.,
letter Ref. DB/JP dated 4-11-80.
4. Relion Ltd.
Diamond tool makers, Birmingham.
5. J.H. Westbrook and H. Conrad,
The Science of hardness testing and its research application,
Symposium ASM, 1971.
6. J.M. Pearson
Field emission tungsten tips, unpublished report,
Department of Physics, The University of Aston in Birmingham,
1976.
7. Williams' monographs,
Hardness techniques
Published by ASM (2000 references), 1942.
8. B.S.18: Methods for tensile testing of metals, 1962.
9. B.S. 427: Methods for Vickers hardness test.
Part I: testing of metals, 1961.
Part II: Verification of Vickers hardness testing machine,
1964.
10. B.S. 891: Methods for Rockwell hardness test.
Part I: Testing of metals, 1962.
Part II: Verification of Rockwell hardness testing machine,
1964.

11. B.S. 240: Methods for Brinell hardness test.
Part I: Testing of metals, 1962.
Part II: Verification of Brinell hardness testing machine, 1964.
12. H. O'Neill
Hardness measurement of metals and alloys.
Second edition, Chapman and Hall, 1967.
13. R.W. Cahn
Physical metallurgy
John Wiley and Sons, 1965.
14. P. Ludwick
Die Kugelprobe, Berlin, 1908.
15. B.W. Mott
Microindentation hardness testing.
Butterworths, London, 1956.
16. T. Yoshino,
Bull. JSME, 1965, 8, 291.
17. E. Orowan
Nature, 1941, 147, 452.
18. N. Gane and J.M. Cox
Phil. Mag., 1970, 22, 881.
19. J. Friedel
Dislocations.
Pergamon, 1961, p.23.
20. T.O. Mulhearn
J. Mech. Phys. Solids, 1959, 7, 85.
21. A.G. Atkins, A. Silvers and D. Tabor
J. Inst. Metals, 1966, 94, 369.

22. L.E. Samuels and T.O. Mulhearn
J. Phys. Mech. Solids, 1957, 5, 125.
23. N.A. Stilwell and D. Tabor
Proc. Phys. Soc., 1967, 78, 169.
24. M. Braunovic, C.W. Howorth and R.T. Weiner
Met. Sci. J., 1968, 2, 67.
25. K.T. Aust and J.H. Westbrook
Acta. Met., 1971, 19, 521.
26. M. Braunovic and C.W. Haworth
Pract. Metallog., 1970, 7(4), 183.
27. V. Ya Ferene, M.I.N. Mikrotverdost and M.M. Khruschov
Nauka, 1965, 171.
28. J.H. Westbrook and D.L. Wood
Nature, 1961, 192, 1280.
29. N.G. Ainslie, V.A. Philips and E. Turnbull
Acta Met., 1960, 8, 528.
30. J.H. Westbrook
A.S.M., Trans. Quart., 1964, 57, 567.
31. J.H. Westbrook and K.T. Aust
Acta Met., 1963, 11, 1151.
32. K.T. Aust, A.J. Peat and J.H. Westbrook,
Acta Met., 1965, 19, 1469.
33. K.T. Aust and J.H. Westbrook
Lattice defects in quenched metals
Academic Press, New York, 1965, 771.
34. W.H. Basset and C.H. Davies
Trans. AIME, 1919, 60, 428.

35. W.J. Babyak and F.N. Rhines
Trans TMS - AIME, 1960, 218, 21 and 1122.
36. P.C. Jindal and R.W. Armstrong
Trans TMS - AIME, 1967, 239, 1856.
37. P.C. Jindal and R.W. Armstrong
Trans TMS - AIME, 1969, 245, 623.
38. R.M. Douthwaite
J. Iron Steel Inst., 1970, 208, 265.
39. K. Farrel and J.T. Houston
Scripta Met., 1971, 5, 463.
40. E.O. Hall
Nature, 1954, 173, 948.
41. R.W. Armstrong
Met. Trans., 1970, 1, 1169.
42. A.T. Churchman
Acta Met., 1955, 3, 22.
43. A.F. Mohrheim
Prakt Metallog., 1968, 5(3), 144.
44. R.M. Douthwaite and N.J. Petch
Acta Met., 1970, 18, 211.
45. C.A. Edwards and L.B. Pfeil
J. Iron Steel Inst., 1925, 112, 129.
Metal handbook, 1948 ed., American Soc. for Metals, 433,
Table XIII.
46. S.I. Bulicher, V.P. Alekhim and M. Shorshoron
Fiz. Khim, Obrab, Met., 1979, 79(5), 69-81.
47. H.T. Angus
Wear, 1979, 54(1), 37-38.

48. E.I. Treiger
Zavod Lab., 1979, 11, 1059.
49. J.I. Parks
Met. Proc. Conf. 83rd annual meeting, Birmingham, Ala 30th
April-4th May, 1979.
(MET A 8008-72-282), 195-202.
50. H. Buckle
Met. reviews, 1959, 4(13), 49.
51. G. Bluebeck, O. Brummer and A. Alam
Phys. Status Solidi(a), 1979, 52(1), 217-221.
52. A. Krupkowski and Truszkowski, W.
Bull. Acad. Pol. d. Sci., 1951, 1, 39.
53. G. Williams and H. O'Neill.
J. Iron Steel Inst., 1956, 182, 266.
54. A.G. Atkins and D. Tabor
J. Mech. Phys. Solids, 1965, 13, 149.
55. R. Boklen
Z. Met., 1964, 55, 371
56. Meyer
Z. d. Ver. Deutsch Ing., 1908, 52, 645-835.
57. E. Kips and J. Sack
Nature, 1939, 138, 328.
58. F. Knoop
J. Res. Nat. Bur. Standards, 1939, 23, 39.
59. B.W. Mott
Microindentation hardness testing
Butterworth, London, 1956.

60. N. Gane and F.P. Bowden
J. Appl. Phys., 1968, 39, 1432.
61. N. Gane
Proc. Roy. Soc (London), 1970, A317, 367.
62. N. Gane and J.M. Cox
Phil. Mag., 1970, 22, 881.
63. D. Tabor
Rev. Phys. in technol. 1970, 1, 145.
64. Stereoscan Micromanipulator
Type 81115 Mk.2, T1 1121-TM, Issue 4, Cambridge Instruments
Ltd.
65. Vickers Micro-hardness testing instructions.
Vickers Ltd., Vickers Instruments.
66. Stereoscan scanning electron microscope.
Type 96113, Mark 2A, Cambridge Instrument Company Ltd.

Appendix 1

Standard Illuminants

Illuminant	Description
S_A	A gas filled tungsten filament lamp operated at a colour temperature* of 2854K, typical of average artificial tungsten lamp illumination.
S_B	Typical of sunlight with a colour temperature of 4900K.
S_C	Typical of an overcast sky (average daylight) with a colour temperature of 6700K.
D_{6500}	Typical of average daylight with a colour temperature of 6500K.
D_{5500}	Represents a yellower daylight, colour temperature of 5500K.
D_{7500}	A bluer daylight (north skylight), colour temperature of 7500K.

* Theoretically the colour temperature is defined as a temperature at which a perfect black body emits light of the same colour as the source in question. Since most light sources only approximate to black bodies the values quoted are in fact correlated colour temperatures.

APPENDIX 2

Programme OK002

(Page 1)

```

MASTER OKCOLOUR3
DIMENSION A(3,70),B(8,70),C(70),D(70)
DO 5 K=1,65
READ(5,700) A(1,K),A(2,K),A(3,K)
5 CONTINUE
X=0
Y=0
Z=0
B(1,1)=380.00
J=1
DO 10 I=1,65
READ(1,800) B(7,I),B(8,I)
II=I+1
B(1,II)=B(1,I)+5.00
B(2,I)=B(8,I)-B(7,I)
B(3,I)=10*(2-B(2,I))
B(4,I)=A(1,J)*B(5,I)
B(5,I)=A(2,J)*B(3,I)
B(6,I)=A(3,J)*B(3,I)
J=J+1
X=X+B(4,I)
Y=Y+B(5,I)
Z=Z+B(6,I)
10 CONTINUE
SUM=(X+Y+Z)
XX=X/SUM
YY=Y/SUM
ZZ=Z/SUM
XYZ=XX+YY+ZZ
IF (XYZ-1) 20,30,20
20 WRITE (2,300) XX,YY,ZZ,XYZ
30 TO 50
30 WRITE (2,400)
DO 40 L=1,65
40 WRITE (2,500) B(1,L),B(2,L),B(3,L),B(4,L),B(5,L),B(6,L)
50 CONTINUE
60 WRITE (2,600) X,Y,Z,XX,YY,ZZ,XYZ

```

Continued.....

Continued from the previous page

Programme 0k002

(Page 2)

```

CALL OPENGINO6P
CALL CHASIZ(3,0,3,5)
CALL SHIFT2(50,0,50,0)
CALL MOVT02(0,0,0,0)
CALL AXIPOS(0,0,0,0,135,0,1)
CALL AXIPOS(0,0,0,0,200,0,2)
CALL AXISCA(1,70,350,0,705,0,1)
CALL AXISCA(1,20,0,0,100,0,2)
CALL AXIDRA(1,1,1)
CALL AXIDRA(-1,-1,2)
CALL MOVT02(45,0,-18,0)
CALL CHAHOL(16HWAVE LENGTH NM*. )
CALL CHANG(90,00)
CALL MOVT02(0,0,0,0)
CALL MOVT02(-15,0,75,0)
CALL CHAHOL(17HREFLECTIVITY %*. )
DO 65 I=1,65
C(I)=B(1,I)
F(I)=B(3,I)
65 CONTINUE
CALL GRACUR(C,D,65)
CALL DPVEND
70 STOP
200 FORMAT (F5.3,2X,F5.3)
300 FORMAT (////,10X,'THERE SHOULD BE A MISTAKE,BECAUSE:',//,15X,'XX=
1,F7.3,/,15X,'YY=',F7.3,/,15X,'ZZ=',F7.3,/,15X,'XYZ=',F7.5)
400 FORMAT (////,7X,'WAVELENGTH',4X,'ABSORPTION',4X,'REFLECTIVITY',7X
1,'X COEFFICIENT',7 X,'Y COEFFICIENT',7X,'Z COEFFICIENT',//)
500 FORMAT (9X,F6-2,8X,F5.3,8X,F6-3,9X,F11.3,9X,F11.3)
600 FORMAT (//,9X,'X=',F12.3,//,9X,'Y=',F12.3,//,9X,'Z=',F12.3,//,9X,'X
1X=',F5.3,/,9X,'YY=',F5.3,/,9X,'ZZ=',F5.3,/,8X,'XYZ=',F5.3)
700 FORMAT (F7.3,2X,F7.3,2X,F7.3)
END
FINISH
***

```

APPENDIX 3

DOCUMENT OK001

(1)

000.013 000.000 000.064
000.025 000.001 000.116
000.051 000.001 000.243
000.103 000.003 000.488
000.212 000.006 001.008
000.376 000.010 001.785
000.763 000.021 003.636
001.504 000.042 007.195
002.823 000.084 013.564
004.860 000.166 023.511
007.005 000.286 034.183
008.705 000.449 043.004
009.956 000.660 049.944
010.746 000.920 055.360
011.250 001.257 065.658
011.306 001.700 061.870
011.002 002.269 063.133
010.110 002.977 061.528
008.376 003.901 055.217
006.473 005.127 047.476
004.614 006.707 039.220
002.958 008.642 031.458
001.726 011.213 025.072
000.837 014.699 020.081
000.294 019.335 016.282
000.153 025.628 013.358
000.616 033.228 010.449
002.018 042.121 007.734
004.587 051.475 005.673
008.309 060.116 004.337
013.094 068.210 003.335
018.634 075.501 002.463
024.959 081.996 001.750

(2)

032.163 087.644 001.198
040.274 092.445 000.810
049.381 096.464 000.556
059.447 099.500 000.386
070.256 101.366 000.276
081.691 102.035 000.221
093.349 101.424 000.191
104.854 099.563 000.176
115.545 096.383 000.159
124.968 092.150 000.141
132.482 087.139 000.121
137.037 081.424 000.098
138.710 075.208 000.075
136.727 068.579 000.051
131.405 061.771 000.039
122.716 054.719 000.028
110.639 047.261 000.021
096.900 039.970 000.010
083.676 033.509 000.008
070.752 027.647 000.005
058.287 022.329 000.002
046.790 017.658 000.001
036.840 013.744 000.000
028.361 010.490 000.000
021.248 007.815 000.000
015.625 005.721 000.000
011.602 004.232 000.000
008.672 003.152 000.000
006.205 002.249 000.000
004.352 001.574 000.000
003.092 001.117 000.000
002.251 000.810 000.000

Appendix 5

Nanotech automatic high vacuum coater

Nanotech coaters have a fully automatic vacuum pumping sequence and are equipped with chamber jiggging necessary for the production of thin films (of carbon or metal) for transmission and scanning electron microscopy. The 'S' models include a comprehensive selection of vacuum and process components to augment the essential equipment in the basic models.

Specification includes:

2 stage rotary pump	2.5m ³ /h
Diffusion pump	150l/sec.
Pirani and Penning guages	2 heads and one standard.
L.T. supply	1kVA-10v/20v.

Appendix 6

Procedure for preparing and mounting metallographic specimens

1. Coated specimens were cut cross sectionwise into pieces at three positions, i.e. middle, left and right.
2. Three such suitable pieces were selected for each specimen and mounted cross-sectionwise in conducting Bakelite.
3. Each mounted specimen was abraded with increasingly fine grade emery paper, i.e. 150, 200, 300, 400, 600 grades.
4. Each specimen was washed with Inhibisol (cleansing liquid), dried and polished on 6 μ grade diamond sprayed cloth.
5. Each dried specimen was then etched for 5 seconds (to show the thin coating clearly) in a solution of 7% FeCl₃, 3% HCl and 90% distilled water.
6. The etched specimens were washed in distilled water twice, dried and then washed with Inhibisol solution and finally polished again on 6 μ diamond sprayed cloth to achieve uniform polishing the substrate coating and interface regions.
7. All the specimens were dried and kept in a desiccator until examined under the projection microscope or scanning electron microscope (S.E.M.).

Appendix 7

Determination of coating thickness

A. Gravimetric method for determining coating thickness.

If the weight of the glass cover slip before coating = x gram

weight of the glass cover slip after coating = x + m gram

Surface area of the coating (assuming it to be uniform) = A cm²

density of the coating material = ρ g/cm³

thickness of the coating = t cm

then
$$t = \frac{m}{\rho \cdot A} \quad \text{---} \quad (1)$$

Density of gold = 19.3 g/cm³

B. Resistivity method for determining coating thickness.

If R is the resistance in ohms (Ω) of a wire l m long, of uniform cross section a = txw² and resistivity ρ is in ohm meters then

$$t = \frac{\rho \times l}{R \times w} \quad \text{---} \quad (2)$$

Resistivity (ρ) of gold is = 0.02 micro-Ω meter.

Appendix 8

Installation Procedure

Unicam SP 8000D spectrophotometer with a Unicam SP 890 diffuse reflectance attachment

The SP 890 attachment (figure 4.20) fits within the cell compartment of the SP 800 instrument and can be used to record the diffuse reflectance spectrum of solid or powder samples throughout the visible and ultraviolet. To install the SP 890 attachment in the main instrument (spectrophotometer):

1. Lift out the cell compartment partition.
2. Remove the plane mirrors M13 and M14 (see figure 4.19) by unscrewing the two 2BA cap screws with the Allen key provided, and lifting the mirror assembly from its locating pins. This assembly can be stored in place of the diffuse reflectance accessory in the carrying case.
3. Install the SP 890 in place of the plane mirror assembly.

APPENDIX 9

Input files
(Page 1)

DOCUMENT	KGSLIP	DOCUMENT	KG01	DOCUMENT	KG06	DOCUMENT	KG07
(I)		(I)		(I)		(I)	
0-38	0-59	0-28	1-14	0-28	1-68	0-38	1-12
0-375	0-59	0-275	1-136	0-275	1-68	0-375	1-12
0-37	0-59	0-27	1-13	0-27	1-68	0-37	1-12
0-365	0-585	0-265	1-12	0-265	1-68	0-365	1-11
0-36	0-58	0-26	1-11	0-26	1-68	0-36	1-11
0-355	0-575	0-26	1-1	0-26	1-68	0-35	1-1
0-35	0-57	0-26	1-07	0-26	1-68	0-35	1-1
0-345	0-56	0-26	1-05	0-26	1-68	0-345	1-09
0-342	0-54	0-26	1-04	0-26	1-685	0-342	1-08
0-34	0-53	0-26	1-03	0-26	1-68	0-34	1-07
0-34	0-51	0-26	1-01	0-26	1-68	0-34	1-05
0-34	0-50	0-259	0-99	0-259	1-675	0-34	1-04
0-335	0-49	0-257	0-98	0-257	1-67	0-335	1-03
0-335	0-485	0-255	0-97	0-255	1-66	0-335	1-01
0-33	0-48	0-25	0-95	0-25	1-654	0-33	1-0
0-325	0-475	0-246	0-93	0-246	1-65	0-325	0-99
0-325	0-47	0-242	0-91	0-242	1-64	0-325	0-975
0-32	0-465	0-241	0-88	0-241	1-63	0-32	0-96
0-32	0-46	0-24	0-87	0-24	1-62	0-32	0-94
0-32	0-455	0-238	0-85	0-238	1-6	0-32	0-93
0-315	0-45	0-235	0-835	0-235	1-595	0-315	0-91
0-315	0-45	0-232	0-82	0-232	1-58	0-315	0-895
0-31	0-44	0-23	0-80	0-23	1-57	0-31	0-88
0-31	0-44	0-224	0-78	0-224	1-55	0-31	0-86
0-305	0-435	0-222	0-76	0-222	1-532	0-305	0-84
0-3	0-43	0-221	0-75	0-221	1-52	0-3	0-83
0-3	0-43	0-22	0-74	0-22	1-51	0-3	0-815
0-3	0-425	0-219	0-73	0-219	1-5	0-3	0-81
0-295	0-425	0-218	0-72	0-218	1-472	0-295	0-8
0-29	0-42	0-214	0-71	0-214	1-47	0-29	0-79
0-285	0-42	0-21	0-705	0-21	1-46	0-285	0-78
0-28	0-42	0-207	0-7	0-207	1-455	0-28	0-77
0-28	0-42	0-205	0-697	0-205	1-45	0-28	0-765

Continued.....

Continued from the previous page

(Page 2)

0.28	0.76	0.203	1.445	0.203	0.695	0.28	0.415
0.275	0.755	0.20	1.44	0.20	0.69	0.275	0.41
0.27	0.750	0.2	1.435	0.20	0.685	0.27	0.405
0.265	0.74	0.2	1.43	0.195	0.68	0.265	0.4
0.26	0.735	0.2	1.428	0.19	0.68	0.26	0.39
0.26	0.73	0.195	1.422	0.186	0.685	0.26	0.38
0.255	0.725	0.19	1.421	0.182	0.687	0.255	0.375
0.25	0.72	0.186	1.42	0.181	0.687	0.25	0.37
0.245	0.715	0.182	1.42	0.180	0.687	0.245	0.365
0.24	0.71	0.181	1.42	0.175	0.687	0.24	0.36
0.235	0.705	0.181	1.42	0.17	0.687	0.235	0.345
0.23	0.7	0.175	1.42	0.165	0.687	0.23	0.34
0.225	0.695	0.17	1.41	0.162	0.687	0.225	0.335
0.22	0.69	0.165	1.4	0.161	0.687	0.22	0.33
0.215	0.685	0.162	1.4	0.16	0.68	0.215	0.3225
0.21	0.68	0.161	1.398	0.155	0.682	0.21	0.32
0.205	0.675	0.16	1.395	0.15	0.685	0.205	0.315
0.2	0.67	0.155	1.392	0.148	0.687	0.2	0.31
0.195	0.665	0.15	1.39	0.145	0.69	0.195	0.30
0.19	0.66	0.148	1.385	0.143	0.687	0.19	0.29
0.185	0.655	0.145	1.38	0.14	0.685	0.185	0.285
0.18	0.65	0.143	1.375	0.138	0.682	0.18	0.28
0.17	0.645	0.14	1.37	0.135	0.68	0.17	0.27
0.16	0.64	0.138	1.365	0.133	0.668	0.16	0.26
0.155	0.635	0.135	1.36	0.13	0.665	0.155	0.255
0.15	0.63	0.133	1.355	0.127	0.663	0.15	0.25
0.145	0.625	0.13	1.35	0.122	0.66	0.145	0.24
0.14	0.62	0.127	1.345	0.121	0.66	0.14	0.23
0.135	0.615	0.122	1.34	0.12	0.66	0.135	0.22
0.13	0.61	0.121	1.338	0.115	0.66	0.13	0.21
0.125	0.605	0.12	1.335	0.11	0.66	0.125	0.205
0.12	0.6	0.115	1.335	END		0.12	0.2
		0.11	1.335	STOP			
		0.11	1.335	***			

380.00	0.650	22.387	0.291	0.000	1.433
385.00	0.660	21.878	0.547	0.022	2.538
390.00	0.659	21.928	1.118	0.022	5.329
395.00	0.660	21.878	2.253	0.066	10.676
400.00	0.660	21.878	4.638	0.131	22.053
405.00	0.665	21.627	8.132	0.216	38.605
410.00	0.665	21.627	16.502	0.454	78.636
415.00	0.665	21.627	32.527	0.908	155.608
420.00	0.670	21.380	60.355	1.796	289.993
425.00	0.670	21.380	103.905	3.549	502.656
430.00	0.672	21.281	149.076	6.086	727.462
435.00	0.674	21.184	184.403	9.511	910.980
440.00	0.670	21.380	212.856	14.111	1067.784
445.00	0.670	21.380	229.745	19.669	1183.576
450.00	0.675	21.135	237.768	26.567	1387.675
455.00	0.665	21.627	244.517	36.766	1338.074
460.00	0.665	21.627	237.942	49.072	1365.389
465.00	0.660	21.878	221.183	65.130	1346.086
470.00	0.660	21.878	183.247	85.345	1208.016
475.00	0.650	22.387	144.912	114.779	1062.855
480.00	0.635	23.174	106.925	155.428	908.882
485.00	0.620	23.988	70.957	207.307	754.625
490.00	0.600	25.119	43.355	281.658	629.780
495.00	0.594	25.468	21.317	374.359	511.429
500.00	0.569	26.977	7.931	521.608	439.246
505.00	0.550	28.184	4.312	722.295	376.480
510.00	0.520	30.200	18.603	1003.470	315.555
515.00	0.500	31.623	63.815	1331.983	244.571
520.00	0.480	33.113	151.890	1704.497	187.851
525.00	0.460	34.674	288.104	2084.443	150.330
530.00	0.445	35.892	469.972	2448.207	119.700
535.00	0.435	36.728	684.394	2773.018	90.462
540.00	0.420	38.019	948.915	3117.401	66.533
545.00	0.413	38.637	1242.672	3386.275	46.287
550.00	0.605	39.355	1584.984	3638.174	31.878
555.00	0.398	39.994	1974.967	3858.027	22.237
560.00	0.390	40.738	2421.754	4053.434	15.725

Continued.....

Continued from the previous page
(The thick gold coating)
(Page 2)

575.00	0.375	42.170	3936.495	4277.015	8.054
580.00	0.370	42.658	4472.857	4247.154	7.508
585.00	0.365	43.152	4985.987	4159.110	6.861
590.00	0.360	43.652	5455.051	4022.493	6.155
595.00	0.355	44.157	5850.014	3847.801	5.343
600.00	0.350	44.668	6121.218	3637.076	4.377
605.00	0.345	45.186	6267.694	3398.318	3.389
610.00	0.340	45.709	6249.630	3134.665	2.331
615.00	0.335	46.238	6075.918	2856.174	1.803
620.00	0.320	47.863	5873.557	2619.016	1.340
625.00	0.315	48.417	5356.835	2288.247	1.017
630.00	0.310	48.978	4745.957	1957.646	0.490
635.00	0.305	49.545	4145.729	1660.204	0.396
640.00	0.300	50.119	3546.000	1385.632	0.251
645.00	0.300	50.119	2921.270	1119.101	0.100
650.00	0.305	49.545	2318.211	874.866	0.050
655.00	0.300	50.119	1846.374	688.832	0.000
660.00	0.300	50.119	1421.417	525.745	0.000
665.00	0.295	50.699	1077.254	396.213	0.000
670.00	0.290	51.286	801.346	293.408	0.000
675.00	0.285	51.880	601.912	219.556	0.000
680.00	0.280	52.481	455.113	165.419	0.000
685.00	0.275	53.088	329.414	119.396	0.000
690.00	0.270	53.703	233.716	84.529	0.000
695.00	0.265	54.325	167.973	60.681	0.000
700.00	0.265	54.325	122.286	44.003	0.000

X = 104060.689

Y = 88608.379

Z = 17687.176

XX=0.495
YY=0.421
ZZ=0.084
XYZ=1.000

APPENDIX 11

A Computer's Output for Programme Ok002 (Thinnest gold coating) (Page 1)

WAVELENGTH	REFLECTIVITY	X COEFFICIENT	Y COEFFICIENT	Z COEFFICIENT
380.00	0.560	0.358	0.000	1.763
385.00	0.555	0.697	0.028	3.232
390.00	0.550	1.437	0.028	6.849
395.00	0.545	2.937	0.086	13.913
400.00	0.545	6.044	0.171	28.738
405.00	0.545	10.720	0.285	50.891
410.00	0.540	22.005	0.606	104.863
415.00	0.535	43.878	1.225	209.909
420.00	0.535	82.359	2.451	395.720
425.00	0.530	143.429	4.899	693.859
430.00	0.522	210.576	8.597	1027.567
435.00	0.518	264.100	13.622	1304.695
440.00	0.515	304.148	20.162	1525.750
445.00	0.513	329.797	28.235	1699.011
450.00	0.510	347.658	38.845	2029.026
455.00	0.500	357.527	53.759	1956.501
460.00	0.495	351.942	72.583	2019.558
465.00	0.495	323.408	95.231	1968.216
470.00	0.490	271.042	126.234	1786.787
475.00	0.480	214.341	169.771	1572.078
480.00	0.475	154.553	224.661	1313.734
485.00	0.470	100.230	292.829	1065.936
490.00	0.460	59.847	388.796	869.339
495.00	0.459	29.089	510.843	697.887
500.00	0.459	10.218	671.961	565.858
505.00	0.450	5.429	909.316	473.960
510.00	0.440	22.366	1206.436	379.380
515.00	0.442	72.933	1522.294	279.514
520.00	0.440	166.544	1868.944	205.974
525.00	0.440	301.682	2182.680	157.467
530.00	0.435	480.919	2505.233	122.489
535.00	0.435	684.394	2773.018	90.462
540.00	0.430	927.315	3046.440	65.019
545.00	0.427	1203.252	3278.005	44.818
550.00	0.425	1513.648	3474.429	30.443
555.00	0.425	1855.923	3625.478	20.897

Continued.....

Continued from the previous page
(Thinnest Gold Coating)
(Page 2)

10.545	3844.964	2664.915	37.931	0.421	570.00
8.364	3861.439	3091.535	37.844	0.422	575.00
7.178	3811.893	3508.405	37.584	0.425	580.00
6.539	3699.116	3895.695	37.154	0.430	585.00
5.976	3622.434	4342.613	37.584	0.425	590.00
5.299	3463.342	4696.765	37.584	0.425	595.00
4.654	3351.294	5095.149	38.459	0.415	600.00
3.813	3167.761	5331.358	38.905	0.410	605.00
2.952	2959.811	5458.933	39.355	0.405	610.00
2.030	2730.179	5443.200	39.811	0.400	615.00
1.553	2459.148	5231.327	39.811	0.400	620.00
1.115	2178.403	4885.412	39.811	0.400	625.00
0.846	1903.281	4455.621	40.272	0.395	630.00
0.407	1628.299	3947.515	40.738	0.390	635.00
0.326	1365.091	3408.795	40.738	0.390	640.00
0.204	1126.284	2882.297	40.738	0.390	645.00
0.081	909.639	2374.497	40.738	0.390	650.00
0.041	727.682	1928.204	41.210	0.385	655.00
0.000	566.387	1518.167	41.210	0.385	660.00
0.000	427.342	1155.371	40.738	0.390	665.00
0.000	322.054	875.625	41.210	0.385	670.00
0.000	238.491	651.358	41.687	0.380	675.00
0.000	176.419	483.652	41.687	0.380	680.00
0.000	131.397	361.509	41.687	0.380	685.00
0.000	93.754	258.667	41.687	0.380	690.00
0.000	65.615	181.422	41.687	0.380	695.00
0.000	46.564	128.896	41.687	0.380	700.00
0.000	33.766	93.837	41.687	0.380	

X = 91487.597

Y = 81813.767

Z = 24858.700

XX=0.462
 YY=0.413
 ZZ=0.125
 XYZ=1.000

Appendix 12

Features of the automatic switch for electropolishing the tungsten wire

The circuit diagram which was shown in Figure 9.10, has the following features:

1. The transistor T_1 begins to conduct if its base is more positive than 1.06v. T_1 is therefore 'off' when the voltage at point 'A' is -1.06V.
2. The potential at the base of T_2 is then determined by the potential divider made up of resistors R1, R2 and R3. The value is approximately -10V and T_2 is thus 'On' or conducting.
3. The potential of 10V is applied to the base of the output transistor T_3 , which is arranged as an emitter follower via the resistance of the relay coil.
4. Supposing that the voltage of A rises until T_1 just begins to conduct, then an incremental positive signal at the base of T_1 will produce a negative signal at the collector, and hence a negative increment at the base of T_2 .
5. T_2 is disarranged as an emitter follower, so this negative signal appears at its emitter, which is fed back to T_1 , because both T_1 and T_2 emitters are coupled. A negative pulse on the emitter of T_1 is equivalent, as far as its collector output is concerned, to a further incremental positive feedback loop. This rapidly causes the base of T_2 to go so far negative that T_2 cuts 'off' at the end of its characteristics and its collector goes much more positive than previously to about - 1.3V.

6. This is fed to the base of T_3 and appears across the relay coil. The overall potential difference applied to the coil fell down enough to release the magnetic switch making the situation reversed, so that T_1 is 'off' and T_2 is 'on' and the potential at 'A' falls back to the last point.

In fact there is always hysteresis in a bistable circuit so that a value at 'A' less than $-1.06V$ will be needed to revert to polishing a state. This is provided by the reset line. The change in the potential at A to cause switching is derived from the change in the resistance at the polishing solution, when the tip breaks. When the polishing current is first started, $4mA$ gives -8.8 Volts at point B.

Appendix 13

Details of specimens used for assessing microindenters

1. 60/40 brass

60% copper and 40% zinc.

Two phases, β is hard and α is soft.

KBI-2 No. 33.321 annealed at 200°C and then water quenched.

KBI-4 No. 33.341 annealed at 400°C and then water quenched.

2. Aluminium

KAl-2 punched discs from a polished sheet of soft aluminium.

Appendix 14

Vickers D M41 microhardness tester

Assembly

The indenter objective and 40 times reading objective are mounted directly into the objective changer, the objective apertures and objectives being coded in the standard manner.

The pneumatic transmitter cylinder is placed on the anti-vibration platform. The larger nozzle on the air line is inserted into the transmitter. The smaller nozzle on the air line is inserted into the indenter objective, care being taken to ensure that this nozzle is only turned clockwise to avoid damage to the air inlet hole sealing. The centering cone with its adjustable graduated draw tube and filar micrometer eyepiece is attached directly to the monocular viewing head on a cone fitting.

Procedure

1. Plug in and switch on light. Fit indenter objective turret and connect air hose.
2. Focus specimen at low magnification (10 times) to find approximate area required.
3. Change to indenter objective, re-focus and position accurately with specimen stage centroids (cross wire on exact position).

4. Set correct lead, press lever down for 30 secs. (views from objective indentation disappear). Raise lever (view re-appear).
5. Change to measuring objective (x 40), re-focus, put in green filter and close down field iris and give sharper definition.
6. Measurement
 - a. Move specimen stage until vertical line is on left hand edge of diamond.
 - b. Rotate measuring eyepiece knob until second vertical line is at right hand corner.
 - c. Note filar micrometer reading and look up hardness reading in correct table.
 - d. Rotate filar 90° repeat for second diagonal.
7. Change back to indenter objective, open field iris, re-focus and move it to a new position. It is now ready for a second check.
8. The hardness values, against the filar micrometer divisions are tabulated in the Vickers microhardness testing instructions (65) booklet.